Journal of Radar and Optical Remote Sensing

Permission to publish Journal of Radar and Optical Remote Sensing

With respect to the Reference Number: **96/ص/87/7**dated 1396/01/14(3th April 2017), the 104th commission session was held to evaluate and approve the scientific journal of the Islamic Azad University. The commission announced to grant permission to establish the journal entitled "Journal of Radar and Optical Remote Sensing".

Acknowledgement
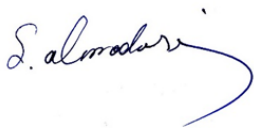
In the Name of God

Dear Readers,

I have the enormous opportunity to share the first journal publication to the readers. The Journal of Radar and Optical Remote Sensing (JRORS) is the first radar journal and the first scientific journal in this area of Islamic Azad University (2017). The first issue will be published this year by the Islamic Azad University, Yazd Branch. The publication of the articles resulting from the scholarly research findings contributes to the advancement of knowledge and performance of remote sensing and radar. This journal focuses on original research papers that develop a basic knowledge in the field of remote sensing and radar.

Over the past years, many research articles have been received in the specialized field and just a few have been accepted for publication in each issue based on the reviewers' and the editorial team's decisions regarding the articles. This has somehow upset the authors. Therefore, an apology on behalf of the editorial team for declining and or delaying the publication of some of these inter-disciplinary scholarly articles. It is hoped to add the scientific richness of the journal by releasing articles that reflect your valuable research activities, providing us with the latest publications in the scientific community of remote sensing and radar.

Finally, I would like to sincerely thank the Editorial Board for their dedication to prepare the first issue. It was their efforts that made it possible to publish the first issue on time.

Sincerely,

Dr. Seyyed Ali Almodaresi

Editor-in-Chief

Journal of Radar and Optical Remote Sensing

www.jrors. ir

INDEX

Estimation Net Groundwater Extraction Using Remote Sensing based on Water Balance Method and Its Comparison by Smart Meter Data (Study Area: Abarkouh-Chahgir Plain)

Mohammad Hossein Bagheri[a*], Saied Ebrahimi[b], Mohammad Mehdi Javadianzadeh[c]

[a*] *Regional Water Authority, Yazd, Iran.*
[b] *Regional Water Authority, Yazd, Iran*
[c] *Regional Water Authority, Yazd, Iran*

Abstract

Calculation of the components of water balance is very important in water resources management. One of the key components of balance is estimation of the amount of water drained by wells, springs and Qanats. Calculation of this parameter is too costly and time-consuming because of the need for field visit and field measurement. In order to solve these problems and to calculate the discharge amount of water resources in short period of time, using remote sensing technology and satellite images can be useful. Accordingly, actual evapotranspiration, the most important component of water-balance equation has been calculated and evaluated using this technology. The scope of the study in this research is the Chahgir plain of Abarkouh where underground water drop has caused many problems in the area. For this purpose, six Landsat 8 satellite images (OLI and TIRS sensors) during the period of June to September (2016) in Julian days 174, 190, 206, 222, 238 and 254 as well as meteorological data of two synoptic stations were used and SEBAL method was applied to estimate actual evapotranspiration. The results of the study and its comparison with the data obtained from smart meters (installed on the wells) with a 7.2 percent error indicates high accuracy of remote sensing data and used methods. Also, the amount of net groundwater extraction is estimated 1.07 million cubic meter (MCM) that comparison by pumping volume data (3.98 MCM), shows low efficiency and high water loss in the case study.

Keywords: Groundwater, Water Balance, Actual Evapotranspiration, SEBAL, LANDSAT 8.

---

* Corresponding author. Tel: +98-9132543541.
Email address: Bagheri.mhb@gmail.com.

1. Introduction

Estimation of the balance and values for input and output components will play a decisive role in any planning for the quantitative and qualitative management of these resources (Bagheri, 2012). In recent decades, there are many qualitative and quantitative problems with groundwater resources. Overuse, lack of attention to exploitation based on sustainable development, climate change and consequently precipitation reduction and drought are the factors that have made this situation. Therefore, management of water resources especially groundwater needs to measure and control its exploitation. Unavailability of statistics on the rate of discharge of aquifers and use of it in different parts are important problems for planners and managers of the country's water sector. The common traditional method of measuring the amount of pumping out of the groundwater table, is based on direct measurement and field visit of water resources by human which in addition to being costly is time-consuming. Estimation of the amount of groundwater harvesting depends on number of active wells, outflow discharge and operating time which is difficult to determine their true value and in some cases unreliable (Ahmad, 2002; Maupin, 1999). Furthermore, lack of cooperation of farmers and unauthorized harvesting make the work more complicated. In line with this need, the legislator has ordered people to install smart meters to measure the amount of volume of water extracted from groundwater table. It is a great move that in addition to the precise measurements of devices, it requires the cooperation of the exploiters on installation and maintenance of intelligent measuring instruments. But since smart meters are installed just on the authorized wells, planners are not able to measure the amount of water extracted from other water resources like aqueducts, fountains and unauthorized wells. In order to solve this problem, collecting data in large amounts and less time, the use of satellite images and Remote Sensing (RS) technique are very effective. RS provides the possibility of estimation of hydrologic parameters on a large scale and spatially with a high accuracy (Bos et al., 2001).

In these regards, several researches has been done on using remote sensing for groundwater studies (Ghulam et al., 2004; Girotto et al., 2019; Jha et al., 2007; Sadaf et al., 2019; Salehi et al., 2018). One of the RS based approaches in groundwater components is using water balance calculation which recently applied by several research (Ahmad et al., 2005; Bagheri et al., 2017; Deus et al., 2013; Gafurov, 2010; Mekonnen, 2005; Muthuwatta et al., 2010; Senay et al., 2011; Thoreson et al., 2009 and Zhang et al., 2016).

The research by Ahmad et al. (2005) is one of the few studies that have been conducted in order to estimate the amount of net groundwater harvesting using this technology and water balance methods. In this study, net ground water use was as a passive component and rainfall, actual evapotranspiration (ET), moisture changes in the soil unsaturated area and the amount of irrigation water by channels were the computational components of their method that they were estimated from October 1993 to October 1994 using images of AVHRR sensors and Landsat satellite in the Rechna Doab in Pakistan. Eventually, the map of the net amount of groundwater used was gained by preparing spatial data, which is one of the main components of water balance. In their study, SEBAL model was used to estimate actual evapotranspiration and Scott, Bastiaanssen, and Ahmad (2003) model was used in order to estimate soil moisture. The comparison of their result with SWAP model showed high accuracy and low error of remote sensing methods in estimating of actual evapotranspiration and soil moisture (Ahmad et al., 2005). In Iran (Bagheri et al., 2017) calculated the net amount of groundwater use by remote sensing technology in the Lake Urmia basin. The satellite images used were from Modis sensor and the study took place from 2000 to 2008. The results and evaluation showed the method used for the study area has had acceptable accuracy.

Lack of ground station for analysis, are the research limitation in RS based models and algorithms, spatially in groundwater modelling. Literally, the hypothesis of the research is based on actual ET calculation, net groundwater extraction can be estimated by Landsat 8 RS-data in agriculture area. In this study, an innovation was applied. The smart meter data which has been installed on the tube wells were used. Also, in this study, using Landsat 8 data with pan sharpening technique to produce 15-meter resolution was another innovation. So, it was tried to estimate and evaluate net volume of water harvested from groundwater resources in Chahgir plain for the first time.

2. Materials and Methods

2.1. Study area

The study area is the Chahgir plain which is sub-basin and a part of Abarkouh desert watershed. This plain is placed in the southwest of Yazd province and northeast of Fars province, between geographical longitudes 53°25′ and 54° and between geographical latitudes 30°30′ and 31°55′. Its medium altitude is 1776 meters above the sea level. Average annual rainfall in this plain is 72.2 millimeters and annual evaporation is 3171 millimeters and the average annual temperature is 16.7°C. Reducing in the groundwater inflow due to drought and also overuse of agricultural wells, increasing the saltwater of playa adjacent to the plain (Abarkouh desert) have caused severe changes in the water quality of the area. In terms of water resources, 39 agricultural wells and two fountains called Beghdaneh and Darehbagh are groundwater drainage resources in this plain. In terms of agriculture, the pistachio is the dominant cultivation. The study area in terms of geology is a part of central Iran Zone and it is in the vicinity of the Sanandaj-Sirjan Zone. Old formations of the area are shale and Silurian sandstone covered by shale, sandstone, coal shale and sometimes yellow and brown Devonian Dolomite. On these formations, there is the huge Jamal formation. Totally, in this area, tectonic and stratigraphy follow the trend of Central Iran Zone. In terms of geology, Chahgir sub-basin is divided into two parts. The northwestern part that some agricultural wells are already drilled in this area and it consists of alluvium and rocks which are mainly carbonate. The wells of this area are usually shallow and they have fresh water with electrical conductivity of two to three thousand micromhos per centimeter. Of course, some wells are salty because of the proximity of evaporative formations and their electrical conductivity is between 3 to 19 thousand micromhos per centimeter.
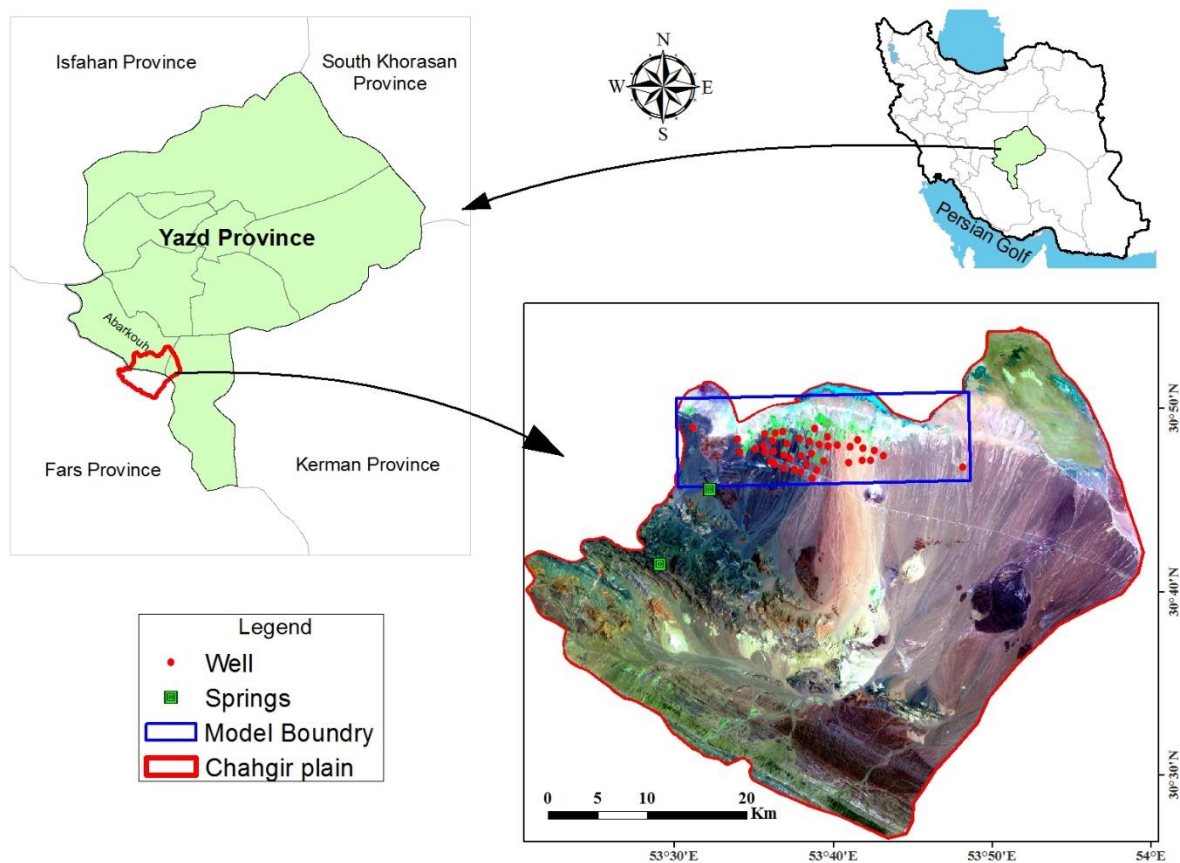
Figure 1. The study area (Abarkouh Chahgir plain)

2.2. Satellite and Ground Data

In this study, in order to use SEBAL algorithm for the quarter period (June to September 2016), six images of Landsat 8 satellite were obtained[1] and used which after pre-processing (Radiometric correction and Atmospheric Correction by FLAASH). The Julian days of satellite passed, were 174, 190, 206, 222, 238 and 254. These images included both OLI and TIRS sensors (all 11 bands except band 9-Cirus). The times that satellite passes were varied from 6:30 to 7 AM (UTC) in all six used imagery. Also, Digital Elevation Model (DEM) were applied. The DEM image at 12.5m in resolution were obtained from VERTEX website[2]. In addition to satellite data, ground meteorological data included air temperature (minimum and maximum), wind speed, daylight hours, and relative humidity (hourly and daily) provided by the Abarkouh and Marvast synoptic stations. This study needed amount of groundwater pumping to assess model results. For this reason, monthly smart meter data which installed on tube wells, were read and used.

2.3. Water Balance

A large amount of water used by plant mass is evaporated and transported and only a small amount of it is absorbed by plants. Accordingly, evaporation and transpiration are considered as good criteria for vegetarian water consumption (Ahmadi, 2014), as long as actual evapotranspiration is important. On the other hand, considering the net amount of consuming water per unit area (for example a pixel of an image satellite) is equivalent to the amount of water extracted from water resources, actual evapotranspiration of a pixel can be equivalent to the amount of water extracted from water resources which goes to pure vegetarian consumption (without losses). In the other words, in aquifers like the study area (Chahgir) which is lack of any rivers or surface water resources and relies on groundwater resources, the main components of water balance are rainfall (P), actual evapotranspiration (ET_a) and moisture changes in the soil unsaturated area (dW_u/dt) which ultimately leads to estimation of the net amount of groundwater use (I_{ngw}). Figure 2 represents an overview of the components related to the balance in a water resource system.

Figure 2. Schematic of balance components in saturated and unsaturated regions (Ahmad et al. (2005) and Bagheri et al. (2017)).

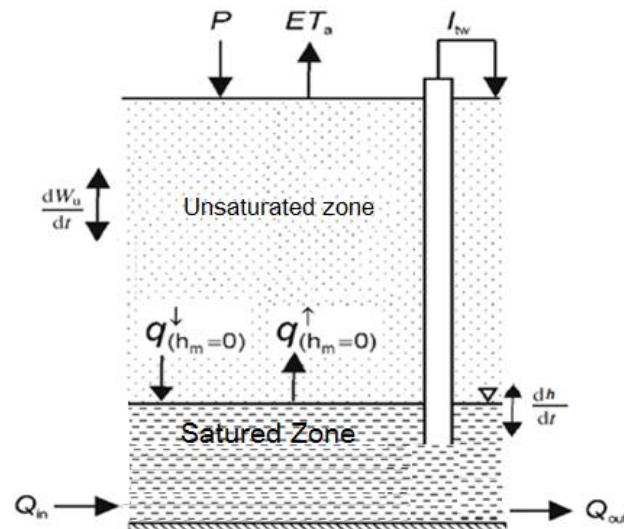 In the aquifer, except tube well extraction (pumping) (I_{tw}), two parameters of capillary penetration and capillary conduction (q ($h_m=0$) & q ($h_m=0$)) and also the amount of recharge and discharge of other aquifers (Q_{in} & Q_{out}) are considered as total input and output of the aquifer (saturation area). As regards the purpose of this study is merely related to unsaturated region, the total equation of the balance for the unsaturated region is according to equation 1:

$$I_{tw} = ET_a - P + \frac{dw_u}{dt} + q \downarrow_{(hm=0)} - q \uparrow_{(hm=0)} \tag{1}$$

The difference between recharge and discharge of the aquifer is equivalent to the net amount of groundwater use at a time. In the other words, the following relationship is confirmed:

$$q_{nr} = q \downarrow_{(hm=0)} - q \uparrow_{(hm=0)} \tag{2}$$

$$I_{ngw} = I_{tw} - q_{nr} \tag{3}$$

In the above relationship q_m is equivalent to the amount of net input water through unsaturated region to the groundwater level. In other word, I_{ngw} is assumed as the difference of all discharge and recharge value of the aquifer. Therefore, from the combination of equations 1 to 3, I_{ngw} is calculated as the follows:

$$I_{ngw} = ET_a - P + \frac{dw_u}{dt} \tag{4}$$

In order to accurately evaluate the research methodology, the period from May to September 2016 was considered. Assuming slight changes in moisture of the soil in unsaturated region and considering the lack of rain during the research period, the amount of net use of groundwater resources is equivalent to actual evapotranspiration ($I_{ngw} \approx ET_a$).

2.4. Actual evapotranspiration

SEBAL is a method based on experimental relationships and atmospheric physics, which estimates the actual evapotranspiration rate with minimum terrestrial and using satellite images with visible, infrared and thermal band. In a lot of researches mentioned SEBAL as an acceptable approach for ET calculation especially in agricultural area (Akbarzadeh et al., 2015; Bagheri et al., 2012; Bagheri et al., 2015; Ziaee et al., 2019). This algorithm represented by Bastiaanssen et al. (1998) for the first time and it was updated in 2000 and 2002 again and has been corrected in some cases. Totally, SEBAL has estimated the components of the energy flux using vegetation indices and surface parameters and their internal relationship. And finally, its passive component, latent heat flux (calculation factor of actual evapotranspiration) is estimated. Actually, in this method latent heat flux which is used for evapotranspiration, according to the amount of remaining energy is determined by the equation 5:

$$\lambda ET = Rn - G - H \tag{5}$$

In the equation above, ET is evapotranspiration, λ is latent heat of vaporization, R_n is net sunlight, H is sensible heat flux and G is soil heat flux (all the components in the equation above are in Watt per square meter). Pure sunlight, is the difference between incident radiation flux and reflected radiation flux and it is considered as a criterion from the amount of energy in the earth surface which is gained by the equation 6:

$$R_n = (1 - \alpha)R_{S\downarrow} + R_{L\downarrow} - R_{L\uparrow} - (1 - \varepsilon_0)R_{L\downarrow} \tag{6}$$

In the equation above, α is surface albedo, R_s is short-wave incident radiation (0.3 to 3 micrometers) (W/m^2), R_L is long-wave incident radiation (3 to 100 micrometers) (W/m^2) and ε_0 is broadband surface emission. Soil heat flux (G) is the amount of heat transfer inside the soil and vegetation due to molecular conductivity which is according to equation 7 (Allen et al., 2002):

$$G = R_n \times \frac{T_s}{\alpha} \times [0.0032 \times \alpha + 0.0062 \times \alpha^2] \times [1 - 0.978 \times NDVI^4] \tag{7}$$

In this equation, T_s is surface temperature in centigrade degrees and α is surface albedo and NDVI is vegetation index. Sensible heat flux (H) as the most complicated component of the energy balance equation, is a waste of energy (or the heat) that is transferred to the air by temperature difference which is calculated by equation 8;

$$H = \rho_{air} \cdot C_p \cdot \frac{T_O - T_{air}}{R_{ah}} \tag{8}$$

In the equation above T_0 is Aerodynamic air temperature (Kelvin), ρ_{air} is air density (kg/m^3), C_p is specific heat (J/Kg/K) and Rah is Aerodynamic air resistance. Reference evapotranspiration ratio daily per hours was used for estimation of daily evapotranspiration from instantaneous evapotranspiration of the satellite. For this purpose, reference evapotranspiration on an hour scale (millimeter per hour) at the moment of the passage of the satellite (ET$_{r\text{-insat}}$) and also its amount on a day scale (millimeter per day) (ET$_{r\text{-24}}$) for the meteorological station representing the area was calculated. Then the amount of daily actual evapotranspiration of satellite models (ET$_{act\text{-24}}$) in millimeter per day was estimated (Allen et al., 2002):

$$ET_{act-24} = ET_{r-24}\frac{ET_{inst}}{ET_{r-inst}} \tag{9}$$

It is possible to estimate total sum of periodic values of ET between two images (ET$_{act\text{-period}}$) for n consecutive days with estimating the amount of daily actual evapotranspiration (ETact-24) for the days having image satellite, like equation 9:

$$ET_{act-period} = \sum_{1}^{n} ET_{r-24}\frac{ET_{act-24}}{ET_{r-24}} \tag{10}$$

In order to daily and hourly reference evapotranspiration, Mantit-Fao method was used (Allen et al., 2002).

2.5. Estimation of Net Groundwater Use

Considering the significant waste of water in the agriculture sector, irrigation efficiency plays an effective role in calculation of net groundwater use. Totally, irrigation efficiency is defined as the ratio of net water required or the consumption of the plant to the total input or extracted water (Abbasi et al., 2017). Therefore, if the extracted water (I_{tw}) is measured by smart meters and irrigation efficiency is applied, the amount of net groundwater use, according to equation 11 will be estimated:

$$I_{ngw} = E_i \times I_{tw} \tag{11}$$

It is noteworthy that in order to control and manage the use, in 2015 with following Yazd Regional Water Company, all agricultural wells of the study area were equipped with smart meters. Accordingly, tube well

extraction (I_{tw}) data for the time period of study was extracted from smart meters. In Figure 3, the research methodology flowchart has been represented. IDL programming in ENVI software was used to apply all equations of the research.
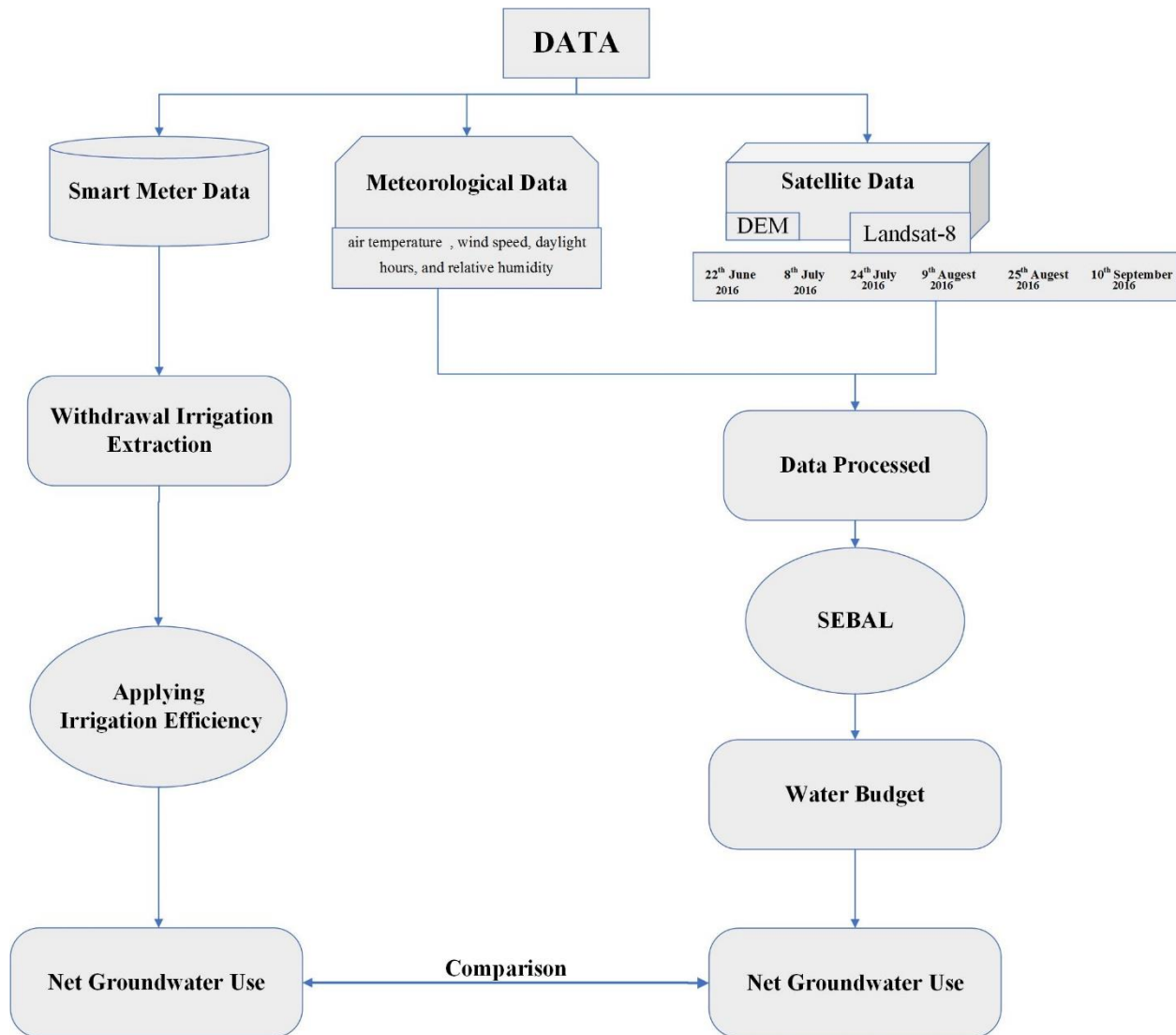
Figure 3. Flowchart of research methodology

3. Results and Discussion

The amount of periodic actual evapotranspiration was estimated with the actual evapotranspiration on a daily scale (for each of the six dates mentioned), using equation 10. Figure 4 (a) represents the spatial distribution map of daily actual evapotranspiration resulted from SEBAL algorithm as a sample for one of the modeling days. As it can be observed the highest value of actual evapotranspiration is related to agricultural land which is irrigated by groundwater resources. The lowest amount of actual evapotranspiration is related to pastures and shrubs. Also, Figure 4 (b) shows total ET from model outputs.
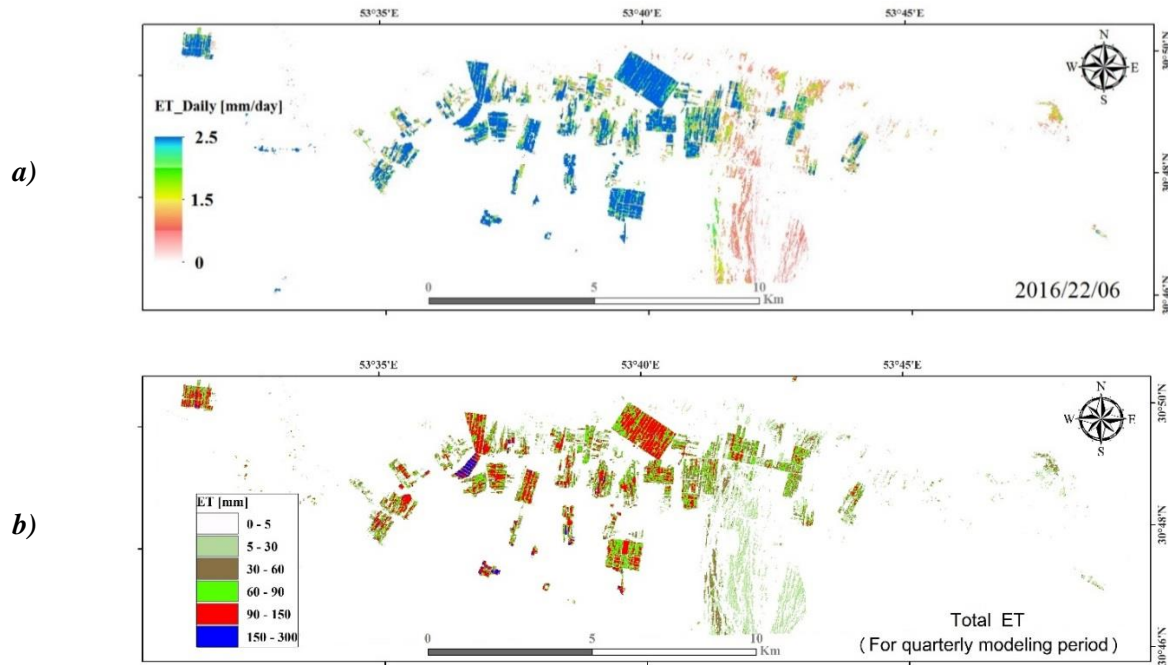
Figure 4. The spatial distribution map of a) daily actual evapotranspiration on June 22, 2016 in the study area (mm/days), b) Total ET (mm)

Figure 5 shows time distribution of actual evapotranspiration in the quarterly modeling period. Maximum chart values are related to agricultural land which according to represented results in the second half of August until mid-September, the most value of actual evapotranspiration and as a result the most amount of net groundwater use are visible.
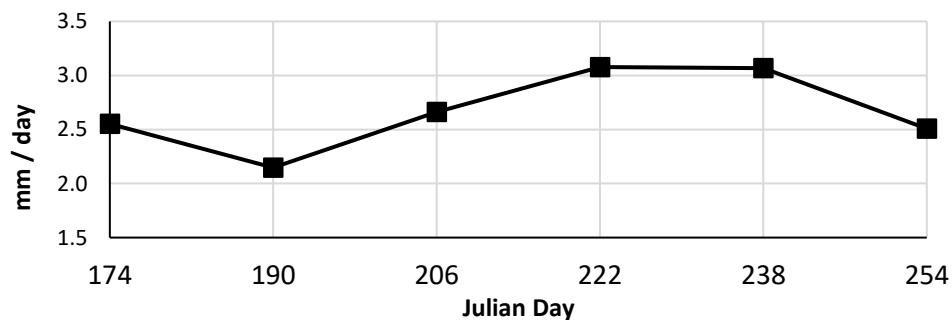
Figure 5. Time changes of the amount of actual evapotranspiration (millimeter per day)

As previously mentioned, failure of rainfall during the modeling period and a month before that (to ensure the removal of the effect of rainfall delay time) for the year, it means that any actual evapotranspiration estimated from pixels of agricultural land, is equivalent to net groundwater use due to pumping of the agricultural wells. Accordingly, Figure 7 represents SEBAL algorithm output based on net groundwater use. As shown in Figure 7, the amount of net water use is variable from 0 to 300 millimeters. In order to evaluate the results more accurately, three wells dispersed in the plain with different specifications and conditions were chosen and the amount of their output was calculated (Figure 6).
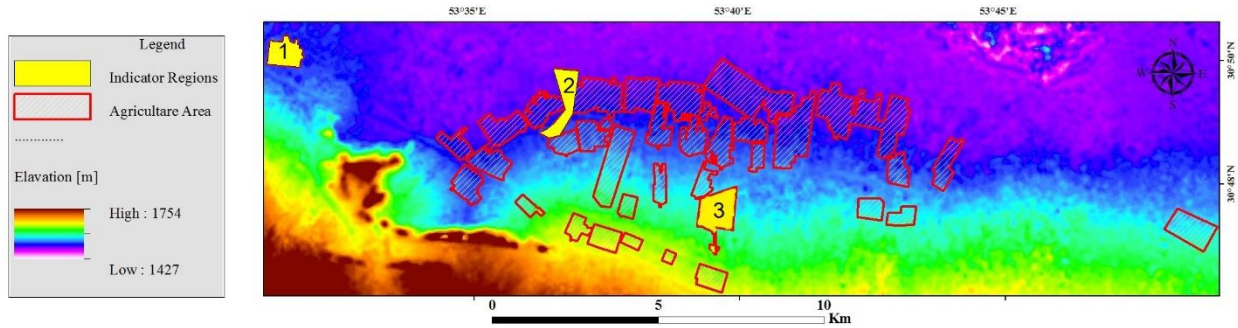
Figure 6. Agricultural land position and three indicator regions
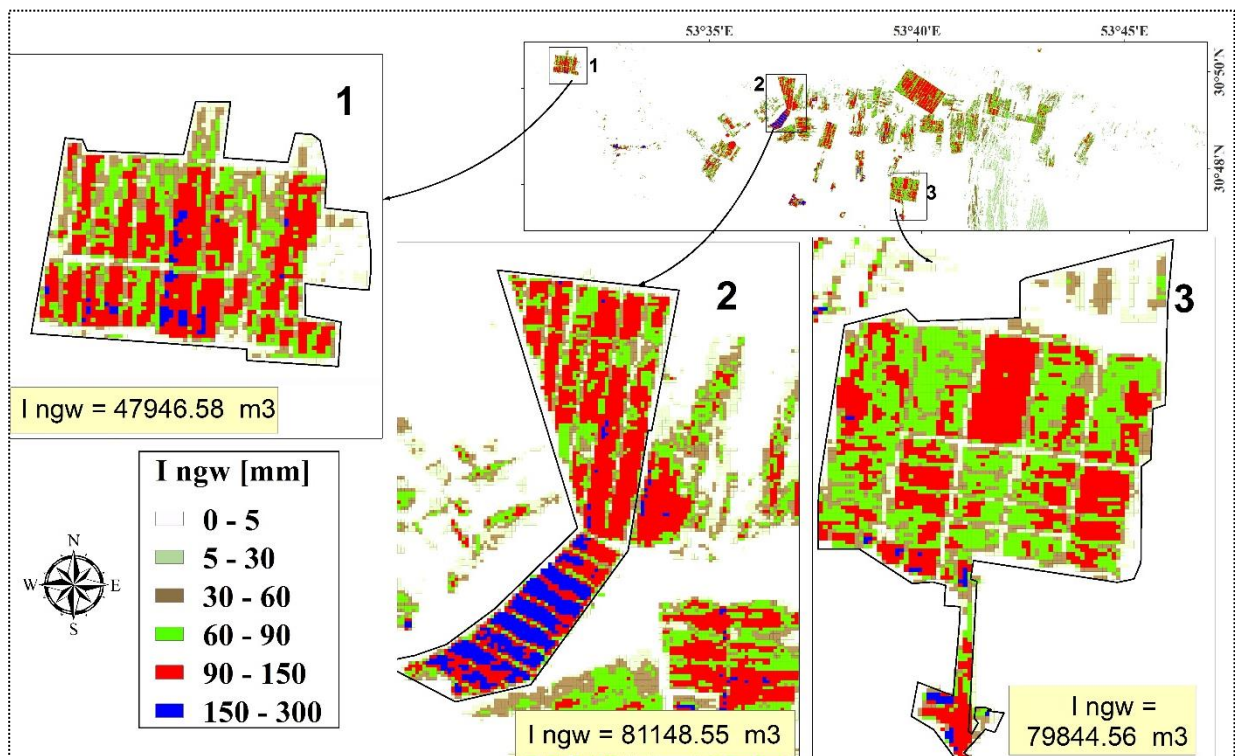
Figure 7. Groundwater net use map for the quarterly modeling period (in millimeters) and situation of research methodology output in the case of index ranges

In order to evaluate and analyze the results of the research methodology, according to Figure 7, the net amount of groundwater use was estimated in the three selected wells. Irrigation efficiency of the case study was used from another research by Ebrahimi et al. (2019). Table 1 shows the specification and parameter calculation of efficiency for wells. Efficiency in each well is very different. Although the water in the well number 3 has better quality than other wells, its efficiency is lower. And this is true for well number 1 in comparison to well number 2. The well number 2 has electrically conductive, but there are increasing water efficiency and significant reduction in waste water because of proper use of low-pressure irrigation system and use of low-width and proper plotting in order to reduce evaporation losses and also setting up regular irrigation. As it can be seen in Figure 7, blue pixels in the well number 2 shows lack of water stress in the farm which expresses the impact of water use management in high productivity and more product performance.

Table 1. Profile of indicator wells with model output amount

Well No.	Water EC	Cultivated area	I_{ngw} (Model)	I_{tw}	E_i	I_{ngw} (Observation) $[\mathbf{I_{ngw}} = \mathbf{E_i} \times \mathbf{I_{tw}}]$	MAPD[1] $[\frac{\sum_{i=1}^{n}[m_i - o_i]}{n} \times \frac{100}{\frac{1}{n}\sum o_i}]$
	μmhos/cm	m^2	m^3	m^3	%	m^3	%
1	6430	686,242.20	47,946.58	73,435.68	60	44061.408	
2	7370	878,264.1	81,148.55	112,597.4	70	78818.18	7.2
3	4500	1,073,250	79,844.56	205,578	35	71952.3	

As shown in the Table 1, error between observed values (resulted from smart meter data and applying efficiency) and modeling values in the three wells is in average 7.2 percent which shows acceptable accuracy of research method and use of remote sensing in estimation of net groundwater use.

Figure 5 shows I_{tw} and I_{ngw} in the quarterly modeling period. As shown in Figure 8, the amount of net groundwater use and well pumping volume (I_{tw}) data for the time period are 1.07 and 3.98 MCM[2] respectively. These values show low efficiency and high water loss in the case study.
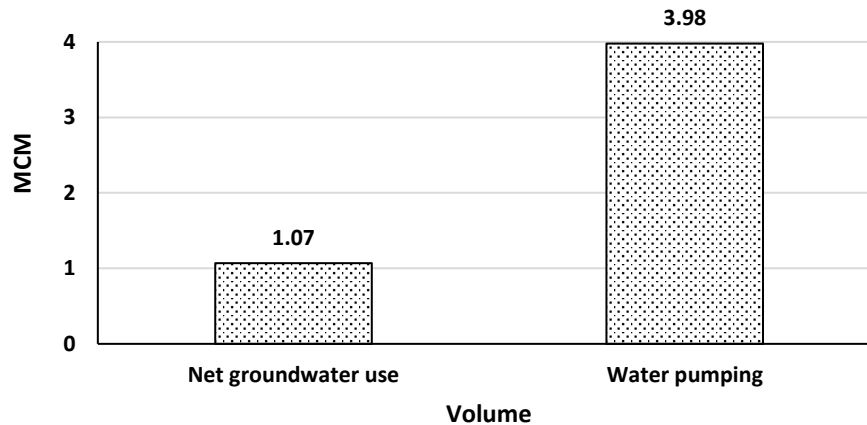
Figure 8. Total volume of I_{tw} and I_{ngw} in the quarterly modeling period

As previously mentioned, in this study high resolution of Landsat 8 imagery was used to calculate I_{ngw} while previous research used other satellite imageries such as MODIS (Bagheri et al., 2017) or AVHRR sensors (Ahmad et al., 2005) with low spatial resolution. So, accuracy of this study methodology was better than other same studies. Also, it is important to analysis ET accuracy. Base on Bastiaanssen et al. (2002), the accuracy of evapotranspiration estimation by satellite data varied from 0% to 10% on a field scale to 5% at regional level. So, the accuracy of this study with 7.2 percent error is acceptable which shows that the results from Landsat 8 imageries are better than other satellite data.

4. **Conclusion**

Water use management in the agricultural sector as the country's largest water consumer plays an important role in water crisis management and reducing the tension that results from water crisis. Estimation

---

1. Mean Absolute Percent Difference.
2. Million Cubic Meter.

of net use of groundwater resources has always been a matter of serious concern for experts and managers in water and agricultural sector. Use of traditional method for estimating the exact amount of water used and wasted has always faced many failures and errors. In this study, it is tried to estimate and evaluate net groundwater use by providing an efficient method based on available data and free satellite images. The six images processed and applied by SEBAL algorithm to calculate evapotranspiration as a major water balance component. To analysis, the smart meter data extracted. The error analysis by MAPD, showed acceptable accuracy of model with 7.2 percent. A solution which can be used both on small scales (such as a farm) and on large scales like plains and catchment basins. Also, as a result, the amount of net groundwater use and well pumping volume (I_{tw}) data for the time period were calculated 1.07 and 3.98 MCM respectively. These values demonstrate low efficiency and high water loss in the study area.

Reference

Abbasi, F., Sohrab, F., & Abbasi, N. (2017). Evaluation of Irrigation Efficiencies in Iran. *Irrigation and Drainage Structures Engineering Research, 17*(67), 113-120. Retrieved from http://idser.aeri.ir/article_109617_56564fd7d1cdc955ba66b818cbca0d84.pdf. doi:10.22092/aridse.2017.109617

Ahmad, M. (2002). Estimation of net groundwater use in irrigated river basins using geo-information techniques: a case study in Rechna Doab, Pakistan. *ITC Dissertation (Netherlands)*.

Ahmad, M., Bastiaanssen, W. G. M., & Feddes, R. A. (2005). A new technique to estimate net groundwater use across large irrigated areas by combining remote sensing and water balance approaches, Rechna Doab, Pakistan. *Hydrogeology Journal, 13*(5), 653-664. Retrieved from https://doi.org/10.1007/s10040-004-0394-5. doi:10.1007/s10040-004-0394-5

Ahmadi, A. (2014). *Using Remote Sensing In Calculation Of Evapotranspiration And Water Demand*. Retrieved from Isfahan University of Technology.

Akbarzadeh, H., Haghighatjoo, P., & Bagheri, M. H. (2015). Estimates of Evaporation from Surface Water Bodies with Sebal Algorithm Using Remote Sensing Techniques (Case Study: Chahnimeh's Fresh Water Reservoirs of Sistan). *Iranian Journal of Irrigation and Drainage, 9*(3), 510-521.

Allen, R., Tasumi, M., Trezza, R., Waters, R., & Bastiaanssen, W. (2002). SEBAL (Surface Energy Balance Algorithms for Land). *Advance Training and Users Manual–Idaho Implementation, version, 1*, 97.

Bagheri, M. H. (2012). Assessment of remote sensing technique for estimation of water balance components in basin scale, emphasizing on net groundwater exploitation: a case study on Urmia lake basin. (Master of science), Universityof Tarbiat Modares.

Bagheri, M. H., Arshad, S., Majnuni, A., & Morid, S. (2012). A comparison of single-source and two-source energy fluxes models to estimate actual evapotranspiration in Tabriz Plain. *Iranian Journal of RS and GIS, 4*(13), 81-96.

Bagheri, M. H., Morid, S., & Arshad, S. (2015). Assessment of remote sensing SEBAL algorithm to estimate actual evapotranspiration in different landuses, a case study in Urmia Lake basin. *Iranian Water Research Journal, 9*(16), 101-110.

Bagheri, M. H., Morid, S., & Arshad, S. (2017). Application of Remotely-Sensed Data to Estimate a Water Budget for Data-Scarce Endorheic Basins: A Case Study of Lake Urmia basin, Iran. *Journal of the Indian Society of Remote Sensing, 45*(1), 101-112. Retrieved from https://doi.org/10.1007/s12524-015-0522-9. doi:10.1007/s12524-015-0522-9

Bastiaanssen, W. G., Ahmad, M. u. D., & Chemin, Y. (2002). Satellite surveillance of evaporative depletion across the Indus Basin. *Water Resources Research, 38*(12), 9-1-9-9.

Bastiaanssen, W. G., Menenti, M., Feddes, R. A., & Holtslag, A. A. M. (1998). A remote sensing surface energy balance algorithm for land (SEBAL). 1. Formulation. *Journal of hydrology, 212*, 198-212.

Bos, M., Dayum, S., Bastiaanssen, W., & Vidal, A. (2001). Remote sensing for water management: The drainage component. Paper presented at the Report on expert consulation meeting organized by representatives of the ICID, IPTRID, ILRI, WaterWatch and the World Bank, Ede-Wageningen May.

Deus, D., Gloaguen, R., & Krause, P. (2013). Water Balance Modeling in a Semi-Arid Environment with Limited in situ Data Using Remote Sensing in Lake Manyara, East African Rift, Tanzania. *Remote Sensing, 5*, 1651-1680.

Ebrahimi, S., Sarkargar, A., Javadianzadeh, M. M., & Bagheri, M. H. (2019). *Calculation of water lossess in agricultural sector using remote sensing (Study Area: Chahgir plain, Yazd)*. Paper presented at the 7th Iranian water resources management conference, Yazd, Iran.

Gafurov, A. (2010). *Water Balance Modeling Using Remote Sensing Information: Focus on Central Asia*.

Ghulam, A., Qin, Q., Zhu, L., & Abdrahman, P. (2004). Satellite remote sensing of groundwater: quantitative modelling and uncertainty reduction using 6S atmospheric simulations. *International Journal of Remote Sensing, 25*, 5509-5524.

Girotto, M., Reichle, R. H., Rodell, M., Liu, Q., Mahanama, S., & De Lannoy, G. J. (2019). Multi-sensor assimilation of SMOS brightness temperature and GRACE terrestrial water storage observations for soil moisture and shallow groundwater estimation. *Remote Sensing of Environment, 227*, 12-27.

Jha, M. K., Chowdhury, A., Chowdary, V., & Peiffer, S. (2007). Groundwater management and development by integrated remote sensing and geographic information systems: prospects and constraints. *Water Resources Management, 21*(2), 427-467.

Maupin, M. A. (1999). Methods to determine pumped irrigation-water withdrawals from the Snake river between upper Salmon falls and Swan falls dams, Idaho*, using electrical power data, 1990-95*.

Mekonnen, S. C. (2005). Assessment of catchment water balance using GIS and Remote Sensing*: Roxo, Portugal*. The Netherlands: ITC.

Muthuwatta, L., Ahmad, M., Bos, M., & Rientjes, T. (2010). Assessment of water availability and consumption in the Karkheh River Basin, Iran-using remote sensing and geo-statistics. *Water Resources Management, 24*(3), 459-484.

Sadaf, R., Mahar, G. A., & Younes, I. (2019). Appraisal of Ground Water Potential through Remote Sensing in River Basin, Pakistan. *International Journal of Economic and Environmental Geology*, 25-32.

Salehi Siavashani, N., Vaquero, G., Elorza, F. J., Candela, L., & Serrat Capdevila, A. (2018). Remote sensing application for investigating groundwater recharge at Lake Chad Basin. *Paper presented at the EGU General Assembly Conference Abstracts.*

Scott, C. A., Bastiaanssen, W. G., & Ahmad, M.-u.-D. (2003). Mapping root zone soil moisture using remotely sensed optical imagery. *Journal of Irrigation and Drainage Engineering, 129*(5), 326-335.

Senay, G., Leake, S., Nagler, P., Artan, G., Dickinson, J., Cordova, J., & Glenn, E. (2011). Estimating basin scale evapotranspiration (ET) by water balance and remote sensing methods. *Hydrological Processes, 25*, 4037-4049.

Thoreson, B., Clark, B., Soppe, R., Keller, A., Bastiaanssen, W., & Eckhardt, J. (2009). Comparison of evapotranspiration estimates from remote sensing (SEBAL), water balance, and crop coefficient approaches. *Paper presented at the World Environmental and Water Resources Congress 2009: Great Rivers.*

Zhang, Y., Pan, M., & Wood, E. F. (2016). On creating global gridded terrestrial water budget estimates from satellite remote sensing. In *Remote Sensing and Water Resources* (pp. 59-78): Springer.

Ziaee, R., Moghaddasi, M., Paimozd, S., & Bagheri, M. H. (2019). Comparison of SEBS and SEBAL Algorithms in Evaporation Estimation from Open Water Surface with the Assessment of the Salinity Effect. *Journal of Water and Soil Science, 22*(4), 317-329. Retrieved from http://jstnar.iut.ac.ir/article-1-3570-en.html. doi:10.29252/jstnar.22.4.317

Spatio-Temporal Analysis of Morphology Distribution and Monitoring of Land Use Change in Yazd

Mojtaba Khezri[a*], Masoud Salman Roughani[b], Ali Sarkargar Ardakani[c]

[a* b]*Ms in GIS, Remote Sensing,Yazd Branch, Islamic Azad University, Yazd, Iran.*

[c] *GIS & RS Department, Yazd Branch, Islamic Azad University, Yazd, Iran*

Abstract

Land use planning is the most important issue of sustainable urban development and a major priority in urban planning. This study was conducted with the aim of investigating the extent of physical expansion of Yazd city, identifying the land use changes to urban use and determining the city growth directions during the years 2013 to 2018, using Landsat 8 satellite imagery over a time period of 5 years for Yazd city. Using the technique of detection of changes by comparative method after classification of images, changes in green space and moor lands were identified for urban use. Then, regional statistics techniques were used to determine the extent of city expansion and the nature of changes were obtained in different geographical directions. From 2013 to 2018, based on the results, 24.73% of the moor lands and 32.22% of the green area has had urban use. The growth of the city during this period were towards the East and South directions in the central and southern sectors in the marginal sector. The greatest amounts of green space changed to urban use were in the central and peripheral sectors, and the largest conversions of the moor land to urban use were in the central eastern region and in the southern marginal sector. The results showed that inappropriate distribution of applications in some parts of the city disrupted the spatial distribution of the land use.

---

* Corresponding author Tel: +98-9133568878.
Email address: Mojkhezri@gmail.com.

1. Introduction

One of the processes in which changes in the city can be studied for a period of several years and thereby predicting the urban development trends for proper planning is modeling the urban development. One of the main challenges in the urban development process of the developing countries is their accelerated growth, which, if this growth be dispersed and unplanned, many problems and difficulties will result in the management process and urban planning. Today, urban land use planning is of great importance by the ever-increasing development of cities and the imbalance in user dispersion. Equitable access to these uses and their optimal use is one of the fundamental components of sustainable development and social justice (Ammanpour et al., 2016).

To be able to plan the future growth of the city in the right direction, it is imperative to know the city growth at different time periods. Today, one of the ways omitted to analyze and inspect a city's change over a period of time is to use data and remote sensing methods. Remote sensing data has many advantages, including access to data at different time periods, low cost, and reduced study time, which in recent decades has dramatically increased its use in various fields, especially in urban studies (Eghbali and Ziari, 2007).

One of the most important applications of remote sensing data is using it to investigate and discover the changes that have occurred in phenomena and are spatial-temporal or, in other words, their position and status change over time. In fact, the discovery of changes to the process of identifying and determining the type and extent of coverage or land use in a time frame is referred to using remote sensing images. The discovery of changes using remote sensing data requires the use of several images at different times to discover and track changes that have occurred over time in relation to the observed phenomenon (Zanganeh Shahraki et al., 2014).

Mehdi Hassan (2017) evaluated land use change, urban growth and analysis in five cities in Bangladesh using Landsat satellite imagery, which results in continually increasing the conversion of agricultural land, blueberries, vegetation and wetlands in urban areas that significantly alter the structure and functioning of ecosystems around cities.

Khezri Ahmadabad et al. (2017) studied land use change in Baharestan using Landsat satellite imagery. For this purpose, Landsat 7 ETM satellite images on May 15, 2003 and Landsat 8 OLI-TIRS satellite images on September 15, 2016, produced a land use map using maximum likelihood method. Then, for evaluation of classification accuracy, overall accuracy and kappa coefficient were calculated for each map. The map produced in 2003 achieved 90% overall accuracy and 87% kappa coefficient and the 2016 map produced 98% overall accuracy and 97% kappa coefficient. The results showed that human factors (buildings and roads) led to the most changes in the city of Baharestan.

Sahle Kibert et al. (2016) undertook a four-decade-long assessment of land-use change and land cover in Ethiopia based on satellite imagery analysis. They used an approach of multi-temporal mid resolution satellite images, combined with visual interpretation and supervised classification, to enhance accuracy of land cover classification and dealing with varying cloud cover, which resulted in improvements of 12–30% over the conventional method. The results of the time series (1972-2013) indicate the impact of human development on environmental degradation. The data analysis also showed that agriculture in lands today has reached its maximum extent and that the marginal lands of forests are more threatened by biodiversity.

Zanganeh Shahraki et al. (2014) investigated the spatial-temporal analysis of the physical development of Mashhad city and the monitoring of land use changes in the period 1987 to 2013 using satellite imagery. Using Landsat satellite imagery, they identified urban land use changes in the city of Mashhad after classifying the images using a change detection technique. The results showed that 343.63 hectares of agricultural lands and 6964.11 hectares of moor land have had urban land use.

Heydarian et al. (2013) studied the land use change in Tehran metropolitan area during the period (1995-1997) using the comparison method after classification of Landsat satellite images. The results of variation detection with Kappa coefficient of 91% and Kramer coefficient of 88% indicated an increase in area in developed areas (4603.68 hectares), parks (650.7 hectares) and blue levels (22.32 hectares) as well as a decrease in the area of open land (4561.4 hectares) and vegetation (715.23 hectares). According to the results, most of changes took place in the western part of Tehran.

Rabiei et al. (2005) studied and rediscovered land use and land use changes in Isfahan using remote sensing and geospatial data using monthly Landsat images. The results indicated a large change in the use of agricultural land adjoining the city of Isfahan to the residential area during the eight years that managers and planners need to oversee the destruction of agricultural land in this area.

The historic city of Yazd is one of the unique examples of the Iranian desert towns, which is now the largest city registered in the UNESCO World Heritage Sites and is undoubtedly the focus of attention of tourists, and due to globalization, the need to study and expand the city is doubled. The present study is to investigate and evaluate the land use status of the city and provide appropriate solutions for balancing the distribution and spread of land use in Yazd in order to achieve a sustainable cities.

2. Materials and Methods

2.1. Study area

Yazd city in the center of Yazd province between latitudes 29 degrees 48 minutes to 33 degrees and 30 minutes north latitude 52 degrees 45 minutes to 56 degrees and 30 minutes east is the source of meridian. This province is limited to north and west of Isfahan Province, northeast to Khorasan province, southwest to Fars province and southeast to Kerman province, due to its remoteness from the borders of Iran, during the history of crises and cultural and ethnic pressures has remain immune (Fig 1). Yazd province has an area of 72156 square kilometers, accounting to approximately 37.4 percent of the country's total land cover.

Table 1. Population density in Yazd in 2013 and 2018

Source: Management and Planning Organization of Yazd Province

Year	City area (hectare)	Population	Population density
2013	14995.2	503114	33.55
2018	14995.2	548193	36.56

2.2. Land Use Map of the Studied Area

The land use map of the studied area for 2013 and 2018, which is provided by the supervised classification method, is shown in Figure 2 and Figure 3. In this research, according to the structure of the city, images were classified in five classes: residential lands, green spaces, moor lands, asphalt roads and trees. Also, based on the obtained maps, the area of each land uses in the study area is calculated and presented in Table 1. The results of this study show that.
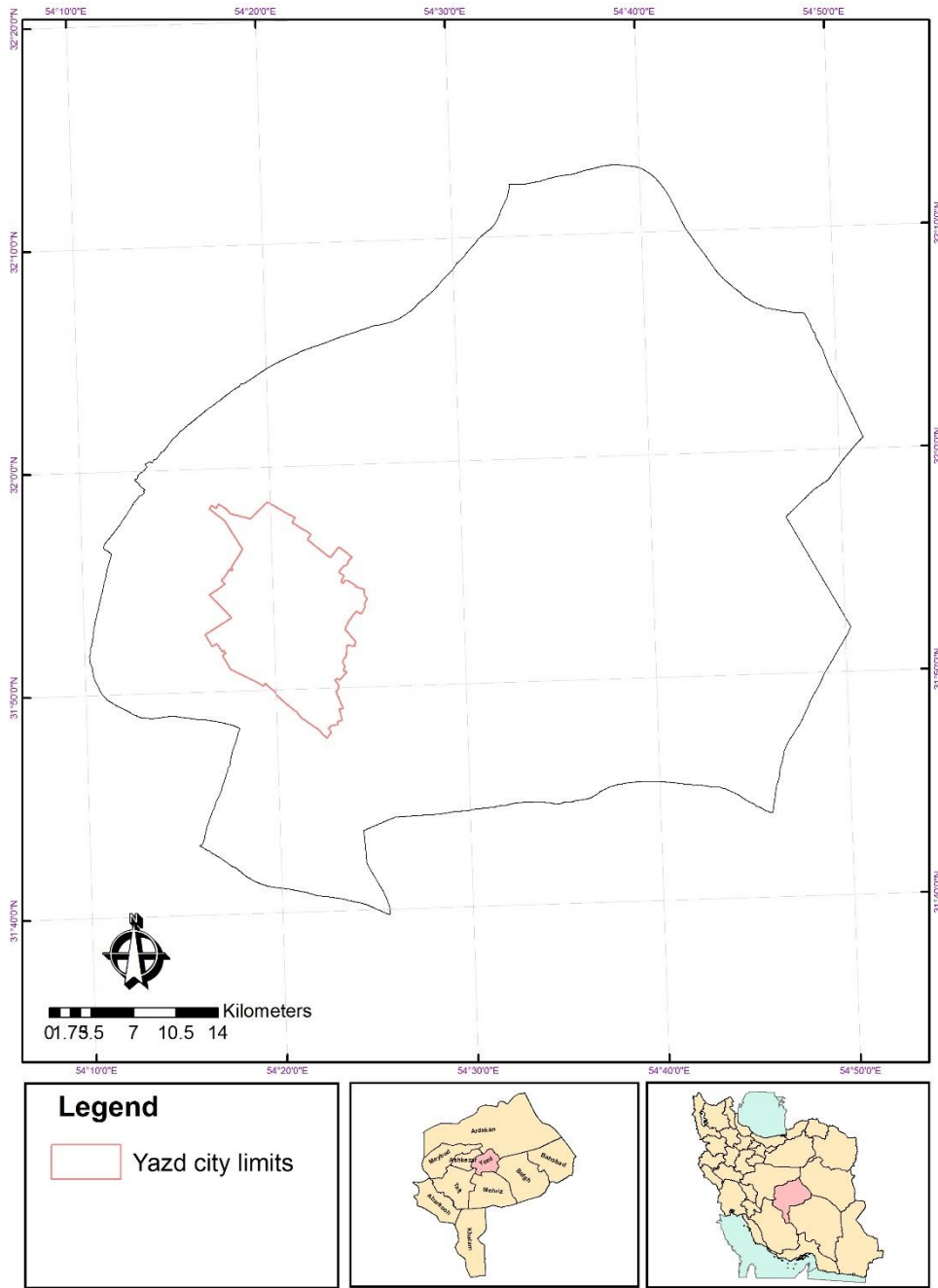
Figure 1. Study area
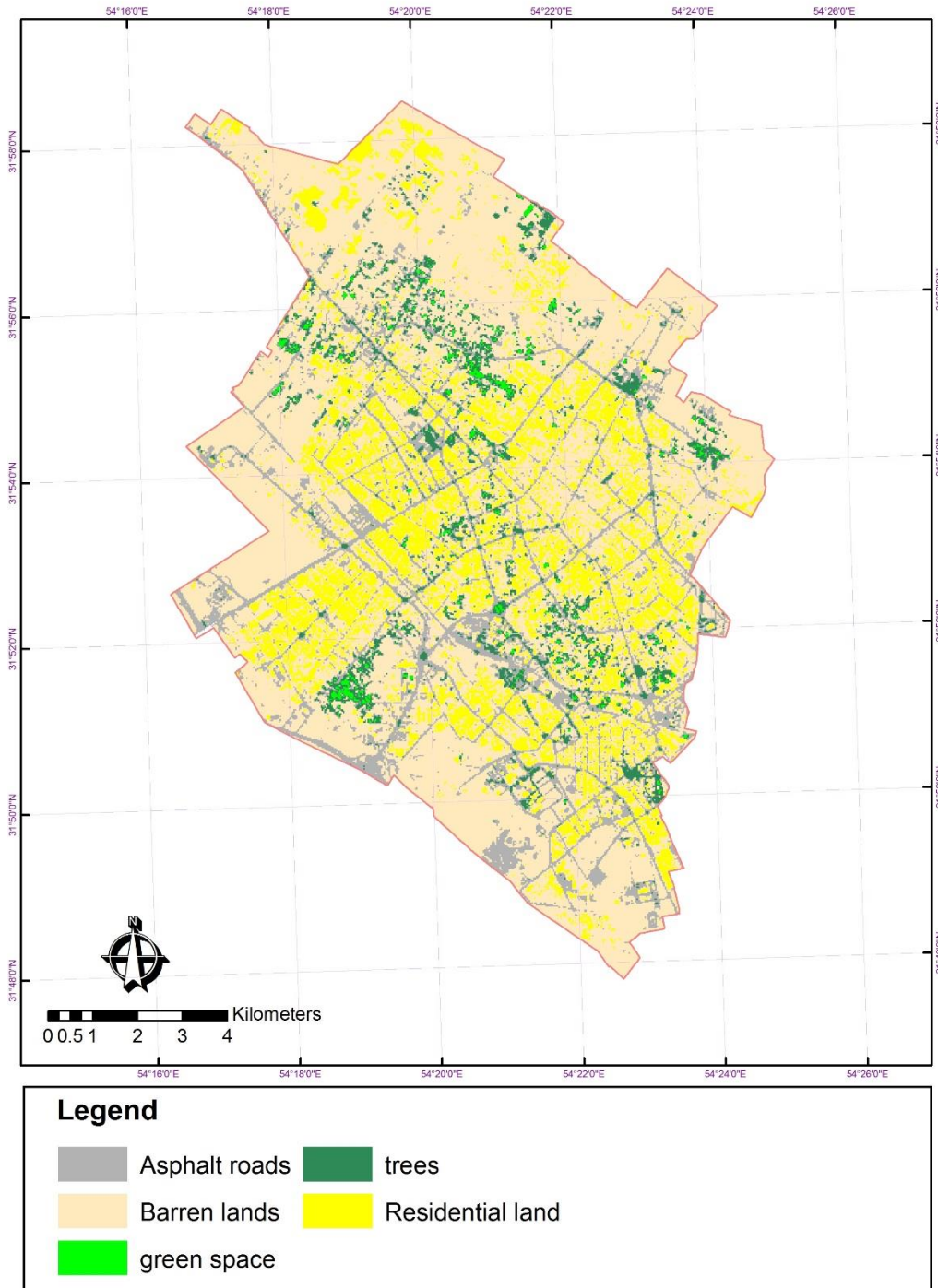
Figure 2. Land use map of Yazd city year 2013
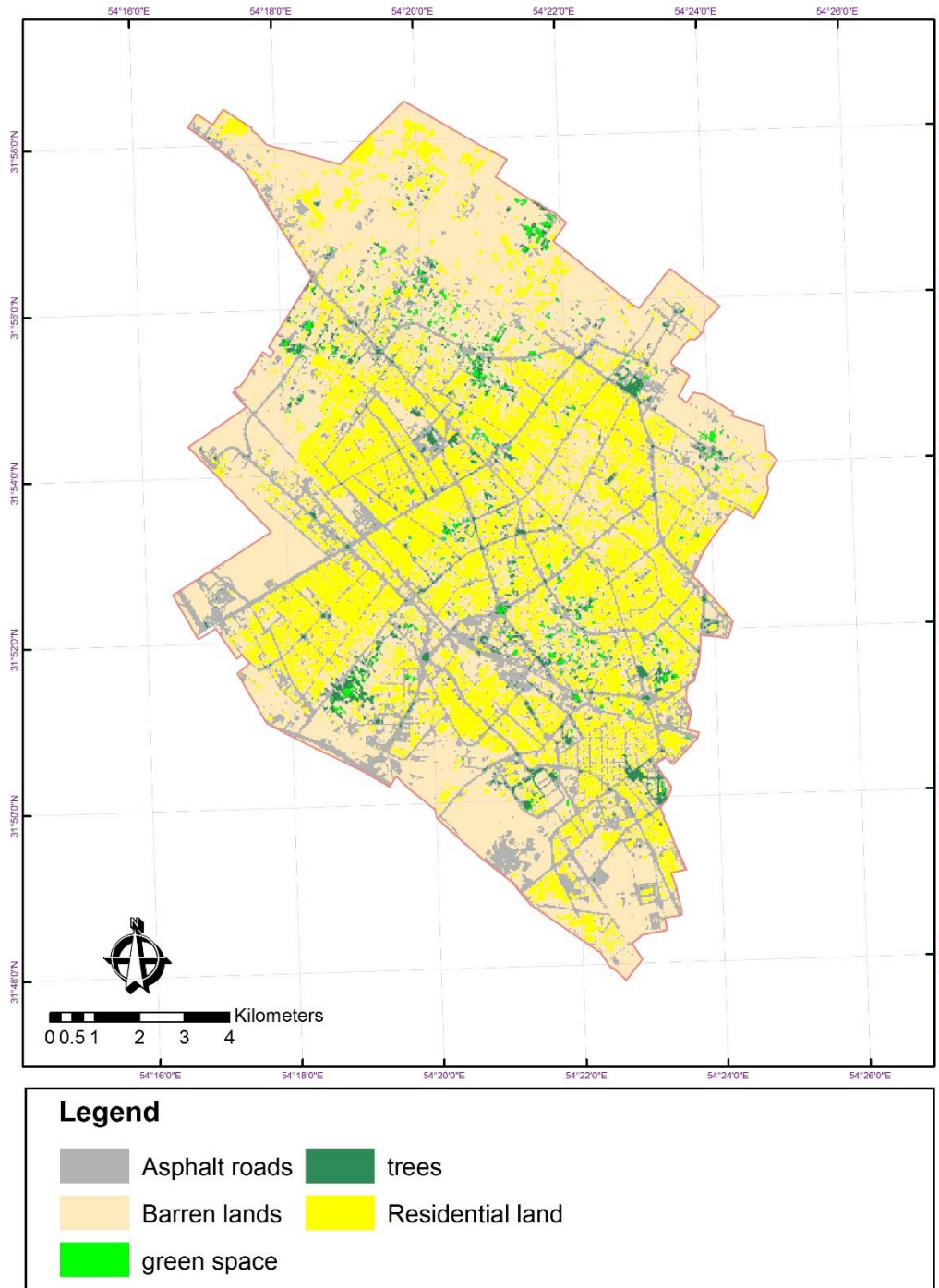
Figure 3. Land use map of Yazd city year 2018

The total area of the area for 2013 and 2018 was set at 14,995.2 hectares. Also, based on the interpretation of satellite images of the mentioned years, the area of residential land, green spaces, land, asphalt roads and trees in 2013 was 2934.72, 133.29, 9046.53, 2149.2 and 753.84 respectively hectares and for 2018 this

amount has changed to 4160.97, 168.12, 7748.1, 2654.64 and 285.66, which indicates an increase in residential lands, green spaces and asphalt roads, and reductions in dry land and trees.

Table 2. Land area based on satellite imagery in 2013 and 2018

Sensor	Residential land (hectares)	Green space (hectares)	Moor lands (hectares)	Asphalt roads (hectares)	Tress (hectares)
LANDSAT 2013	2934.72	133.29	9046.53	2149.2	753.84
LANDSAT 2018	4160.97	168.12	7748.1	2654.64	285.66

2.3. Satellite data

Landsat 8 launched on February 11, 2013, from Vandenberg Air Force Base, California, on an Atlas-V 401 rocket, with the extended payload fairing (EPF) from United Launch Alliance, LLC. The Landsat 8 satellite payload consists of two science instruments—the Operational Land Imager (OLI) and the Thermal Infrared Sensor (TIRS). These two sensors provide seasonal coverage of the global landmass at a spatial resolution of 30 meters (visible, NIR, SWIR); 100 meters (thermal); and 15 meters (panchromatic).

Landsat 8 instruments represent an evolutionary advance in technology. OLI improves on past Landsat sensors using a technical approach demonstrated by a sensor flown on NASA's experimental EO-1 satellite (Fig 4). OLI is a push-broom sensor with a four-mirror telescope and 12-bit quantization. OLI collects data for visible, near infrared, and short wave infrared spectral bands as well as a panchromatic band. It has a five-year design life. The graphic below compares the OLI spectral bands to Landsat 7′ s ETM+ bands. OLI provides two new spectral bands, one tailored especially for detecting cirrus clouds and the other for coastal zone observations (https://landsat.gsfc.nasa.gov).
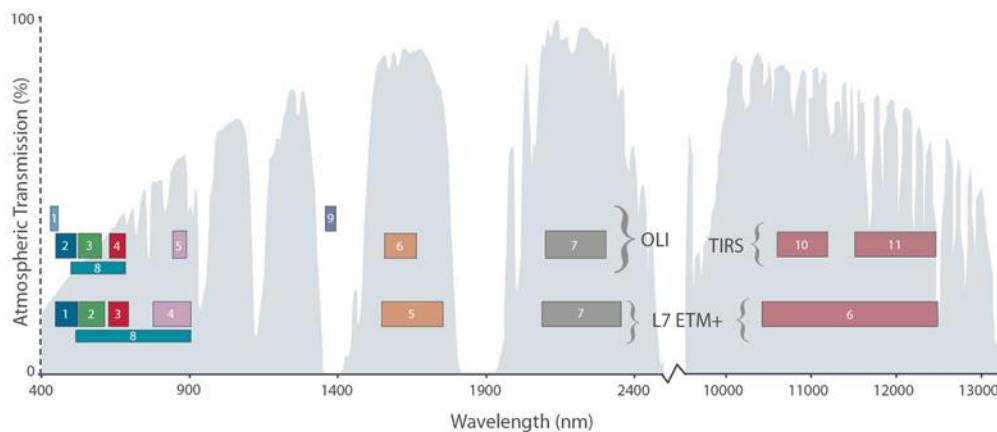
Figure 4. Wavelengths received in Landsat 7 and Landsat 8

Satellite images of the OLI Sensor, 2013 and 2018, downloaded on the USGS site in two dates of (16/07/2013 and 30/07/2018).

2.4. Methodology

The above satellite image is capable of displaying surface-to-surface effects to a 30-meter resolution, so that it is suitable for updating the effects of circular blocks, parks and green spaces in the passageways, as well as surveying changes in coverage and usage over the past years. This image was taken after processing operations which includes radiometric and geometric corrections. The classification method was used to classify the Spectral Information Diversion (SID). For this, 25 samples were collected for each class, 20 samples were taken for the classification map, and 5 samples were used for classification analysis.

2.4.1. Classification of Images by Spectral Diversion (SID)[1]

This method measures the difference between the probability distributions of two spectral characteristics. The SID criterion considers the spectral characteristic of each pixel vector as a random variable and uses its statistical probability distribution to calculate the spectral similarity between two spectral characteristics. In the metaphysical images, each pixel appears as a vector, and each spectral behavior curve, along with the reflection values associated with each wavelength which can also be represented by $X = (x_1, x_2 ... x_L)^T$, each component x_1 pixels of the band B_1 is obtained at wavelength λ_l. Thus, the vector of each pixel can be modeled as a random variable in an appropriate probabilistic space. Given the fact that the reflection values are always positive values, the probability P for x is calculated by the following equation (1), (Bigdeli et al., 2015).

$$P(\{\lambda_j\}) = P_j = \frac{x_j}{\sum_{l=1}^{L} x_l} \tag{1}$$

Where the vector $p = (p_1, p_2,..., p_L)^T$ is the probability vector of x. With these interpretations, each vector $x = (x_1, x_2,..., x_L)^T$ can be considered as an information source that follows its own statistics and describes the spectral variations of each pixel, such as the above equation. The probability vector of the pixel or other behavior curve $y = (y_1, y_2,..., y_L)^T$ is also calculated as $q = (q_1, q_2,..., q_L)^T$. According to the information theory, the self-information band l of the pixels or spectra x and y can be obtained using the following equation (2):

$$I_l(y) = -\log(q_l) \ , I_l = -\log(p_l) \tag{2}$$

Using the equations, the relative entropy x (3) and the relative entropy of y (4) are calculated as follows:

$$D(y||x) = \sum q_l D_l(y||x) = \sum_{l=1}^{L} q_l(I_l(x) - I_l(y)) \tag{3}$$

$$D(x||y) = \sum q_l D_l(x||y) = \sum_{l=1}^{L} q_l(I_l(y) - I_l(x)) \tag{4}$$

The sum of the above equations calculates the SID (5) criterion, which is defined as follows (Bigdeli et al., 2015):

$$SID(x,y) = D(y||x) + D(x||y) \tag{5}$$

In a simpler way, in this method, the entropy of each spectral characteristic is introduced as a measure of the measurement of information per pixel. If the discrepancy of this information is negligible between the

---

1. Spectral Information Divergence

two characteristics of the spectrum, it is understood that these two characteristics of the spectrum are not new to each other and are similar to each other.

2.4.2. Classification Accuracy Assessment

After extracting the land use map, it is essential to ensure the accuracy of the maps. There are different methods for assessing the accuracy of the classification. In this project, the general accuracy and kappa coefficient method were used based on comparing the map extracted from satellite data with ground-based information such as field observations, aerial photographs, existing maps and expert knowledge.

Table 3. Classification of error for images of 2013 and 2018

Desired year	Overall accuracy	Kappa coefficient
2013	86.48	0.82
2018	92.30	0.89

3. Results and Discussion

3.1. Identify the Extent of City Expansion and Changes in Green Space and Land to Urban Use

Since one of the objectives of this research is to investigate the extent of the expansion of Yazd, the amount of green space and land changes to urban construction will be determined using the technique of discovery of changes. The built-in user is comprised of buildings and streets. The changes mentioned above are listed in Table 4 over the period 2013 to 2018. Based on this table, from 2013 to 2018, 285.84 hectares of green space has been built into the use of the city. In addition, over the same period, 2237.13 hectares of moor lands have been made into use. The area of use omit in 2013 has been 5083.92 hectares, while in 2018 this area has reached 6815.61 hectares. Based on the data extracted from the statistical maps of the management and planning organization of the area of Yazd city is 14995.2 hectares. But the urban boundary covers not only the built areas, but all the land that lies within the municipality's boundaries of governance (including those that are considered for future growth of the city). In addition, green space in the city is not considered as built-in urban use.

Table 4. The amount of green space and land use change for urban use in 2013 to 2018 (hectares)

User built in 2013	**5083.92**
Change green space to urban use	285.84
Change of moor land to urban use	2237.13
Total area added	2522.97
Change lands built to Bayer	762.21
Change lands made to green space	29.07
User built in the city in 2018	**6815.61**

As indicated in the map guide, the sections marked with yellow color are land-use change to urban use, and green points are the change of the green space to urban use.
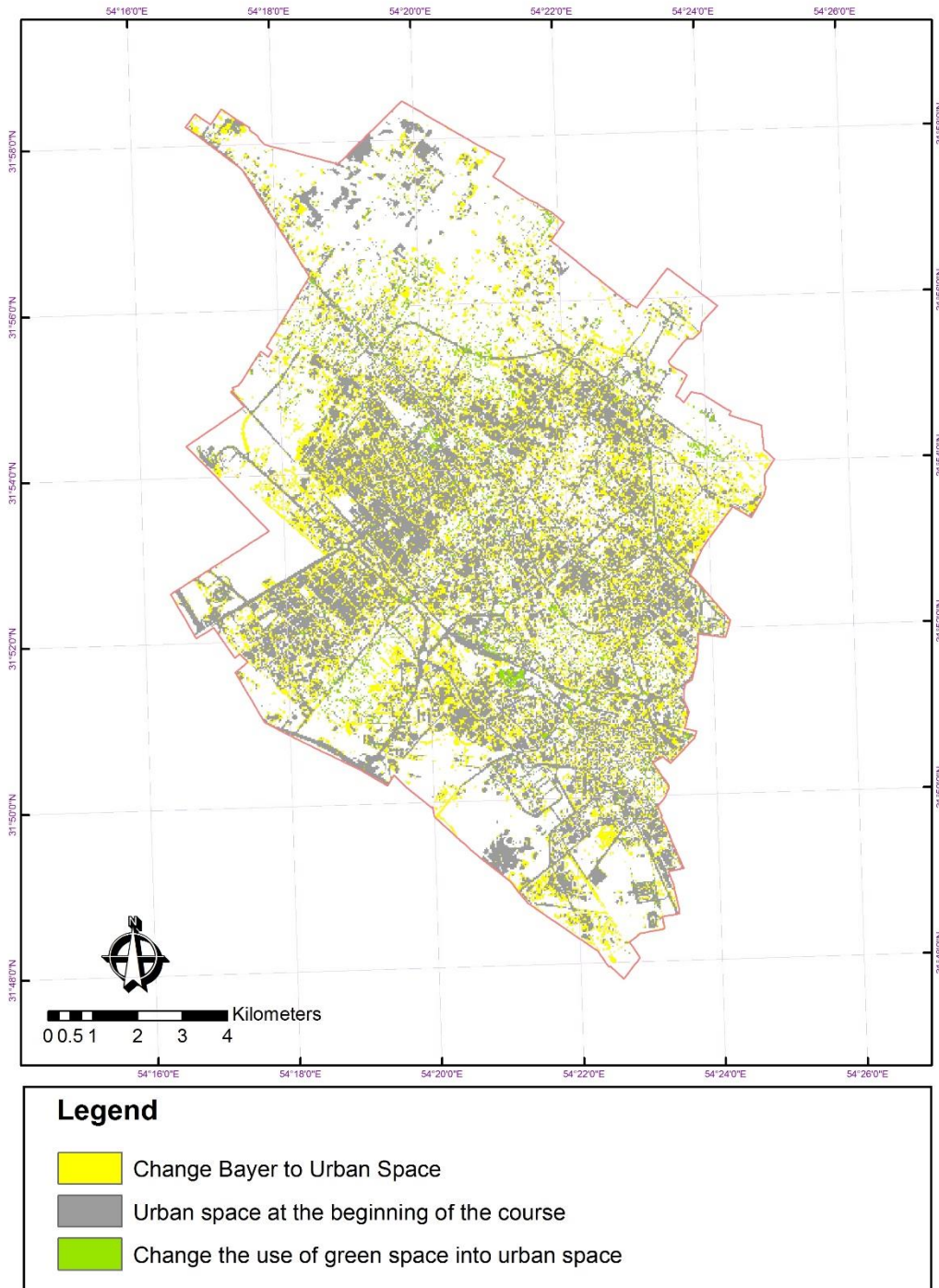
Figure 5. Land-change and green space for urban use in the period 2013 to 2018

3.2. Identification of the Main Directions of the Expansion of Yazd in 2013 to 2018

In the previous section, the extent of the city expansion of Yazd in dry land and green space based on the results of discovery of changes was presented in general. However, determining the extent of city expansion in different geographical directions is also one of the issues that can be useful for understanding the main

directions of city growth in the future. In this section, using the regional statistics method, the total amount of development of the city as well as the extent of the city expansion in dry land and green space will be determined in different geographical directions. The way this method works is that the target area is divided into several regions, and then different statistical information is extracted for each region.

To determine the extent of the city expansion in different directions, the scope of surveillance should be divided according to geographic directions into several regions. First, the city's geometric center was originally built for the areas built in 2013, followed by 16 areas in the north-central, north-eastern, northeastern, eastern-central, eastern margin, south-east central, southeastern margin, south-central, southern margin, south-west central, southwestern margin, west central, western margin, north west central and northwest margin with 45 degrees. The zoning and distribution of the changes are shown in Figure 6.

The extent of the expansion of the city in different geographical directions is given in Table 5. According to the data of this table, during the period 2013 to 2018, the highest growth has been in the central region in the east which was 266.85 hectares and the south was 248.31 hectares and in the southern marginal area 257.49 hectares. On the other hand, the least growth was observed in the central region in the south east due to the existence of a worn-out texture of 178.2 hectares and in the marginal area in the north-east due to the fact that the area of Yazd was 31.32 hectares. The situation of the city expansion in the moor lands in different directions is as follows: In the central region, the largest changes of moor land use to the urban land in the east were 254.16 hectares and in the marginal area of the south to 245.25 hectares and the lowest changes in the central region in the south-east were 146.97 hectares and in the marginal area in the north-east were 28.08 hectares.

The situation of the city expansion in green areas in different directions is as follows: In the central area, the greatest amount of changes of green spaces to urban lands in the north to 50.22 hectares and in the marginal area in the north to 25.2 hectares and the least amount of changes in the central sector in the west were 4.86 hectares and in the marginal sector in the west were 1.62 hectares.
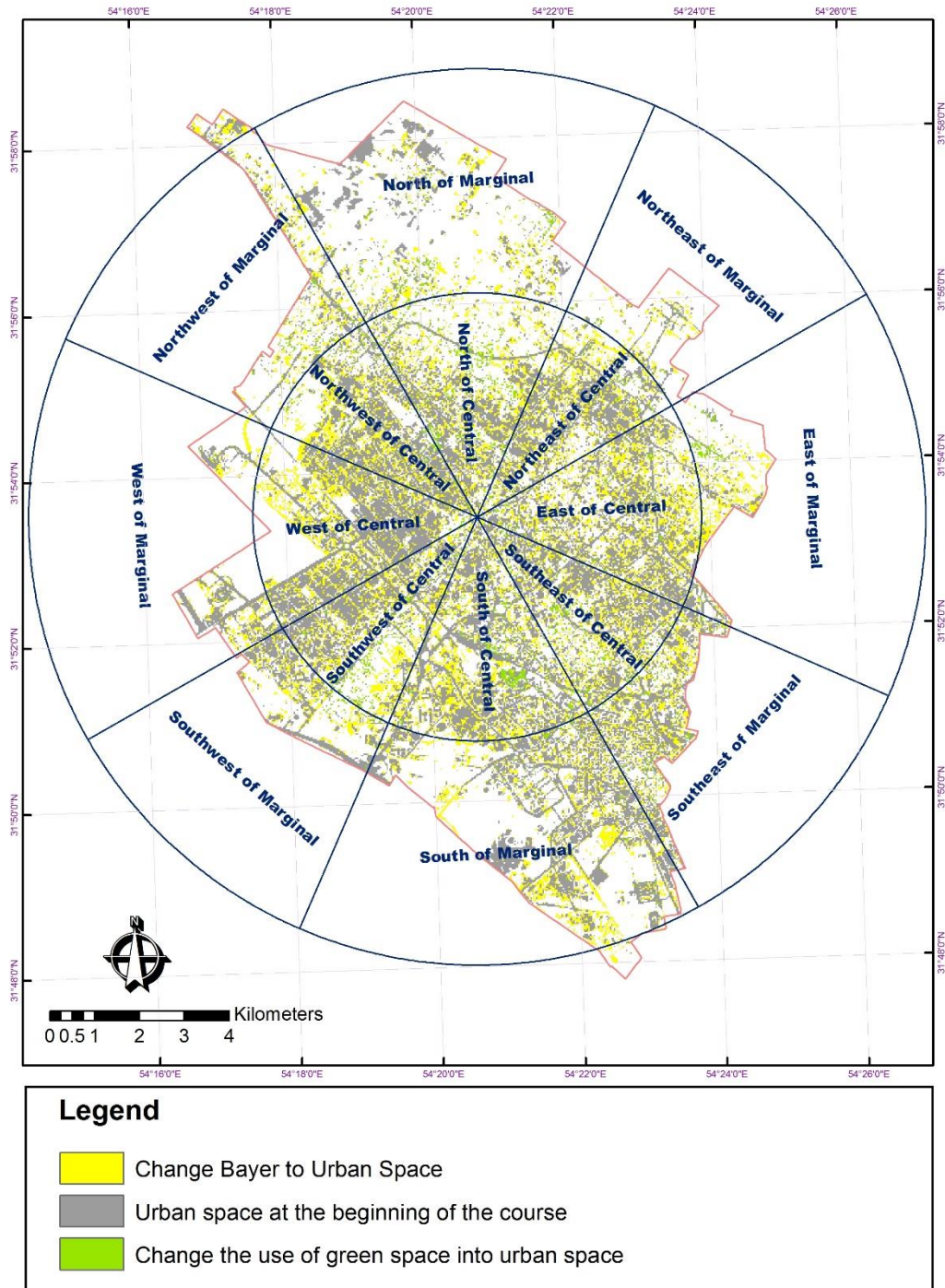
Figure 6. Expansion of the city in different geographical directions from 2013 to 2018

Table 5. Expansion of the city in dry land and green space (hectares)

Geographic directions		Change of moor land to urban use	Change green space to urban use	The overall expansion of the city
Central	North	173.16	50.22	223.38
	Northeast	158.13	10.89	169.02
	East	254.16	12.69	266.85
	Southeast	146.97	31.23	178.2
	South	209.7	38.61	248.31
	Southwest	153	28.35	181.35
	West	211.86	4.86	216.72
	Northwest	174.71	16.2	190.91
Marginal	North	116.19	25.2	141.39
	Northeast	28.08	3.24	31.32
	East	63.63	13.14	76.77
	Southeast	115.2	18.18	133.38
	South	245.25	12.24	257.49
	Southwest	66.69	6.3	72.99
	West	49.68	1.62	51.3
	Northwest	71.73	13.32	85.05

4. Conclusion

The aim of this study was to investigate the expansion of Yazd city using satellite imagery and GIS techniques and remote sensing. Many studies have been done in the field of land use maps and their changes using remote sensing data in different cities. However, the review of studies carried out in relation to the expansion of Yazd shows that satellite imagery in growth studies and the expansion of this city is less useable.

The results of this research show that from 2013 to 2018, the amount of 2237.13 hectares of urban land has been urbanized. In addition, during this period, 285.84 hectares of green space has had urban use. This is if the user area made in 2013, 5083.92 hectares, has reached 6815.61 hectares in 2018. In the same period, 762.21 hectares of land were built in urban areas changed to moor and 29.07 hectares of urban lands made to green space.

The main directions of the expansion of the city of Yazd in the period 2013 to 2018 were in the central sector, respectively, in the east and south and in the marginal south. In the central part of the East and in the marginal sector of the South, there are the most significant changes in the land use change in urban areas; while in the central northern sector and in the marginal sector, the north has turned green space into more urban land uses.

The important and spectacular observation of the comparison of satellite images in 2013 and 2018 can be seen in the change of the area of trees from 753.84 hectares to 285.66 hectares. As trees are seen as key ecosystems which can be found in reducing air pollution, noise pollution and wind intensity, as well as preventing soil erosion, and due to the lack of permeability of urban green space, results in damage to urban green space, negative environmental consequences such as increased environmental pollution and negative social consequences, such as reduction of pleasure and joy of citizens.

Comparison of the change of green space and land to urban use indicates that in the central sector in the east and south, the expansion of the city in the green area is more than land. But in the marginal area of the northern, northwest, west, southwest, south, east and north-east directions, the expansion of the city has been more inferior to green areas.

The horizontal expansion of the city has left many lands in the city's center and the worn-out texture of the city center empty. Only in the marginal area to the south-east of the city expansion the moor lands was more than green space.

It is important to note that the growing centers are mainly in areas where most of the greenery is located, and if the city continues to expand in these directions, much of the land will have urban land use. According to the mentioned points, the results and maps presented and the satellite images of Yazd city, it can be concluded that the most suitable direction for the future growth of this city is the restoration of the worn-out texture. Therefore, in order to prevent the transformation of green space into urban land use, it is possible to limit the expansion of the city and, instead, direct the growth of the city into a worn out and empty territory.

References

Ammanpour, S., Kamelifar, M., & Bahmani, H. (2016). An analysis of land use change in metropolitan cities using satellite image analysis in the ENVI environment (case study: Ahwaz metropolis). *Quarterly Journal of Geographic Information, 26*(102), 139-150.

Bigdeli, B., Valadan zoj, M., & Maghsoudi Mehrani, Y. (2015). Evaluation of OLI Sensor Images Potential in the Separation of six Iranian Wheat Varieties Differentiation using Spectral Library. *Geographical Information Research Journal (Sepehr)*, *24*(93), 5-26.

Eghbali, N., & Ziari, Y. (2007). Analyzing the application change of urban lands by using satellite images Case: Tehran area 6 of district one (1358-83). *Geographic Quarterly of Territory*, *3*(10), 1-8.

Heydarian, P., Rangzan, K., Maleki, S., & Taghizadeh, A. (2013). Monitoring land use change using comparison method after Landsat satellite images (case study: lands of Tehran). *Remote Sensing and Geographic Information System*, *4*(4), 1-10.

Https://landsat.gsfc.nasa.gov/landsat-data-continuity-mission

Khezri Ahmadabad, et al. (2017). Monitoring Land Use Change Using Satellite Images and RS & GIS Techniques (Case Study: Baharestan), *Geographic Quarterly Territory*, *24*.

Mehdi Hassan, M. (2017). Monitoring land use/land cover change, urban growth dynamics and landscape pattern analysis in five fastest urbanized cities in Bangladesh. *Remote Sensing Applications: Society and Environment*, 69-83.

Rabiei, H., Zeaiean, P., & Alimohammadi, A. (2005). Detection of Land Use/Cover Changes of Isfahan by Agricultural Lands around Urban Area Using Remote Sensing and GIS Technologies. *Quarterly Journal of Human Sciences*, *9*(4), 41-54.

Sahle Kibert, K., Marohn, C., & Cadisch, G. (2016). Assessment of land use and land cover change in South Central Ethiopia during four decades based on integrated analysis of multi-temporal images and geospatial vector data. *Remote Sensing Applications: Society and Environment*, 3, 1-19.

Zanganeh Shahraki, S., Kazemzadeh, A., & Hashemi Darebadam, S. (2014). Time-based analysis of the physical expansion of Mashhad city and monitoring of land use changes. *Geographical Research of Urban Planning*, *2*(4), 483-499.

.

The Need for Environmental Assessment and Field Surveys in Landfill Location Studies (Case Study: Yazd City)

Sara gilvari[a*], Alireza Mazloumi Bajestani[b], Seyed Abolfal Kashfi[c], Alireza Sarsangi Ali Abad[d]

[a] MSc of Environmental geology, Mahabad Branch, Payame Noor University, Iran

[b] Department of Geology, Payame Noor University, Tehran 19395 4697, Iran.

[c] Ph.D. student of Environmental geology, Shahroud Branch, Islamic Azad University, Shahroud, Iran.

[d] Ph.D. student of GIS and Remote Sensing, University of Tehran, Iran

Abstract

The need for a comprehensive management of sustainable environmental development is more than ever due to the growth of population and more waste production. In order to achieve the goals of sustainable development, environmental assessment before, during and after each project is needed. The purpose of the environmental impact assessment is to ensure that managers and experts meet the goals set in a project in accordance with government and environmental regulations. The first step towards achieving this goal will be exploring the study area. In this research, the Leopold matrix was used for environmental assessment of landfill location in Yazd. Environmental assessment was done on the problems resulting from landfill on the environment and living organisms of the area in the environmental assessment area by visiting the field of the current landfill site of Yazd. The total score of the results of the Leopold Environmental Assessment Matrix related to the current landfill site was -214. Therefore, it is possible to carry out management solutions to improve the status of the current landfill. By performing location studies using the hierarchical analysis method, zone one was designated as a suitable landfill site. The soil permeability gradient curve of the selected region was prepared and the soil type of this region was clayey silt. Which will be suitable for landfill.

Keywords: environmental impact assessment, hierarchical analysis, landfill, Yazd city.

---

* Corresponding author Tel: +98- 9130977801.
Email address: sara.gilvary@yahoo.com.

1. Introduction

Environmental impact and environmental pollution caused by solid waste management is a global and inclusive issue in the cycle of pollution of water, air and soil. This mismanagement in developing countries is more harmful to the environment and human society (Ferronato and Torretta, 2019). In order to determine the best choice with the highest profitability and efficiency, the evaluation is used as a method for assessing the environmental impacts of engineering projects. Environmental impact assessment predicts possible potential positive and negative results of the project on the environment before and during the project implementation. This assessment identifies a negative impact management method. Consequently, experts and decision makers will be guided to start or continue the project. The ultimate goal is to decrease environmental pollution so that its adverse effects on plant species, animals and human health are reduced. Environmental impacts of the implementation of the engineering-sanitary landfill project on the parameters of the surrounding physical environment, directly and indirectly, can be separated in two phases including construction phase and exploitation phase. The effects of activity in the construction phase on the physical environment about activities in the short term are irreversible and immediately after the completion of this phase, the exploitation phase will last for about 20 years, which will also have an impact on the environment around the project (Hafezi Moghadas and Hajizadeh, 2007).

These effects whatever they are, there are efforts to reduce or eliminate them in order to achieve the least negative impact on public health, the least negative impacts of the site on the environment, the highest level of service and the lowest cost for users (Yao, 2013).

This issue should be considered that the final selected site is not capable of answering all the problems. Therefore, this site should be less damaging to its environment than other sites. In other words a special tool should be used to identify the negative effects of the project. There are many ways to determine the priority which has the characteristics and properties that experts have considered. Therefore, there are several methods for assessing the environmental impacts that require a variety of technical and information layers to use and analyze them. The best and most practical methods should organize a large amount of data, summarize the data in a smaller format and display raw data related to each other. The spatial information system provides the spatial information necessary for users to evaluate the site. In other words, the system will be a useful tool in environmental assessment of management and decision making (Zamorano et al., 2008).

Kapilan and Elangovan (2018) did a research titled "Selection of the potential landfill for solid waste disposal using GIS and multi-criteria decision analysis" in Coimbatore in India. The model used for weighing in location using geographic information system was a hierarchical analysis method. The data layers used in multi-criteria decision analysis included population density, underground water depth, drainage density, slope, soil texture, geology and geomorphology. By applying the final weight of each layer by this method, seventeen locations in this area were identified. By reviewing through the field survey of the area, eventually, four areas were identified as suitable for landfills.

Jafari et al. (2015) did a research titled "The final choice of landfill site in Ardebil based on methods similar to the ideal option and environmental impact assessment". The model used for weighing in location using geographic information system was a hierarchical analysis method. After creating a final map of waste landfill by conducting field visits from designated and collecting necessary information from these places, four suitable landfills were placed in the appropriate category. Then, to determine the most suitable location using a method similar to the ideal option and the Leopold matrix method these four places were evaluated. The results of the assessment by using two methods indicated that the prioritization of the options with a method similar to the ideal option is equivalent to prioritizing options by assessing the environmental impacts of the Leopold Matrix and the first option is the first priority. They finally said since the groundwater level in this place is low, the depth of soil is high and access to borrow pits is easier, urban waste disposal in a trench method would be more appropriate at this location.

Gilvari et al. (2015) conduct an investigation titled "Environmental assessment (EIA) and optimum locating of solid municipal waste landfill using GIS, SAW method and the Leopold matrix (case study: Yazd city) ". Required information layers including geology, land use, distance from city boundary, slope,

distance from road, vegetation, permeability and hydrology were provided to weighting using simple additive weighting. To determine the proper burial location three stages were carried: location of susceptible areas of landfill, field visit to study the characteristics of susceptible areas and environmental assessment using the Leopold matrix to rank the areas and select the optimal location. Initially, the final map of the appropriate places for landfill was classified, and four locations were in the appropriate category for landfill dumping. Then, field visits were conducted from selected areas in order to confirm the locations according to limitations of their ability to landfill. Finally, using Leopold Matrix method, region 1 was identified as the optimum location for sanitary-engineering waste landfill. Moreover, using this matrix, it was found that the greatest environmental impacts of landfill construction in the study area are physical effects which the construction and operation of landfill can create in the area and adjacent lands. Therefore, it takes a lot of care to run and operation landfill to minimize these effects.

2. Materials and Methods

2.1. The Study Area

Yazd city, the center of Yazd County, with a total area of 107 square kilometers, is located in the center of Yazd province. The city is located on the coordinates of 54 ° and 9′ to 54 °, 31 ′ east longitude and 34 °, 31 ′ to 32 °, 10′ north latitude. In this study, the radius of 30 km from the legal boundary of Yazd city was considered (Figure 1).
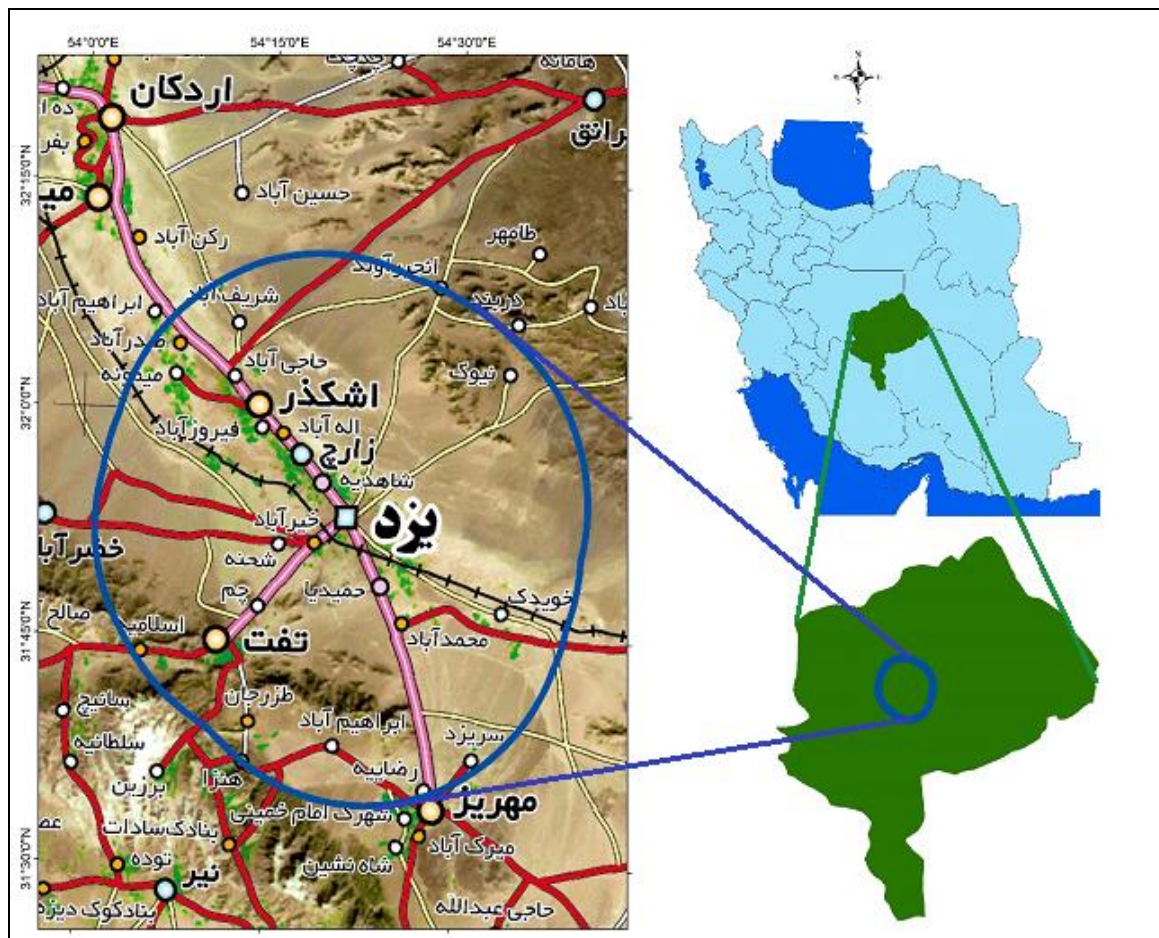

Figure 1. Location of the study area in the country and provincial divisions

2.2. Methodology

Initially, the environmental assessment of the current landfill site of Yazd city was done using the Leopold matrix method and then using the hierarchical analysis method in the arcgis10.9 software environment. The final selected area was evaluated by field surveys and soil permeability tests. The first step in assessing environmental impacts is studying the status of the study area, including environmental elements influenced by the project as well as the target chain which different levels of pollution have different effects on it (Zamorano et al., 2008; Butt et al., 2008).

For this reason, the physical, biological, economic and social parameters and in the next step, the effects of the project on each of these parameters will be investigated. One of the things which can make the landfill undesirable is the stench of waste in the landfill site; climate changes will affect the intensity of odor (Naddeo et al., 2018).

Table 1 shows the environmental impacts on the landfill site during the construction and operation phase on the physical environment (Farhadi and Hafezi Moghadas, 2006).

Table 1. The environmental impacts on the landfill site during the construction and operation phase on the physical environment (Farhadi and Hafezi Moghadas, 2006).

Effects	Construction stage	Operation stage
Effects on the biological environment	• The probability of invading some non-native species of plants due to destruction of vegetation cover of native species and the cultivation of non-native species • Destruction of the natural habitat of animals living there • Possibility of few changes in wild life	• Effects on plants due to gasses from the landfill site • The probability of increasing non-native plant species • Destruction of wildlife habitats due to land occupation • Reduction of animal population due to the movement of machinery
Air pollution	• Partial increase of air pollutant gases • Increasing suspended particles due to the movement of machinery	• Gas production from waste • Production of organic compounds from waste
Pollution of water resources	• Changing the channel of the area causing changes in the hydrologic regime • Making bad changes in the water due to the construction of the production workshops which are resulted during rainy season and runoff	• pouring and spread of pollutants, industrial and oil waste along roads • Oil and fuel leakage and distribution on the surface of the soil and entry into groundwater resources
Pollution of soil resources	• Destruction of soil at the site of construction workshop • Destruction of soil for leveling the path of the road • Excavation in the area to supply borrow soil • Leakage of leachate into soil	• Distribution of solid waste on the soil • Leakage of leachate into soil • Soil subsidence due to lack of waste consolidation
Noise pollution	• Noise pollution caused by Vehicles traffic • Noise pollution due to drilling tools and equipment	• Noise pollution due to the operation of load-carrying devices such as forklift and trucks

One of the methods of environmental assessment is the use of the two-dimensional and matrix comparison method. Matrices are, in fact, two-dimensional checklists which the project activity is based on an axis (horizontal axis) that effective activities are in the process of disposal and landfill. On the other axis (vertical axis) is the effects of project activity on the physical, social and biological environment around the selected

area (Canter, 1996). This method is used to identify cause-and-effect relationships, between specific activities and effects, and it provides a special contribution to further studies. The most common type of matrices is the Leopold matrix (Farhadi and Hafezi Moghadas, 2006). Each unit of the matrix represents two values of the relationship between the activities and the project as a positive or negative number. Below the fraction of each unit of the cell is the magnitude of the effect and its value varies from 1 to 5 (low to high). At the top of the fraction of each unit of the cell is the value of the cell and its value varies from -5 to +5 (harmful to useful) (Leopold, 1971). The matrices only represent the direct effects and emphasize biophysical issues. In other words, the timing or duration of the impact period is not mentioned. In this method, the best location with the highest degree of importance and positive intensity of the layers is determined (Shariat, 2000). The expert, by visiting a field of the desired areas, determines the severity and significance of the effects in the scoring of each of the factors in the candidate regions. Zoning and locating susceptible areas for waste dumping using hierarchical analysis technique were done which were established based on the three principles of analysis of the problem, the creation of a paired comparison matrix together with determining the relative weight of the priority of the variables and achieving the real value of the weights after determining the adjustment rate. Firstly, for each of the information layers, the comparison matrix is formed. A higher score indicates the value and importance of the layer in the locating process (Gilvari et al., 2016). A higher score indicates the value and importance of the layer in the locating process and the value of each layer is determined by the other (Guiqin et al., 2009).

3. Results and Discussion

The current landfill site of Yazd city is located at km 4 Azadegan Cement Road, 4 km from the legal border and 11 km from the city center of Yazd city. This place has been used for this purpose for at least 45 years ago. This location is located in the geographical coordinates at 31º55 ′ 55 ″ on the north latitude and 54º25′59″ on the east longitude, in the northeast of Yazd. Figure 2 shows the current location of the landfill site of solid waste in Yazd.
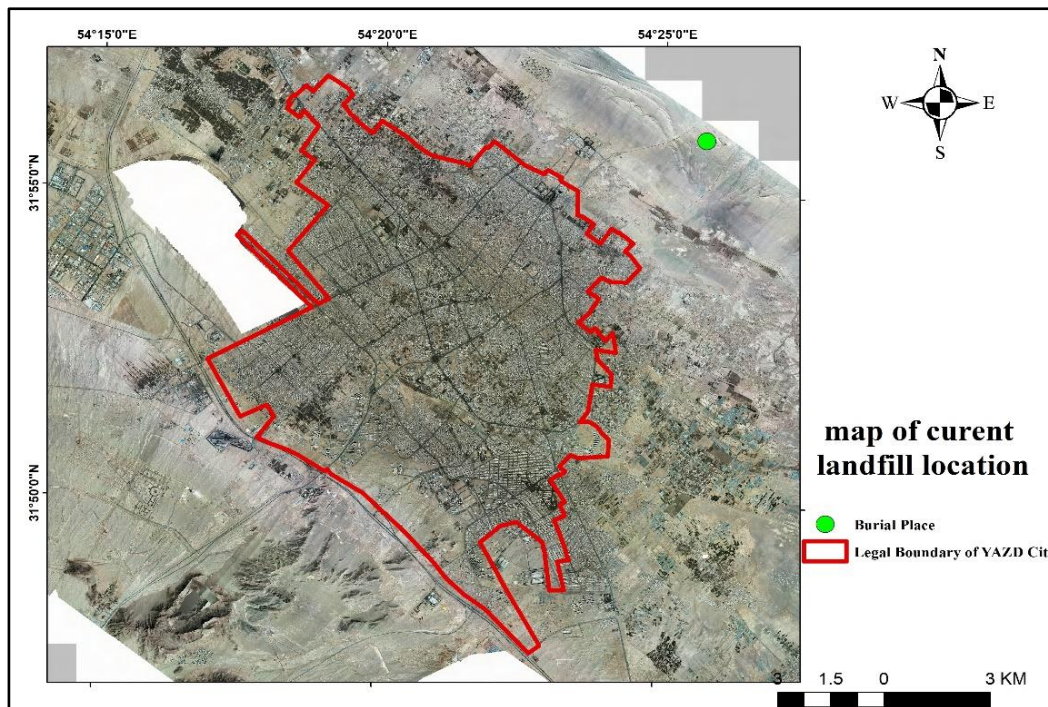

Figure 2. Current location of the landfill site of solid waste in Yazd

The problems encountered in field visits and surveys include:

- Unusual and non-engineering waste landfill (The burial is carried out continuously for years without daily coverage without compression of the layers, which is likely to cause leachate leakage, gas leakage and slippage in the landfill location),
- No specific scheduled landfill (landfill in different places in the last 45 years),
- Infectious waste landfill and construction and demolition waste beside urban waste near the border and without proper burial coverage,
- Urban sewage drainage near the municipal landfill and becoming sewage lake,
- Absence of landfill fence,
- The presence of unlicensed separators that search inside infectious and urban waste,
- Presence of birds (rare species such as Eagle and Hawk) and wild animals that feed on garbage,
- The landfill around the road is sometimes done and the privacy of the main road is not met,
- High distances from the current landfill site (about 8 km) from the composting plant,
- Bad smell, mosquitoes and flies that it annoys passengers who cross the road because of proximity to the main road,
- Non-separation of waste for the purpose of consuming garbage fuel and a composting plant,
- Absence of observation wells around the landfill site to investigate the risk of contamination caused by leachates,
- Extreme rainfall, though short-lived, causes leachate and animals feed on garbage in relation to it.

Table 2 shows the Leopold matrix for assessing the environmental status of the current solid landfill site in Yazd.

Table 2. The Leopold matrix for assessing the environmental status of the current solid landfill site in Yazd (Gilvari et al., 2014).

Total	Leakage of leachate	Methane gas leakage	Traffic machines	Extraction of loan resource	Daily burial	Construction of landfill infrastructure	flatten	Excavated	Construct Access road	Environmental impact		
-140	-3 / 2				-4 / 4					Soil pollution	soil	Physical
							-4 / 3	-4 / 3		Soil erosion		
	-3 / 3				-3 / 3					Surface water quality	water	
	-4 / 4				-3 / 4					Groundwater quality		
				-4 / 3			-4 / 3	-4 / 3		Dusty production	air	
		-4 / 3								Creating an unpleasant odor		
-60					-2 / 1		-1 / 1	-1 / 1	-2 / 1	plant species	environment	Biological
			-3 / 2							Animal species		
	-4 / 3	-4 / 2			-3 / 2					Public health	Human	
		-3			-4					Sickness (by animal)		

	2			4								
						1 3	1 1			1 2	Create a job	economic	social – economic
										-1 1	Agriculture		
						-1 1	1 1				Animal husbandry		
						-4 1	1 1			1 1	Land values		
-14						-2 1	1 1			1 1	Future development	social	
		-2 1									Creating traffic		
						-3 3					Beauty Landscape		
						-2 2					Area tourism		
		-2 1									Increased accidents		
-214			Total results of Leopold's environmental assessment matrix related to the current burial site									

In this study, ten layers of information including geology, topography, soil permeability, land use, distance from the city, vegetation, the distance from the main road, the distance from the power lines, the quality and depth of the groundwater have been used. Depending on the extent of the impact on locating these layers are classified by the expert choice software in the software environment of arcgis10.9 into four classes including: highly suitable (class 1), suitable (class 2), relatively suitable (class 3) and inappropriate (class 4). Figures 3 to 12 represent the map of classification of these layers in Yazd city.
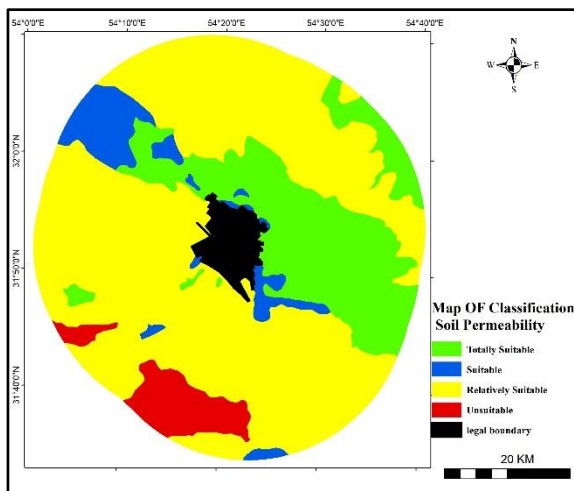
Figure 3. Map of classification layer soil Permeability of the study area (Gilvari et al., a.2019).
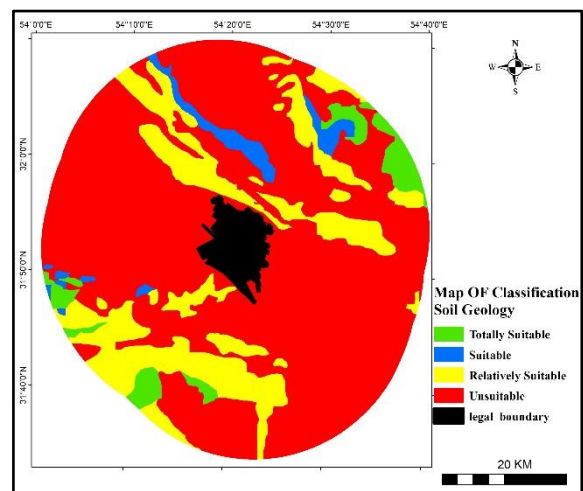
Figure 4. Map of classification layer Geology of the study area (Gilvari et al., a.2019).
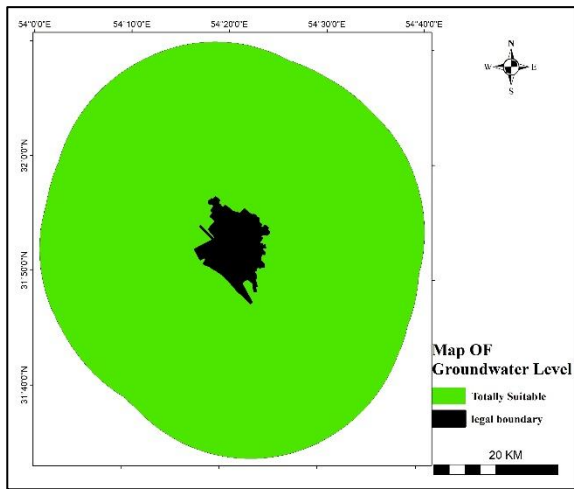
Figure 5. Map of classification layer Underground water depth of the study area (Gilvari et al. a.2019).
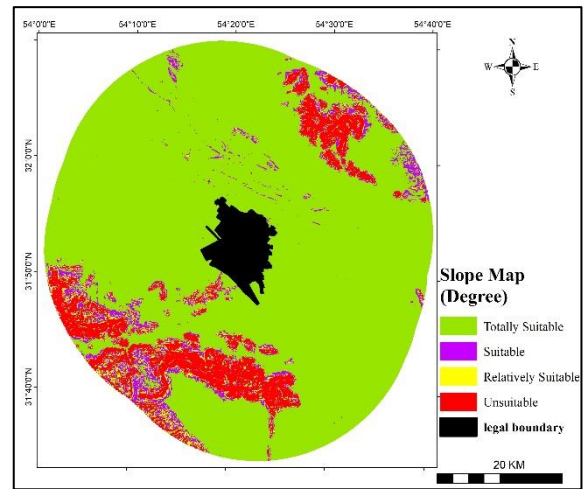
Figure 6. Map of classification layer slope of the study area (Gilvari et al. a.2019).
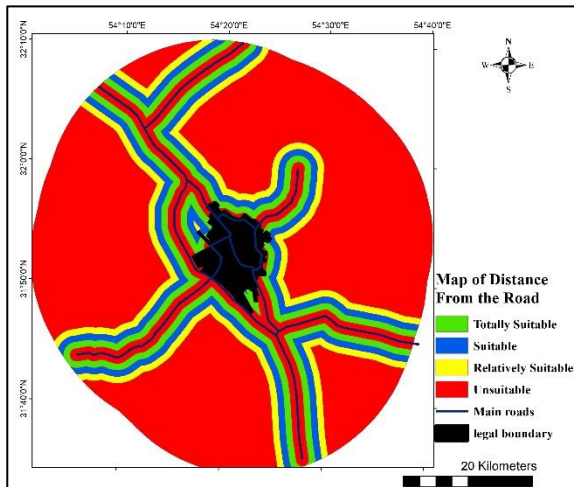
Figure 7. Map of classification layer Distance from the road (km) of the study area (Gilvari et al., a.2019).

Figure 8. Map of classification layer Distance from the city (km) of the study area (Gilvari et al., a.2019).
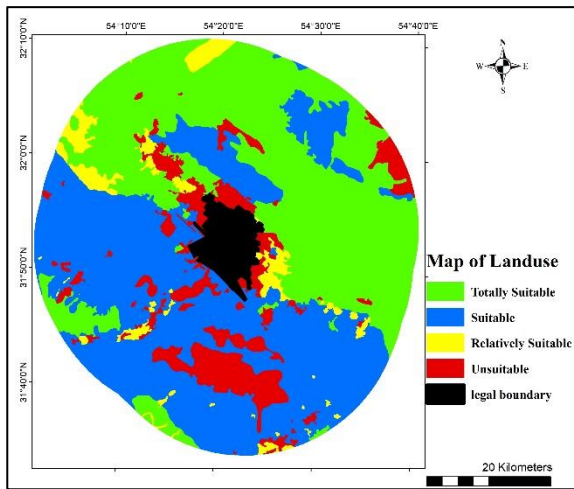
Figure 9. Map of classification layer Land use of the study area (Gilvari et al., a.2019).
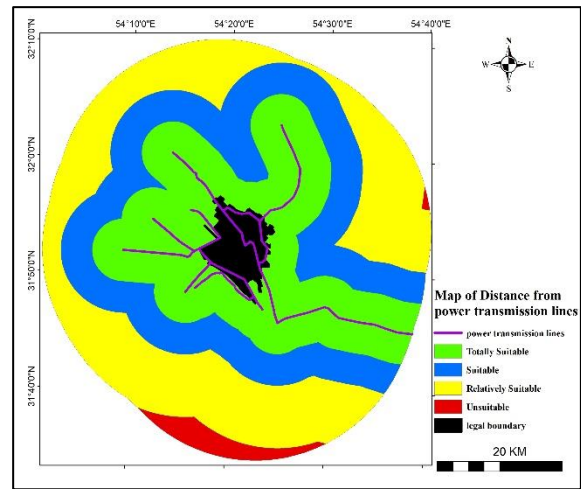
Figure 10. Map of classification layer Distance from power transmission lines (km) of the study area (Gilvari et al., a.2019).
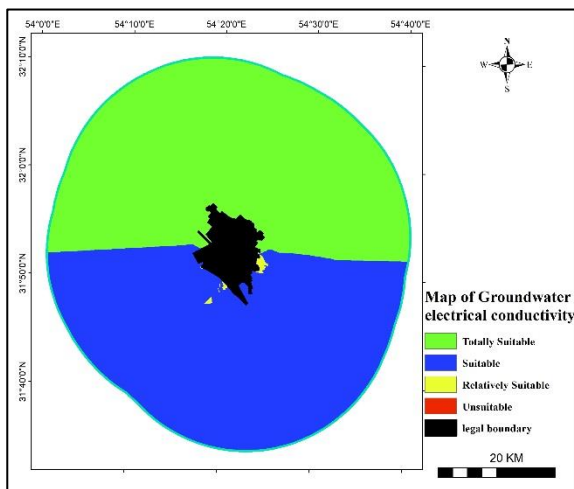
Figure 11. Map of classification layer Groundwater electrical conductivity of the study area (Gilvari et al., a. 2019).
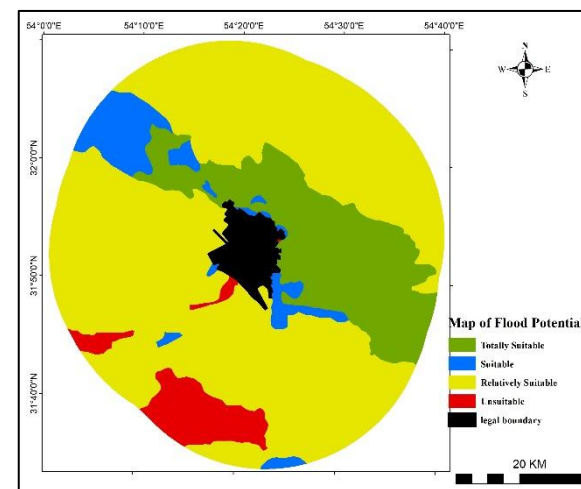
Figure 12. Map of classification layer Flood potential of the study area (Gilvari et al., a.2019)
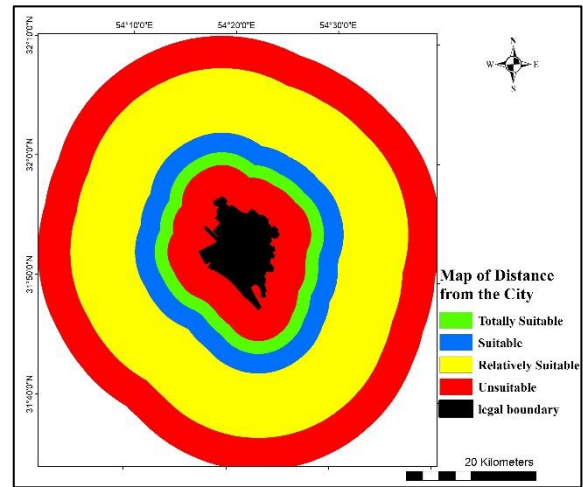
Figure 13 shows the final map of suitable areas for landfill with weighting through the hierarchical analysis method.
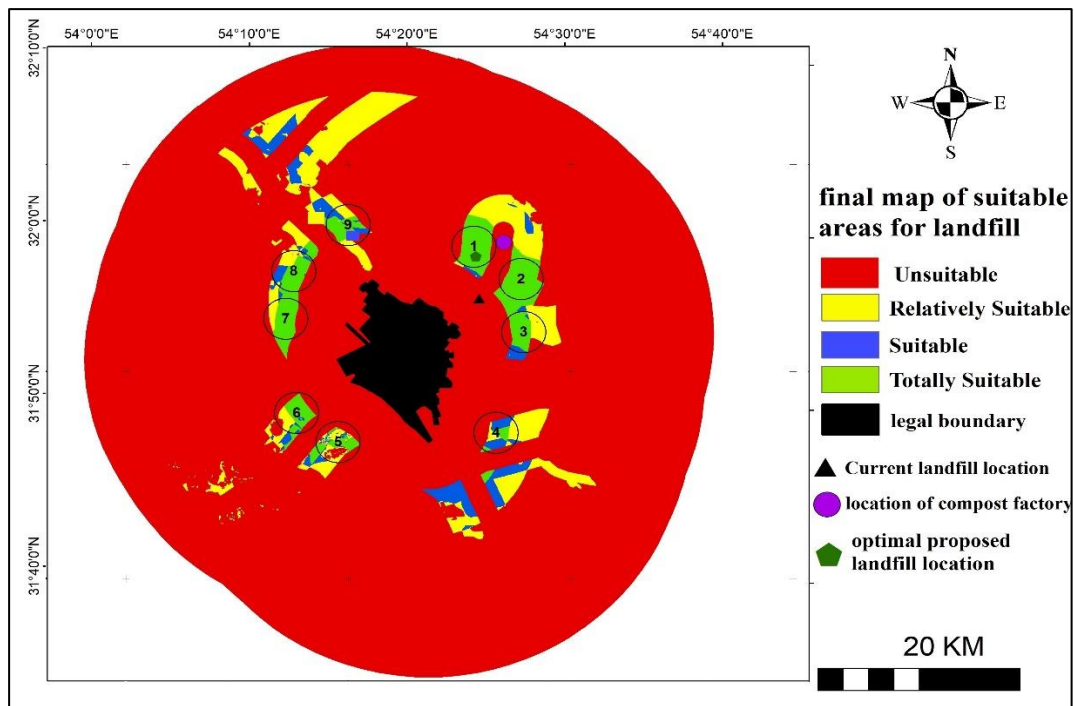
Figure 13. The final map of suitable areas for landfill with weighting through the hierarchical analysis method at a radius of 30 km from the border of Yazd city (Gilvari et al., b. 2019).

Here, it is necessary to ignore some of the selected locations, due to limiting factors such as dominant wind direction, minimum area required for landfill, in a multi-year perspective (at least 20 years), given the volume of waste generated and etc. Since the dominant wind direction is Yazd, the west is northwest and southeast As well as taking into account the minimum area required in the 20-year horizon for landfill, with areas larger than 278 square kilometers, all areas except 1, 2 and 3 will be unsuitable. By conducting a field survey of these three areas, considering the environmental assessment of experts and considering such things as view perspective, access to compost plant, road access geological conditions and etc, Area 1 is appropriately detected.

Then the final selected area was examined by field visit. The field survey results are presented in table 3.

Table 3. Field survey of the proposed solid landfill site in Yazd city

Parameter checked in selected region	Results
Groundwater and surface water	The groundwater level in the study area is over 50 meters, there were no main and secondary streams in the area, in terms of flooding, the area is in a relatively suitable area
Plant and animal species	The area is idle with scattered vegetation, there was no specific animal species in the region
Agricultural and animal husbandry activities	In the region, agriculture and animal husbandry activities are not carried out
Distance from the main road	Distance from the main road is appropriate, road traffic is low
The value of the land	The area is idle and is not in the urban development plan

Tourism and protected areas	The area is not in the tourism and protected plan
Distance from prohibited zone	The selected area is not limited by any limiting factors
Infrastructure and power lines	Because of its proximity to the composting plant, power lines and infrastructure are available

In Figure 14, an overview of the final selected zone (area 1) is presented using a hierarchical analysis method.

Figure 14. Overview of the final selected zone (area 1) for a new landfill site in Yazd

To ensure the soil conditions of the final selected area, permeability and granulometric composition of soil were investigated. For this purpose, about 3 kg of soil area was investigated in Yazd soil mechanics laboratory. According to figure 15, sieve analysis curve is 6.2×6 cm / s. The soil type is clayey silt. This type of soil is suitable for landfill (Niknami et al., 2009). Due to the high depth of water in the area, trench method with a high depth can be used in the area as well.

Particle size analysis and soil classification

Clay / Silt		Sand	Gravel	Rub ble
29/38		33	–	–

U.S. standard soil classification	D10	D30	D50	D60	Cc	Cu	LL(%)	PI(%)
CL-ML	0.001	0.0033	0.0073	0.009	1.22	>6	31	9
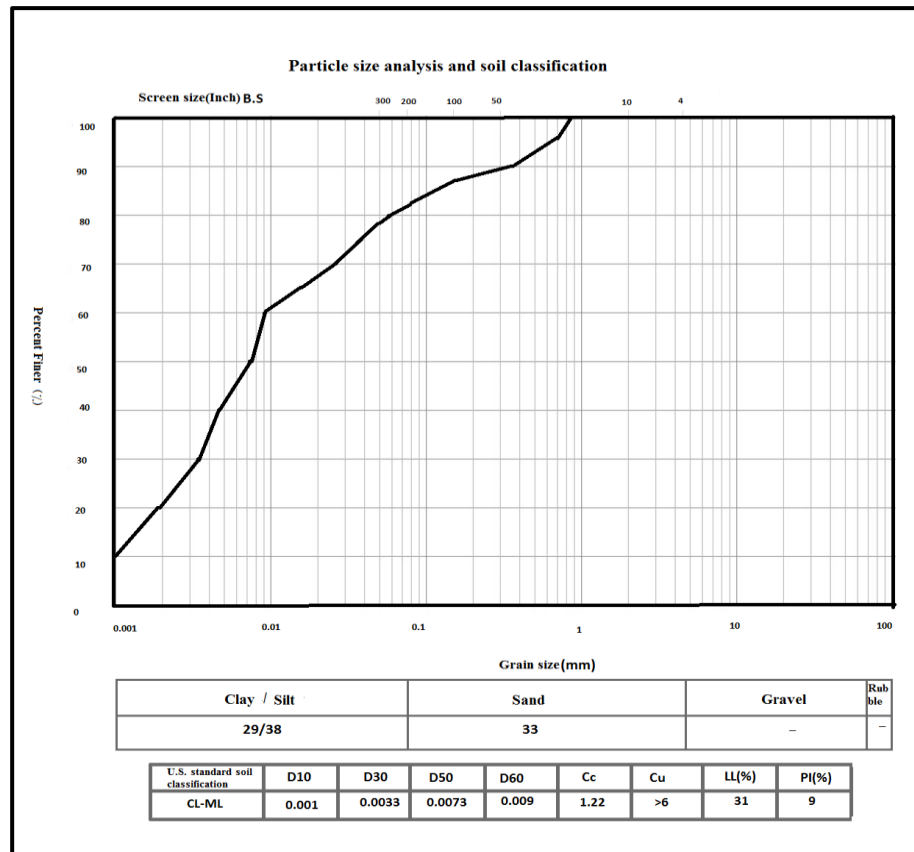
Figure 15. The soil permeability gradient curve of the selected region

4. Conclusion

In this study, the need for environmental assessment in landfill location studies of solid landfill in Yazd using the Leopold matrix method has been emphasized. By field visit from the current landfill site, bad effects of landfill on the environment and living organisms were studied ecologically. The total results of the Leopold Environmental Assessment Matrix related to the current landfill were -214. Since the most environmental impacts of landfill construction in the study area related to the physical effects that the construction and operation of landfill can create them in the area and the surrounding lands and areas, it is necessary to be very careful in the implementation and operation of landfill to minimize these effects. Therefore, management solutions can be developed to improve the status of the current landfill. Since the dominant wind direction is Yazd, the west is northwest and southeast As well as taking into account the minimum area required in the 20 year horizon for landfill, with areas larger than 278 square kilometers, all areas except 1, 2 and 3 will be unsuitable. Locating the burial place was determined by analyzing the hierarchy. By conducting a field survey of these three areas and considering the environmental assessment of experts, area 1 appropriately detected. The sieve analysis curve of the selected area was created and the soil type of this region was determined as clayey silt. Table 4 presents technical proposals for the construction of engineering-sanitary of landfill site in Yazd city.

Table 4. Technical proposals for a better landfill operation in Yazd city

Actions	Description
surface drainage	Surface drainage is required to reduce the risk of rain or flood entry, of course, it is not a flooding area and the main stream was not seen and the gentle slope of the area also helps to collect water.
Excavation and embankment	Since the area is flat and the slope is gentle, no need to transfer too much soil and it saves time and cost.
Substrate preparation	Since the soil in the area is clayey silt, the substrate is isolated by soil compression and no need for costly isolating materials.
Wall preparation	The wall is suitable with slopes of 135 degrees or less, since the depth of the underground water is high, it is possible to construct deep trench about 8 meters.
Leachate collection system	At the beginning, digging and filling the pit should be taken from the lowest point of collecting leachate in order to from the beginning of the work, the leachate is collected by the tube, then it is transferred to the tank next to the burial site to evaporate.
Gas collection	Tubes and wells are required to collect gas to reduce the smell, reduce the risk of fire and generate electricity
Wind and water erosion control	The excavation should be stopped during stormy and rainy days (heavy rainfall), moreover the erosion is reduced by planting around the landfill site
Underground water monitoring sump	A deep sump should be built to control underground water in terms of waste and leachate regularly
Reuse	After the landfill closes, after 10 years, buildings can be built on it with compression and also it can be used to create green space and playground
Geotechnical study	To study the land conditions for creating, stabilizing and keeping the landfill, geotechnical and geophysical studies will be needed
Vegetation	Vegetation of the area is low density, it is possible to plant trees and plants in the crown of the landfill to reduce erosion and create a beautiful view.
Fencing	Lightweight fencing is recommended to prevent unauthorized and also domestic and wild animals entry
Creating Infrastructure	Since its proximity to plant composting, it is possible to create infrastructure with low cost
Design of landfill cells	The complete map of the landfill, along with the location of the cells, the location of collecting leachate and gas is required, it is also possible to isolate the material inside the cells by creating a bump inside the cells not to be in contact
Waste separation	Waste separation is done before landfill for use at the composting plant
Control of insects	Regular and periodic spraying of the landfill site to prevent the spread of vermin, especially phlebotomus mosquito that it exists in Yazd
Preparation of evaluation report	It is need to prepare environmental reports before and during operation and after closing to control effects of landfill on the environment
Daily coverage	During day, waste compression should be done by heavy weight or bulldozer and at the end of the day with a meter of soil, the surface of the garbage should be covered.

References

Butt, T.E., Lockley, E., & Oduyemi, O.K. (2008). Risk assessment of landfill disposal sites – State of the art. *Waste Management*, 28, 952–964.

Canter, L.W. (1996). *Environmental Impacts Asessment*. Mc Grew Hill Book Co. Baltimore.

Farhadi, M., & Hafezi Moghadas, N. (2006). *Investigating the environmental impacts of solid waste sites during the construction and operation phase*. Master's dissertation. Shahrood University of Technology. (In Farsi).

Ferronato, N, & Torretta, V. (2019). Waste Mismanagement in Developing Countries: A Review of Global. J. Environ. Res. *Public Health*, (16) 6, 1-28.

Gilvari, S., Hafezi Moghadas, N., Mazlomi Bajestani, A. R., & Mazhari, S. A. (2015). *Environmental Assessment and Locating of Waste Landfills in Yazd Using Remote Sensing and Geographic Information Systems*. MA Thesis for Environmental Geology, Payame Noor University, Mashhad Center. (In Farsi).

Gilvari, S., Hafezi Moghaddas, N., Mazlomi Bajestani, A. R., Mazhari, S. A., & Sarsangi Aliabad, A. R. (2016). Environmental Assessment (EIA), and Optimal Locations of Urban Solid Waste Landfill using SAW, GIS and Leopold Matrix a Case Study of Yazd City. *Tolooe Behdasht*, (14) 6, 149-162. (In Farsi).

Gilvari, S., Mazlomi Bajestani, A. R., & Kashfi, S. A. (2019a). The need for environmental assessment in landfill site studies of solid waste in Yazd using Leopold matrix method. Third National Conference on Application of Advanced Space Models (Remote Sensing and GIS) in the alignment of the land. *Islamic Azad University, Yazd Branch*. (In Farsi).

Gilvari, S., Mazlomi Bajestani, A. R., & Sarsangi Ali Abad, A. R. (2019b). The evaluation of the solid waste landfill location in Yazd by comparing the similarity technique with the ideal option and the Leopold matrix. The 3rd National Conference on the Application of Advanced Space Models (Remote Sensing and GIS) in Land Reconciliation. *Islamic Azad University, Yazd Branch*. (In Farsi).

Gilvari, S., Sarsangi Ali Abad, A. R. Mazlomi Bajestani, A. R. Hafezi Moghaddas, N., & Mazhari, S. A. (2014). Landfil Urban Location Using GIS, Analytical Hierarchy Process and Similarity to Ideal Option (Case Study: Yazd City), *First Conference National Application of Advanced Space Models (Remote Sensing and GIS) in Land Use. Islamic Azad University, Yazd Branch*. (In Farsi).

Guiqin, W., Li, Q., Guoxue, L., Lijun, C. (2009). Landfill site selection using spatial information technologies and AHP: A case study in Beijing, China. *Journal of Environmental Management*, 90, 2414–2421.

Hafezi Moghadas, & N., Hajizadeh, H. (2007). Environmental assessment of proposed options for landfill in Khorasan Razavi province. *Fifth Iranian Conference on Geology and Environment*. (In Farsi).

Jafari, K., Hafezi Moghaddas, N., Mazlomi Bajestani, A. R., & Ghazi, A. (2015) Selection of Urban Waste Landfill Options in Ardebil Based on Ideal Option and Environmental Impact Assessment. *Journal of Health*, (6)4, 404 – 420. (In Farsi).

Kapilan, S. Elangovan, K. (2018). Potential landfill site selection for solid waste disposal using GIS and multi-criteria decision analysis (MCDA*), J. Cent. South Univ*. 25, 570−585.

Leopold, L.B. (1971). Procedur for evaluating environmental impact, *circular 645, U.S. Geological Survey, Washington. D.C*.

Naddeo V., Zarra T., Oliva G., Chiavola A., Vivarelli A. and Cardona G.(2018). Odour impact assessment of a large municipal solid waste landfill under different working phases, *Global NEST Journal*, (20)3, 654-658.

Niknami, M., Hafezi Moghaddas, N., & Dahr Azma, b. (2009). *Locating landfill in Golpayegan city*. Master's thesis, Shahrood University of Technology. (In Farsi).

Shariat, S. M. (2000). Environmental Impact Assessment of Seven Gardens of Heaven. *Third Environmental Health Conference*. (In Farsi).

Yao, P. (2013). Perspectives on technology for landfill leachate treatment. *Arabian Journal of Chemistry, Article in Press*.

Zamorano, Montserrat, Molero, Emilio, Hurtado, A´lvaro, Grindlay, Alejandro, Ramos, A´ngel. (2008). Evaluation of a municipal landfill site in Southern Spain with GIS- aided methodology. *Journal of Hazardous Materials,* 16,473–481.

Feasibility of Using Landsat OLI Images for Water Turbidity Estimation in Gandoman Wetland, Iran

Ghazal Lotfi[a], Mozhgan Ahmadi Nadoushan[a*], Mohammad Hadi Abolhasani[b]

[a] Department of Environmental Sciences, Isfahan (Khorasgan) Branch, Islamic Azad University, Isfahan, Iran.

[b] Waste and Wastewater Research Center, Isfahan (Khorasgan) Branch, Islamic Azad University, Isfahan, Iran.

Abstract

Change detection of wetlands is one of the essential requirements for the management and assessment of wetlands. Monitoring water quality is a crucial issue for assessing the environmental consequences of human interventions in wetland ecosystems. The present study aims to study the capability of satellite images in assessing the water turbidity and comparing their capability with ground sampling. Four stations in four directions were chosen in Gandoman wetland, located in Chaharmahal and Bakhtiari Province. Samples were taken three times in the wetland with the intervals of 30 days from September to December 2017. The turbidity index was calculated and the relationship between the data obtained from ground-based measurement and from satellite images was studied using linear regression analysis and correlation coefficient. The comparison between the amounts of turbidity observed in different stations in different months revealed that the turbidity value was at its highest point (214.49 NTU) in station number three in September, and its lowest point (2.25 NTU) in station number four in October and, therefore, there was a significant difference between the values ($p<0.05$). The results were also indicative of a significant correlation between the measured amounts of turbidity and the reflectance values of blue and red bands in the satellite images. Remote sensing techniques can overcome the limitations of traditional methods and be used as appropriate substitutes in monitoring the quality of water.

---

* Corresponding author Tel: +98-9131697106.
Email address: m.ahmadi@khuisf.ac.ir.

1. Introduction

Wetlands are complex and fragile ecosystems that hardly have the ability to self-purify (Engin et al., 2016; Yumun and Once, 2017). Wetlands are useful resources for supporting groundwater recharge, biodiversity, flood control, and the quality of water. Increase in the human population, anthropogenic activities, failure in the proper functioning of wastewater treatment plant, land use changes and the destruction of natural systems such as wetlands all lead to the increase of water pollution (Ahmed et al., 2017). Wetland water generally regulates functions such as conserving nutrients and filtering and cleaning pollutants (Alam et al., 2017).

With the extension of human communities over time and consequently, increase in the use of water resources, increasing changes in the qualitative features of water resources have occurred. Population growth and the pollution resulted from the emission of municipal, industrial and agricultural wastewater, leachate from landfills and surface runoffs are the factors that have resulted in water pollution and limitation of water resources (Masocha et al., 2017). Exploiting natural water resources requires raising awareness toward quantity and, more importantly, quality of water since water resources are the ultimate recipients of the pollution caused by human activities. Qualitative characteristics of water are among those factors that are important to be taken into consideration in planning for the management of water resources, assessing health factors of watershed basin, and making managerial modifications (Gigloo et al., 2013).

Wetlands have been identified as one of the most threatened habitats and received greater attention for monitoring the ecological functions (Ahmed et al., 2017). Many studies have reported that a decrease in the quality of water is a terrible threat to the society. To take corrective steps, it is required to assess the quality of water and provide a management system in which priority is given to monitor the quality of water (Mushtaq and Nee lala, 2016). As far as quality is concerned, water is defined in terms of physical, chemical and biological parameters. The conventional methods adopted to monitor the quality of water are generally expensive, time-consuming and not capable to give a proper temporal and spatial perspectives for the water resources from which few samples have been taken (Mohamed, 2015; Mushtaq and Nee lala, 2016). Water turbidity is an important index in defining the quality of water which, in turn, is a determining factor for other variables such as Chlorophyll a, total nitrogen and phosphorus, and trophic state (McCullough et al., 2012).

Remote sensing and Geographic Information System (GIS) have been generally used in study of water quality. Remote sensing as a method for monitoring water quality was introduced in 1978 when Coastal Zone Color Scanner (CZCS) was launched; however, the first satellite started in 1961 (Chawira et al., 2013). Wetlands affect such physical aspects of water as color in much the same way as they affect people and their financial activities (Abdelmalik, 2016). Factors such as agricultural activities in the area, and seasonal changes are effective in the amount of pollution (Yumun and Once, 2017). Part of the pollutants are analyzed through biological processes and others, such as heavy metals, because of being poisonous (Migani et al., 2016) and not being able to self-purify, may be accumulated in suspended particles and sediments and, thereby, enter into the food chain (Feng et al., 2017). This will cause many problems particularly for the aquatic animals in the region and decreases their normal lifespan (Liao et al., 2016). To prevent and control water pollution, it is necessary to implement plans for monitoring surface water resources (Markogianni et al., 2014). In-situ measurements of qualitative parameters of water entail collecting water samples from different areas and analyzing them in laboratories; this is a time-consuming and expensive process (Sharif et al., 2014). However, remote sensing techniques are potent enough to overcome the limitations of traditional methods and are appropriate substitutes for monitoring the quality of water; they allow for displaying the results in terms of temporal and spatial scales, and are appropriate especially for wider areas (Mumtaz Bhatti, 2008). In recent studies about the pollution of the environment, geographic information system has been increasingly used to detect the sources of the pollutants. Geographic information system is used as a perfect tool for the interpretation, processing and presentation of the data (Moore et al., 2015). Remote sensing is from among those methods of data collection that keep the direct physical contact with the objects to be measured at a minimum. From this perspective, they are in contrast with ground methods in which human agent is responsible for data collection and analysis. Geographic information system and remote sensing provide appropriate tools for supervising and monitoring the patterns of change in wetlands and determining their state (Rebelo et al., 2009). Recent advances in remote sensing will facilitate the study of patterns of change in vegetation, land cover, and their management (Zomer et al., 2009). Turbidity is

defined as the haziness of water, which is the result of the accumulation of suspended sediments in water. An increase in turbidity and its aftermaths will change the composition of the aquatic animals' community.

Turbidity is one of the important factors that can be used to assess the water quality and also to determine the amount of suspended sediments. It represents an optical determination of water clarity (Constantin et al., 2016). The kind of turbidity that is caused by suspended solids can result in a decrease in the amount of light that passes through water (Rangzan et al., 2012). Determining turbidity is one of the common procedures taken to evaluate the quality of water. In an area with a large number of dams, taking samples even from small parts for evaluating the quality of water is costly. Satellite remote sensing is a powerful tool for assessing the quality of water in large areas. Since 2013, a new satellite of the Landsat series is available, called Landsat-8 OLI, which was designed with similar characteristics to Landsat-5 and Landsat-7 ETM+ sensors in terms of spatial resolution (Yepez et al., 2018). The OLI (Operational Land Imager) sensor on Landsat-8 has the potential to meet the requirements of remote sensing of water color (Wang et al., 2019). The main objectives of this study are to investigate the water turbidity through ground-based measurement and compare the findings with those obtained from satellite images in Gandoman wetland. The innovation is that remote sensing was not used for quantifying water turbidity in this area. The main hypothesis of this study is that satellite images could be used for assessing water turbidity.

2. Materials and Methods

2.1. Study Area

Gandoman wetland as one of the wetlands of Aqyalaq drainage basin, located not far from Choqakhor wetland. A part of the water getting out of Choqakhor wetland falls into this wetland. The wetland is situated near Gandoman, a town in Borujen County, Charmahal and Bakhtiari Province, Iran. The minimum altitude of the wetland from the sea level is 2219 meters. It is located between 31° 49' N to 31° 53' N and 51° 05' E to 51° 07' E. The area of the wetland exceeds 1200 hectares; however, taking the encroachments into consideration, the area is reduced to 980 hectares. In high-water seasons, the depth of the wetland reaches an average of 30 centimeters. The majority of the lands have low infiltration capacity and mild slope of 0 to 2 percent. The level of sweat underground water is high and at the depth of 75-120 centimeters. The name of this wetland is recorded in the list of 10 best wetlands for bird-watching in Iran and its name is also recorded in the International Waterfowl Research Burea in London. The permanent water coverage is around 700 hectares (Mokhtari and Ghaderi, 2008). Figure 1 shows the location of study area.
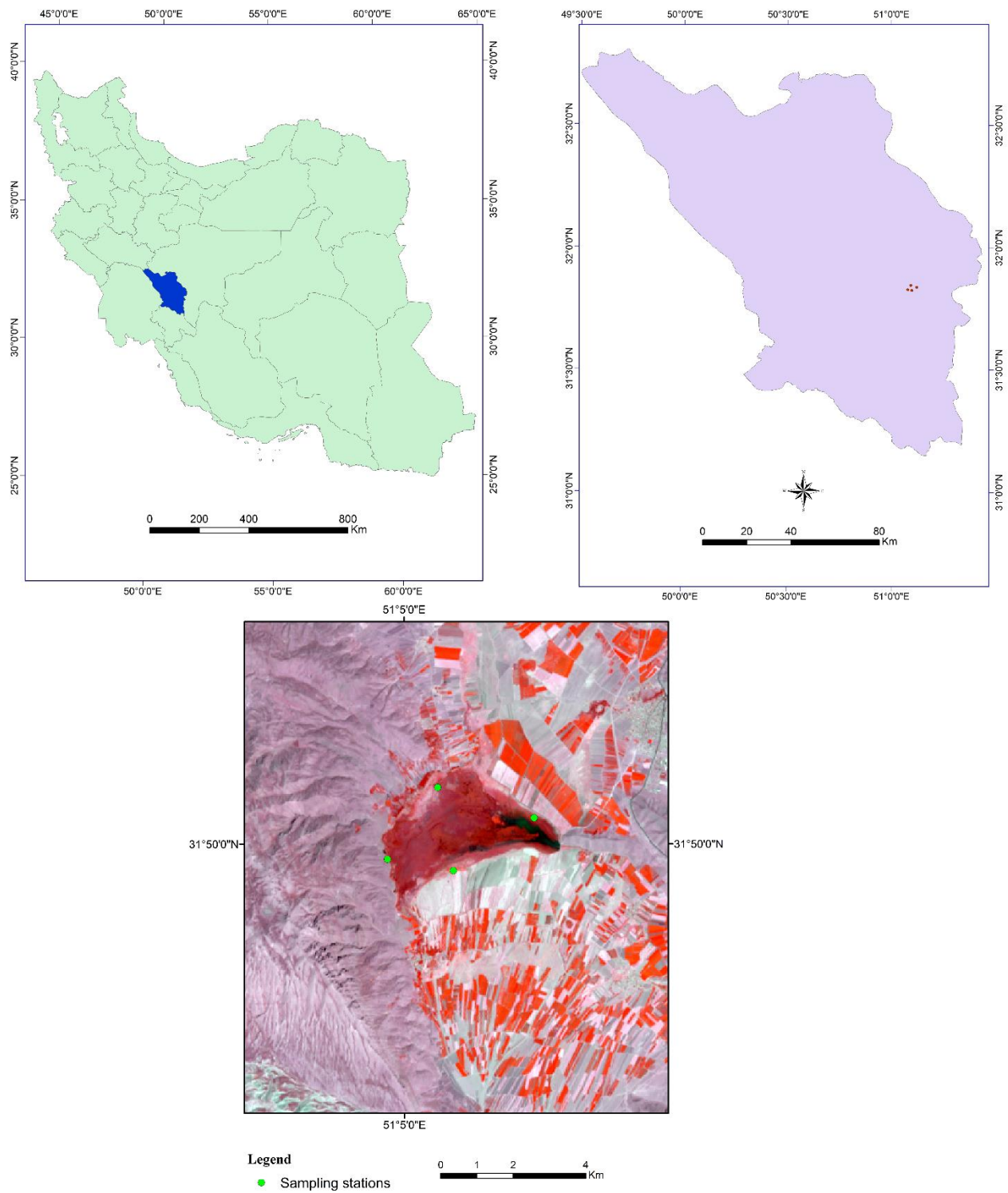
Figure 1. Location of study area

2.2. Methods

In the present study, Landsat OLI (2017) and Landsat TM (2000) images were used. OLI has a deep blue visible channel that is designed specifically for water resources and coastal zone analysis (Hancock, 2015). The images were georeferenced. They are available in the U.S. Geological Survey website. The image pertaining to the year 2017 was downloaded using Ortho Photo download application; therefore, geometric correction was not needed. Geometric correction of the Landsat TM image of the year 2000 was performed using ground control points and topographic maps on a scale of 1:2500. To do so, 32 ground control points, which were mostly such landmarks as junctions and known buildings, with an appropriate dispersion were used. The images were georeferenced using first degree polynomial model. After performing geometric correction, the intended area for investigation was separated creating AOI in ERDAS Imagine 8.4 software. Figure 2, shows the flowchart of the study.
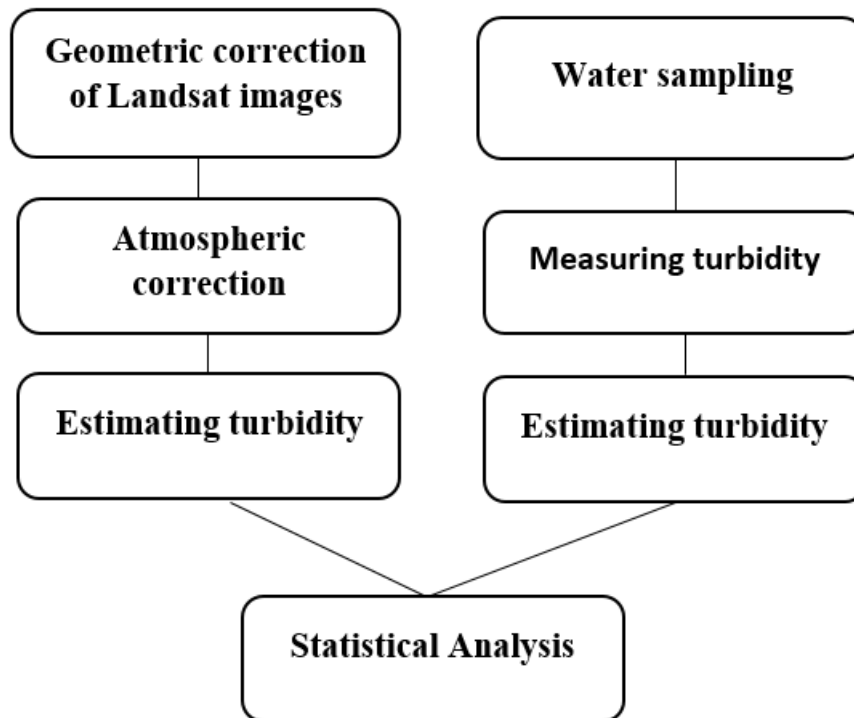
Figure 2. Flowchart of the study

2.3. Water sampling

Water samples were gathered three times from the depth of 20-30 centimeters from four stations (north, south, east and west) on the fifteenth day of each month. In the same location, water and air temperature were measured. The depth of water in the sampling area was between 50 to 80 centimeters. Before delivering the water samples to the laboratory for analysis, they were kept in special containers in a cool and dark place so as to minimize any negative effect on the quality of the water. During this fieldwork, GPS 76csx with an accuracy of three meters was used to determine and record the coordinates of sampling stations.

Table 1. The geographical position of the sampling stations

January	December	November	October	September	Parameter	Months / Stations
29.61 ± 0.86^{AB}	27.47 ± 0.93^{AB}	11.16 ± 0.36^{C}	16.97 ± 0.43^{C}	12.72 ± 0.04^{D}		1
27.72 ± 0.38^{B}	24.05 ± 2.17^{cB}	79.19 ± 0.27^{A}	94.13 ± 0.48^{B}	51.02 ± 0.41^{B}	Turbidity	2
31.02 ± 1.42^{A}	28.38 ± 0.87^{A}	48.64 ± 0.02^{B}	127.91 ± 1.26^{A}	214.49 ± 0.91^{A}		3
21.03 ± 1.36^{C}	20.63 ± 1.38^{C}	$2.48\pm.02^{D}$	2.25 ± 0.01^{D}	15.12 ± 0.50^{C}		4
9.34 ± 0.48^{A}	9.71 ± 0.07^{A}	8.88 ± 0.07^{AB}	5.88 ± 0.04^{B}	7.45 ± 0.01^{B}		1
9.40 ± 0.56^{A}	9.56 ± 0^{B}	8.50 ± 0.21^{C}	9.47 ± 0.53^{A}	7.52 ± 0.02^{AB}	pH	2
9.90 ± 0^{A}	9.79 ± 0.01^{A}	9.15 ± 0.13^{A}	6.08 ± 0.04^{B}	7.66 ± 0.09^{A}		3
9.75 ± 0.07^{A}	9.77 ± 0.02^{A}	8.72 ± 0^{BC}	6.05 ± 0.03^{B}	7.59 ± 0.07^{AB}		4
600.50 ± 47.37^{C}	570.50 ± 43.13^{C}	352.50 ± 0.70^{C}	316.00 ± 1.41^{D}	304.50 ± 4.94^{D}		1
872.00 ± 7.07^{A}	824.00 ± 7.07^{A}	268.00 ± 1.41^{D}	$984.00\pm.65^{A}$	653.00 ± 2.82^{B}	EC	2
758.00 ± 2.82^{B}	726.00 ± 9.89^{B}	580.00 ± 8.48^{A}	669.00 ± 1.41^{B}	914.50 ± 0.70^{A}		3
376.50 ± 2.12^{D}	354.50 ± 10.60^{D}	386.50 ± 16.26^{B}	340.00 ± 1.41^{C}	339.50 ± 2.12^{C}		4
0.10 ± 0.02^{A}	0.06 ± 0.05^{A}	0.96 ± 1.07^{A}	0.70 ± 0.14^{A}	0.13 ± 0.07^{A}		1
$0.06\pm.02^{A}$	0.04 ± 0.02^{A}	0.02 ± 0.02^{A}	$6.60\pm.84^{A}$	0.04 ± 0.02^{A}	TSS	2
0.29 ± 0.21^{A}	0.08 ± 0.02^{A}	0.53 ± 0.43^{A}	9.60 ± 12.72^{A}	1.73 ± 1.28^{A}		3
0.05 ± 0.01^{A}	0.12 ± 0.11^{A}	0.05 ± 0.01^{A}	0.70 ± 1.14^{A}	0.24 ± 0.11^{A}		4

0.80±0.28[A]	0.14±0.11[A]	1.67±2.33[A]	1.30±0.98[A]	1.41±23.26[A]	1
0.01±0.01[B]	0.07±.04[A]	0.81±0.09[A]	0.64±0[A]	18.49±23.26[A]	2
				TDS	
0.03±0.01[B]	0.25±0.29[A]	0.28±0.25[A]	7.59±8.72[A]	2.99±0.43[A]	3
0.05±0.01[B]	0.18±0[A]	0.15±0.01[A]	0.10±0.08[A]	1.15±1.56[A]	4

2.4. Measuring turbidity

Clay particles, sand particles, minerals, particles of organic materials, planktons and other microscopic organs which are suspended in the water and do not let the light transmit through water result in water turbidity. Turbidity is measured under controlled conditions comparing light intensity scattered by the sample with the light intensity scattered by the standard method. The more intense the scattered light at 90 degrees from the incident light beam, the higher the degree of turbidity. Bubbles, color and dirty glasses are from among intervening elements. To measure water turbidity, L21 Raspina Co. turbidimeter was used. Using the available standards and considering the turbidity range of the samples, the intended range was chosen, the standard was put in the related container of the turbidimeter, and the number was read. As the next stage, the samples were completely mixed so that no bubble existed in them. Then, they were put in the turbidimeter's cell, and the external surface of the cell was wiped and dried. Finally, it was put in the container and the number displayed was directly read and recorded.

2.5. Estimating turbidity using satellite images

After geometric correction, radiometric correction was applied to the images so that the numeric values of the pixels could be turned into reflectance values. Then, atmospheric correction was done to eliminate the negative effect of atmosphere on the images. Dark Object Subtraction method was used for atmospheric correction and the value of dark pixels was reduced using ATMOSC in the TerrSet; this helped the quality of the images to be enhanced. Then, the reflectance values in the bands of satellite images were extracted from sampling sites in different months starting from September 2017 and ending with January 2018.

Landsat 8 has been widely used in water and coastal area management. Landsat 8 OLI has been innovated with 12 bits of radiance resolution in comparison with 8 bits for Landsat 5 TM and Landsat 7 ETM (Quang et al., 2017). OLI has a deep blue visible channel that is designed specifically for water resources and coastal zone analysis (Hancock, 2015).

2.6. Statistical analysis

The values of turbidity in different stations were compared using randomized complete block design in SAS 9.4. To analyze the data two-way ANOVA was used, and to compare the means Duncan test with a confidence level of 95% was conducted. Excel software was used to draw diagrams. To determine the relationship between the reflectance values and the measured amounts of turbidity, regression analysis was

applied. In so doing, the measured turbidity and the amount of reflectance were considered as dependent and independent variables, respectively.

3. Results

3.1. Statistical Analysis

The randomized complete block design was used to compare the mean values of turbidity in different months. The results are reported in Table 2.

Table 2. The comparison of mean values of turbidity in different months and different stations

TDS	TSS	EC	PH	Turbidity		Factors / Months
5.56±11.73[A]	0.54±0.88[B]	526.7±266.20[AB]	7.36±0.09 [C]	67.11±88.62[A]		September
2.46±4.63[A]	4.94±6.33[A]	614.4±291.99[AB]	7.02±1.61 [C]	66.46±55.97[A]		October
0.72±.09[A]	0.39±0.60[B]	396.8±122.34[B]	8.81±0.27[B]	35.37±32.79[A]	Months	November
0.16±0.13[A]	0.07±0.05[B]	618.8±190.37[AB]	9.70±0.10[A]	25.13±3.44[A]		December
0.22±0.37[A]	0.12±0.13[B]	651.8±199.52[A]	9.59±0.37[AB]	27.35±4.17[A]		January

As Table 2 presents, the comparison of turbidity amounts in different months and different stations revealed that station number three had the highest amount of NTU (214.49) in September and station number four had the lowest amount of NTU (2.25) in October. A significant difference between these amounts was observed ($p<0.05$).

As it is observed in Table 2, the values of turbidity were studied and compared from September 2017 to January 2018. The highest and lowest values were observed in September with 67.11 NTU and in December

with 25.13 NTU, respectively (p<0.05). These factors did not have significant differences in different months.

3.2. Estimating turbidity using satellite images

The results of regression analysis and the correlation analysis between the values of reflectance in satellite images and turbidity revealed that the highest amount of correlation was between the values of reflectance of red and blue bands and turbidity. As shown in Figures 3 and 4, the correlation coefficient of more than 0.9 was observed between the measured turbidity and the values of reflectance of red and blue bands.
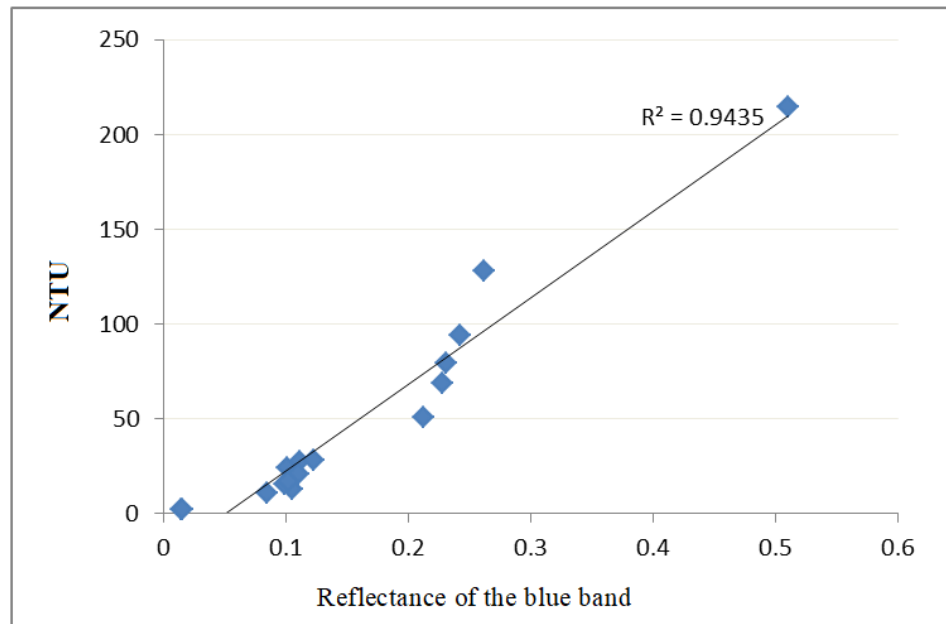

Figure 3. The correlation between the values of reflectance of the blue band and the measured turbidity
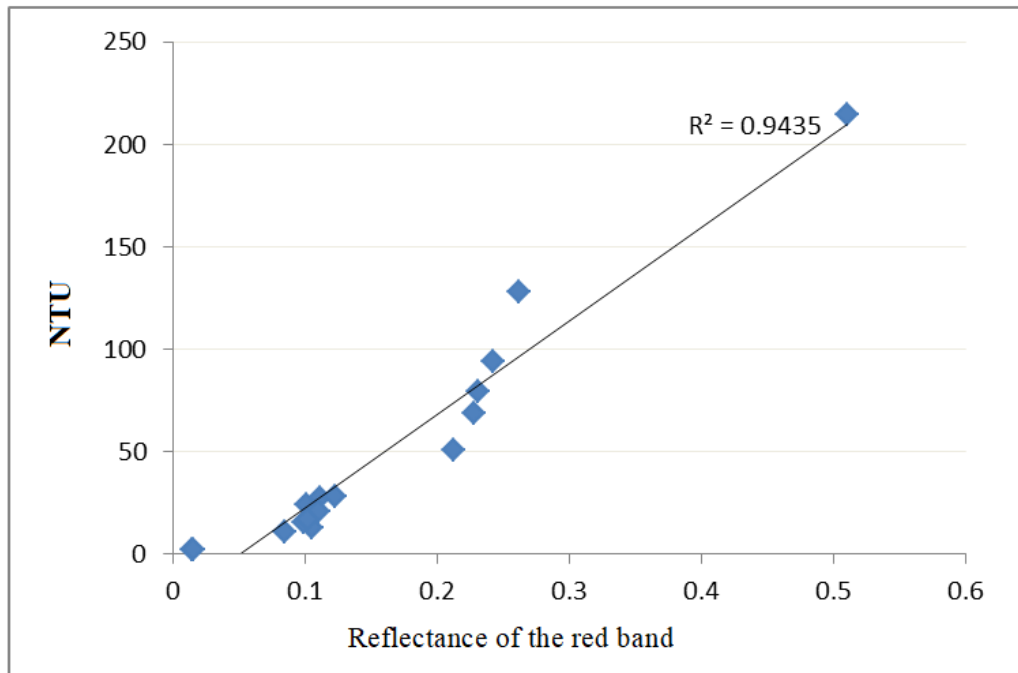
Figure 4. The correlation between the values of reflectance of the red band and the measured turbidityThe regression equation for the values of reflectance of the blue band and turbidity is as follows:

Turbidity: - 23.048 + 455.996 (Reflectance of the blue band) $R^2= 0.94$
The regression equation for the values of reflectance of the red band and turbidity is as follows:
Turbidity: - 21.616 + 378.974 (Reflectance of the red band) $R^2= 0.97$

4. Discussion

This study showed that it is possible to determine the water turbidity using satellite images. This method not only is time saving and cost-effective but also enjoys a high degree of precision. The findings of this study are consistent with those reported in Alrababah, Alhamad (2006), Koutsias, Karteris (2003) and Sadr et al. (1995) that these studies support the usefulness of the data obtained from Landsat in determining turbidity considering their availability. Other researchers also acknowledged the applicability and usefulness of these images in determining turbidity. Dena et al. (2015) are among these researchers. They conducted a research article entitled "Monitoring lake water quality status of the Albufera de Valencia in Spain" and verified the usefulness of Landsat TM and +ETM images in the daily estimation of some of the parameters that have a role in the quality of water such as Chlorophyll A and turbidity. They used MODIS and Landsat TM and ETM[+]. Mohammad (2015) used data from Landsat 5 and 7 for mapping the quality of water of the lake of Mosul Dam located in the northern part of Iraq. The purpose of the study was to extract a simple and accurate algorithm for assessing the parameters related to the quality of water. Measuring the quality of water entailed the measurement of temperature, turbidity, Chlorophyll A, nitrite, nitrate, phosphate, Total Organic Carbon (TOC), dissolved organic carbon, total dissolved solids and pH. The results of the spatial analysis revealed that it was possible to use TM5 and +ETM images for investigating the quality of the water of the lake of Mosul Dam. Abdelmalik (2016) also estimated the parameters involved in water quality through remote sensing in the Himalayan lake of Kashmir using images from Landsat 8 OLI. The purpose of the study was to extract a simple and accurate algorithm for assessing such parameters of water quality as DO, COD, pH, alkalinity, hardness, chloride, TSS, TDS, turbidity, electrical conductivity, and phosphate. The results indicated that remote sensing had a great potential in improving the way the quality of water was monitored and assessed. The study, further, revealed that satellite sensors could measure the values of sunlight's reflection from the surface of water in different wavelengths and these reflectance values usually showed a significant correlation with different parameters of water quality. Satellite images are devices that

reduce the cost and energy needed for water sampling and determining such parameters as turbidity. The results of regression and correlation analyses between the reflectance of the bands of satellite images and the measured amount of turbidity revealed that the highest degree of correlation existed between the values of reflectance of blue and red bands and turbidity. The findings are in line with those obtained from the studies conducted by Hadjimitsis et al. (2006), McCullough (2012) and Kulkarni (2011) in which it has been confirmed that the most appropriate bands for investigating turbidity are blue and red bands. In a like manner, Lambriks and Nagel (2003) conducted a study to assess the potential of Landsat TM and ETM$_+$ satellite images in monitoring water turbidity in Kentucky Lake. The results of correlational study between the reflectance of images and turbidity indicated that there was a significant correlation between the red band and the values of turbidity. The findings are consistent with the findings of Nabizadeh, Binesh Barahmand, Nadafi, and Mesdaghinia's (2012) study in which the turbidity of water in a part of the southern coast of the Caspian Sea was studied. They found that it was possible to quantitatively estimate water turbidity using Landsat OLI and ETM images. Moreover, the results of the present study confirm those obtained from Aghighi et al.'s (2009) study. They conducted their study in Gorgan Gulf and reported that it was possible to use satellite images for estimating important parameters in water quality including turbidity. Turbidity is one of the important parameters that have a role in water quality. It can be claimed that it is the second most important parameter with BOD5 as the most important determining factor. In winters, when rainfall increases, water turbulence and runoffs streaming toward wetlands are the factors that add to water turbidity. Moreover, the depth of water is effective in water pollution and turbidity. The total amount of suspended solids is also a determining factor as an increase in this value leads to an increase in turbidity. In this study, the latter relationship was observed.

5. Conclusion

It is necessary to have long-term precise programs for monitoring water quality and managing wetlands. Remote sensing has an important and effective role in managing and monitoring water quality. Satellite images measure the values of sunlight's reflection from the surface of water. The reflectance of water depends on the concentration of water and those parameters involved in determining water quality, including turbidity. Therefore, the reflection of images is indicative of the amount of turbidity. The findings of regression analysis conducted to study the relationship between in-situ turbidity and turbidity of satellite images revealed that there was a significant relationship between the values of reflectance of red and blue bands and the measured turbidity.

Remote sensing techniques can overcome the limitations of traditional methods and be used as appropriate substitutes in monitoring the quality of water. They provide the possibility of displaying the results at varying temporal and spatial scales and are used especially in wider areas. The features of remote sensing include appropriate return period, high capacity in spatial segmentation, non-stop monitoring, and large-scale data collection. Such characteristics turn remote sensing into a new effective method for monitoring the quality of water. Spectral reflectance measured by the satellite remote sensing system has the relationship with a number of parameters of water quality. One of these parameters is turbidity. An increase in turbidity and its negative consequences in water mass lead to some changes in the composition of the aquatic animals' community. The turbidity that is the result of suspended solids can reduce the amount of light that passes through water.

References

Abdelmalik, K.W. (2018). Role of statistical remote sensing for Inland water quality parameters prediction. *The Egyptian Journal of Remote Sensing and Space Sciences*, *21*(2), 193-200. https://doi.org/10.1016/j.ejrs.2016.12.002

Aghighi, H., Alimohammadi, A., Saradjian, M. R., & Ashourloo, D. (2009). Estimation of water turbidity in Gorgan Bay using IRS-ILSS-III Images. *The Journal of Spatial Planning*, *13*(2), 55-72.

Ahmed, R., Sahana, M., & Sajjad, H. (2017). Preparing turbidity and aquatic vegetation inventory for waterlogged wetlands in Lower Barpani sub watersheds (Assam), India using geospatial technology.

The Egyptian Journal of Remote Sensing and Space Sciences, *20*, 243–249. https://doi.org/10.1016/j.ejrs.2016.11.001

Alrababah, M. A., & Alhamad, M. N. (2006). Land use/cover classification of arid and semiarid Mediterranean Landscapes using Land use ETM. *International Journal of Remote Sensing*, *3*, 2703-2718. https://doi.org/10.1080/01431160500522700

Banaś, J., Nieć, M., & Salamon, W. (1993). Bismuth tellurides from the Jarmuta Hill (Pieniny Mts.). Mineralogia Polonica, 24(1-2), 33-40.

Dona, C., Chang, N., Caselles, V., Sanchez, JM., Camacho, A., Delegido, J., & Vannah, B. W. (2015). Integrated satellite data fusion and mining for monitoring lake water quality status of the Albufera deencia in Spain. *Journal of Environmental Management*, 151, 416-426. doi: 10.1016/j.jenvman.2014.12.003

Chawira, M., Dube, T., & Gumindoga, W. (2013). Remote sensing based water quality monitoring in Chivero and Manyame lakes of Zimbabwe. *Physics and Chemistry of the Earth*, 66, 38–44. https://doi.org/10.1016/j.pce.2013.09.003

Constantin, S., Doxaran, D., & Constantinescu, S. (2016). Estimation of water turbidity and analysis of its spatio-temporal variability in the Danube River plume (Black Sea) using MODIS Satellite data. *Continental Shelf Research*, 112,14-30. DOI:10.1016/j.csr.2015.11.009

Feng, J., Liu, Z., Cao, Y., Qiu, L., Xu, F., Xua, F., & Tiand, X. (2017). Assessment of heavy metal contamination in urban river sediments in the Jiaozhou Bay catchment, Qingdao, China Fangjian. *Journal Catena*, 150, 9-16. https://doi.org/10.1016/j.catena.2016.11.004

Fohrer, N., Kaneyuki, N. & Heidari, A., 2011. Investigation on function of wetlands under influence of land uses (A case study: Higashi-Hiroshima, Japan). *Iranian Journal of Natural Resources*, 64(1), 15-24.

Fridgigloo, B., Najafinejad, A., Moghani Bilehsavar, B., & Ghiyasi, A. (2013). Evaluation of water quality variation of Zarringol River, Golestan province. *Quarterly of Water and Soil Conservation*, 20(1), 77-95. DOI: 10.22059/JRWM.2017.109430.779

Hadjimitsis., Diofantos, G., Marinos, G., Chris C., & Brian, A. (2006). Determination of turbidity in Kourris Dam in Cyprus Utilizing Landsat TM Remotely Sensed Data. *Water resources management*, 20(3), 449-465. https://doi.org/10.1007/s11269-006-3089-y

Hancock, M. J. (2015). Predicting water quality by relating Secchi disk transparency depths to Landsat 8. Master of Science in the Department of Geography, Indiana University.

Jones, K., Lanthier, Y., Voet, P., Valkengoed, E., Taylor, D., & Fernandez-Prieto, D. (2009). Monitoring and assessment of wetlands using Earth Observation, the GlobWetland project. *Journal of Environmental Management*, 90, 2154-2169. DOI:10.1016/j.jenvman.2007.07.037

Koutsias, N., & Karteris, M. (2003). Classification analyses of vegetation for delineating forest fire fuel complexes in a Mediterranean test site using satellite remote sensing and GIS. *International Journal of remote Sensing*, 24, 3093-3104. https://doi.org/10.1080/0143116021000021152

Kulkarni, A. (2011). Water Quality Retrieval from Landsat TM Imagery. *Conference Organized by Missouri University of Science and Technology*. Procedia computer Science. 6, 475-480.

Liao, J., Chen, J., Ru, X., Chen, J., Wu, H., & Wei, C. (2017). Heavy metals in river surface sediments affected with multiple pollution sources, South China: Distribution, Enrichment and source apportionment. *Journal of Geochemical Exploration*, 176, 9-19.

Markogianni, V., Dimitriou, E., & Karaouzas, I. (2014). Water quality monitoring and assessment of an urban Mediterranean lake facilitated by remote sensing applications. *Environmental Monitoring Assessment*, 186, 5009–5026. https://doi.org/10.1007/s10661-014-3755-0

Masocha, M., Murwira, A., Magadza, C., Hirji, R. & Dube, T. (2017). Remote sensing of surface water quality in relation to catchment condition in Zimbabwe. *Physics and Chemistry of the Earth*, 100, 13-18. Doi: 10.1016/j.pce.2017.02.013

McCullough, I. M., Loftin, C. S., & Sader, S. A. (2012). Combining lake and watershed characteristics with Landsat TM data for remote estimation of regional lake clarity. *Remote Sensing of Environment*, 123, 109-115. https://doi.org/10.1016/j.rse.2012.03.006

Migani, F., Borghesi, F., & Dinelli, E. (2016). Geochemical characterization of surface sediments from the northern Adriatic wetlands around the Po River delta. Part II: aqua regia results. *Journal of Geochemical Exploration*, 169, 13-29. https://doi.org/10.1016/j.gexplo.2016.06.012

Mohamed, M. F. (2015). Satellite data and real time stations to improve water quality of Lake Manzalah. *Water Science*, 29, 68-76. https://doi.org/10.1016/j.wsj.2015.03.002

Mokhtari, Z., & Ghaderi, F. (2008). An ecosystem approach to wetland management. *Paper presented at the First National Conference of Iranian Wetlands*, Ahwaz, Iran.

Moore, F., Keshavarzi, B., & Ebrahimi, P. (2015). A GIS-based approach for detecting pollution sources andbioavailability of metals in coastal and marine sediments of Chabahar Bay, SE Iran. Chemie der Erde, 75, 185-195. Doi: 10.1016/j.chemer.2014.11.003

Mumtaz Bhatti, A. (2008). Modelling and monitoring of suspended matter in surface waters using remotely sensed data. (Master's thesis), Kochi University of Technology, Japan.

Mushtaq, F., & Nee Lala, M. G. (2016). Remote Estimation of Water Quality Parameters of Himalayan Lake (Kashmir) using Landsat 8 OLI Imagery. Geocarto International, 32, 274-285. https://doi.org/10.1080/10106049.2016.1140818

Nabizadeh, R., Binesh Barahmand, M., Nadafi, K., & Mesdaghinia, A. (2012). Qualitative analysis of coastal waters in the Caspian Sea in Gilan province: Determining the environmental health indicators in swimming areas. *Journal of Mazandaran University of Medical Sciences*, 22(88), 41-52.

Quang, N. H., Sasaki, J., Higa, H., & Huan, N. H. (2017). Spatiotemporal Variation of Turbidity Based on Landsat 8 OLI in Cam Ranh Bay and Thuy Trieu Lagoon, Vietnam. Water, 9(8), 570-595.

Rangzan, K., Fattahi Moghaddam, M., & Mobed, P. (2012). Estimating the quality of Karun River near the city of Ahvaz by ground data, Field Spec 3 spectrometer and hyperspectral data from Hyperion. *Journal of Advanced Applied Geology*, 1(4), 98-108. https://doi.org/10.3390/rs11050578

Rebelo, L. M., Finlayson, C. M., & Nagabhatla, N. (2009). Remote sensing and GIS for wetland inventory, mapping and change analysis. *Journal of Environmental Management*, 90, 2144-2153. DOI: 10.1016/j.jenvman.2007.06.027

Sader, A., Ahl, D., & Liou, W. (1995). Accuracy of Landsat TM and GIS rule-based methods for forest wetland classification in Maine. *Remote sensing of Environment*, 3, 133-144. https://doi.org/10.1016/0034-4257(95)00085-F

Shareef, M. A., Toumi, A., & Khenchaf, A. (2014). Estimation of Water Quality Parameters Using the Regression Model with Fuzzy K-Means Clustering. *International Journal of Advanced Computer Science and Applications*, 5(6), 151-157. DOI: 10.5942/jawwa.2016.108.0012

Soner Engin, M., Uyanik, A., & Cay, S. (2016). Investigation of trace metals distribution in water, sediments and wetland plants of Kızılırmak Delta, Turkey. *International Journal of Sediment Research*, 32(1), 90-97. DOI: 10.1016/j.ijsrc.2016.03.004

Wang, D., Ma, R., Xue, K., & and Loiselle, S. A. (2019). The Assessment of Landsat-8 OLI Atmospheric Correction Algorithms for Inland Waters. *Remote Sensing*, 11(169), 1-23. doi:10.3390/rs11020169

Yepez, S., Laraque, A., Martinez, J., De Sa, J., Carrera, J. M., Castellanos, B., Gallay, M. & Lopez. J. L. (2018). Retrieval of suspended sediment concentrations using Landsat-8 OLI satellite images in the Orinoco River (Venezuela). *Comptes Rendus Geoscience*, 350, 20-30.

Yumun, Z., & Once, M. (2017). Monitoring heavy metal pollution in foraminifera from the gulf of edremit (northeaster aegean sea) between Izmir, Balikesir and Canakkale (Turkey). *Journal of African Earth Sciences*, 130, 110-124. DOI: 10.1016/j.jafrearsci.2017.03.015

Zahangeer Alam, M., Carpenter-Boggs, L., Rahman, A., Manjurul Haque, M., Uddin Miah, R., Moniruzzaman M., Abdul Qayum, M., & Muhammad Abdullah, H. (2017). Water quality and resident perceptions of declining ecosystem services at Shitalakka wetland in Narayanganj city. Sustainability of Water Quality and Ecology, 9-10, 53-66. DOI: doi.org/10.1016/j.rsase.2017.11.005

Zomer, R. J., Trabucco, A., & Ustin, S. L. (2009). Building spectral libraries for wetlands land cover classification and hyperspectral remote sensing. *Journal of Environmental Management*, 90, 2170-2177. DOI: 10.1016/j.jenvman.2007.06.028

Using EO1 Hyperspectral Images for Geological Units Mapping

Ali Asghar Torahi [a*], Parisa Safarbeyranvand[b], Hasan Hasani Moghaddam[b], ParvizZiaeian Firoozabad[c], Ali Hosseingholizade[d]

[a] Assistant Professor Remote Sensing and GIS, Kharazmi University of Tehran.

[b] Master of Remote Sensing and GIS ,Kharazmi University of Tehran.

[c]Associate Professor of Remote Sensing and GIS, Kharazmi University of Tehran.

[d]PhD Student of Remote Sensing and GIS, University Tehran.

Abstract

The issue of mapping geological units during an evolving process has now reached a point where the detection and classification of geological units is carried out with the aid of hyperspectral sensing. In this study, using hyperspectral image of Hyperion sensor, related to Khorramabad area in Lorestan province, and using Spectral Angle Mapper (SAM) and SVM (Support Vectors Machine) algorithms for detecting and separating geological units after performing the necessary preprocesses, the MNF conversion and PPI algorithm were used to reduce data and extract pure pixels on the image, respectively. From overlapping of pure pixels with geological units and ground data, the average range for each member was extracted and then these net members were used as inputs for the above mentioned algorithms and class B DVD image was done. Field surveys performed at the points provided by the Spectral Angle Mapter (SVM) confirm the superiority of the SVM method in separating geological units. Finally, by verifying the accuracy of the algorithms by calculating the error matrix, the accuracy of the classification of each method are (68.83) and (81.70), for SAM and SVM respectively it was found that at the end of the SVM algorithm with a total accuracy of 81.70 was introduced as the best classification algorithm.

* Corresponding author Tel: +98-9197951476.
Email address: atorahi@khu.ac.ir.

1. Introduction

Using remote sensing technology and using satellite data reduced the costs and increased accuracy and speed of data collecting (Alvipanah, 2013). The use of satellite technology in the last decades as one of the most important means of information acquisition attracted the attention of many experts and specialists of various sciences, including geology, mining, environment, meteorology, agriculture and etc. From years of 1980, by introducing of Hyper-spectroscopic sensors, a major step has been taken in the area of remote sensing technology (Hasani Moghaddam, 2019). Hyper-spectral sensors, in comparison with multi-spectral sensors, produce much more accurate spectral data and therefore allow for more accurate identification of ground targets (Campsvalls et al., 2014). As the Hyper-spectral sensors are used of bands extremely large spectra produce a large amount of spectral data, so it is also necessary to use methods that are capable of processing and extracting valuable information from this high dimension data. The relationships of geological and remote sensing are nearly thirty years old (Waske et al., 2009). In the most hyper spectral sensors, reflection measurements of surface phenomena with a spectral width of 0.01 μm and spectral ranges of 0.4 to 2.5 μm are acquired, so this property makes it possible for geological unit's investigations. The existing maps of the geological units are prepared by traditionally ways; in this research, used of remotely sensed hyperspectral images to produce more accurate maps of geological units. The data obtained from the measurements in terms of providing a wide coverage of the area and providing quantitative parameters can be a suitable source for updating geological maps (Rajendran et al., 2007). Images from remote sensing technology provide efficient data that requires processing on the image to extract information from them. Among different methods of remote sensing, the classification techniques have a special role in analyzing, separating and detecting various geological units. Image classification is one of the main process components of the information extracting from an object that are obtained by examining the relationship between spectral effects and classes (Oommen, 2008).

Ramakrishnan and Bharati (2015), review the potential of Hyperspectral Remote Sensing (HRS) technique in various geological applications ranging from lithological mapping to exploration of economic minerals of lesser crustal abundance. This work updates understanding on the subject starting from spectroscopy of minerals to its application in exploring mineral deposits and hydro-carbon reservoirs through different procedures such as atmospheric correction, noise reduction, retrieval of pure spectral endmembers and unmixing. Besides linear unmixing, nonlinear unmixing and parameters attributed to nonlinear behaviour of reflected light are also addressed. A few case studies are included to demonstrate the efficacy of this technique in different geological explorations. Finally, recent developments in this field like ultra-spectral imaging from unmanned aerial vehicles and its consequences are pointed out.

Kurz et al. (2017), developed a novel geological mapping technique for subsurface construction sites. A major result of this work is that the use of artificial halogen light sources, at ranges suitable for imaging rock faces of similar size to the TT-Niche, is possible and allows good quality hyperspectral data to be obtained. The importance of this result must be stressed, as there were many uncertainty factors with respect to the strength, emitted wavelengths and stability of the required light sources prior to the start of the study. Although complex illumination variations were present in the data, especially at long range, due to the number and configuration of lights used, the data quality was suitable for mapping the large scale geology.

Blackburn (2007), appraised the developing technologies and analytical methods for quantifying pigments nondestructively and repeatedly across a range of spatial scales use of hyperspectral remote sensing. The results of this study showed that hyperspectral images is a better way for evaluating pigments ranges and it can be used in agriculture, forest, environmental, Eco physiological and etc.

Bordoloi et al. (2013), for involving a pot experiment with twenty acidic soils varying widely in properties, evaluated six chemical indices of soil N-availability. Of all the indices evaluated, PBB-N showed the best correlation with plant parameters. Based on the highest correlation of PBB-N with biological indices as well as plant responses, they proposed PBB-N as an appropriate singular of N-availability in the acidic soil of India and other regions with similar soils.

Torahi and Rai (2011), developed a methodology to map and monitor land cover changes using multi temporal Landsat TM and ASTER data. Their data classified into forestland, rangeland, water bodies, agricultural lands and residential area. The MLC algorithm was used and results evaluated by collected GCP. Results showed that image classification of Zagros mount by satellite data have good results in order to ground studies.

This research tries to increase the accuracy of Geological maps by classifying and detecting on the basis of the obtained spectra to identify geological units with the help of satellite images of Hyperion.

2. Study Area

The study area is located at the west of Iran, Lorestan province, Khorramabad city. Khorramabad is geographically located at 33 degrees, 29 minutes north latitude and 48 degrees, 21 minutes east.
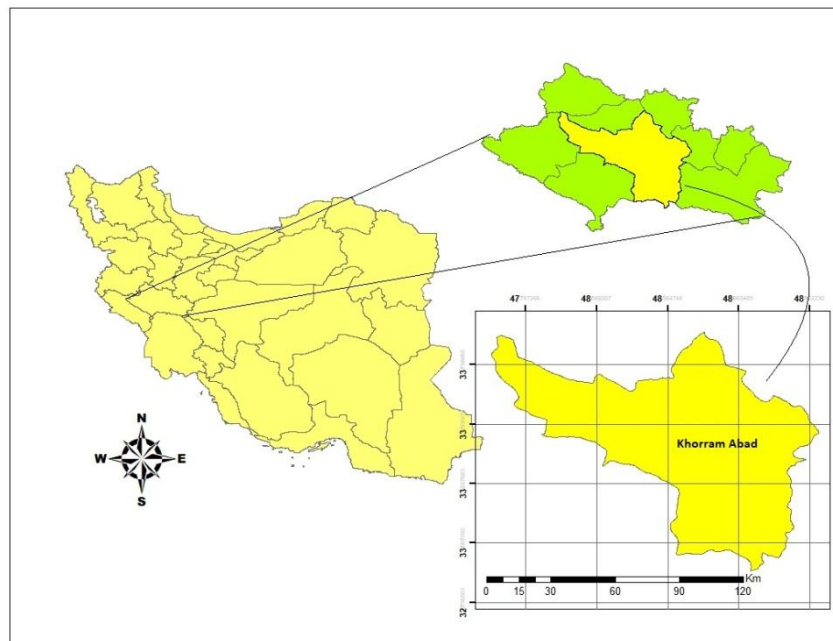
Figure1. Geographic location of study area

The sedimentary status of the province shows this fact that different parts of it during the course of time, have different geological characteristics and differentiated from each other. Therefore, considering tectonic activities and building styles of different units of age, units or sedimentary basins and types of sediments related and also magmatic and metamorphic activities of Lorestan province based on geological and structural units of Iran in two zones are as follows:

A) Zagros Zone**:** wrinkled Zagros Sub-Zone – high Zagros Sub-Zone

B) Sanandaj-Sirjan Zone

In the studied area, we describe the characteristics of the units that are outcropping in the area, including the stone units of the Gachsaran, Sarvak, Bakhtiari, Asmari, Keshkan units.

Table 1. The introduction of the most important available lithology units (studied goals) in the studied zon

No	sign	Lithology
1	PIbk	Cement conglomerate with intense alteration and slightly weathered sandstone with cross- stratification
2	Mgs	Anydrite, salt, red and gray marl of bamiyan plasters, argillite lime and limestone (Gachsaran unit)
3	Emassb	Seperated stenes of Shahbazan and Asmari Units
4	ReKn	Red conglomerate, siltstone and sandstone (Kashkan unit)
5	Ksv	Gray limestone, dolomitic lime

3. Materials and Methods

3.1. Satellite Image of EO-1 Hyperion Sensor

The image used in this study was captured in September 5, 2010, with a route number 166 and a row number 37. Its dimensions are 7.65 km wide and 185 km long. The center of this area is the coordinates of 31° 37' 00.09 "north and 47° 53' 19.11" east.

3.2. Preprocessing satellite data

The preprocessing operations required for data preparation include two general stages of radiometric correction and geometric correction. One of the corrections for Hyperion data is the correction of the spectral curvature in the image, which is due to the push broom technology of imaging has been developed in all Hyperion data (Sidine et al., 2014). Correction of this error was done by means of modulating the mean of the column in the radiative space in the ENVI software. In this method, for each single band of Hyperion data, the mean value of each column is equal to the average value of the band. Vertical stripes are other errors in Hyperion images that were repaired using the De-stripping method. The image data, which was digital, was first converted to radiance and then to reflection. The digital values of Hyperion Level 1 products were 16-bit radiants. VNIR[1] bands have a scale factor of 40 and SWIR[2] bands have a scale of 80. Thus, according to the relation, radian values for the bands of this image were corrected:

VNIRL: Digital Number/40
SWIRL: Digital Number/80

Atmospheric correction converts radian values to reflection values in pixels. Reflection information in comparison with radiance, because reflective information is relatively similar in everywhere in the world and depends on the characteristics of each substance; while radiance information is different, it is affected by various atmospheric indices. Hyperion image correction and radionuclide conversion to reflection were performed using the FLAASH[3] atmospheric correction pattern.

After radiometric correction, geometric correction was applied on the images. For geometric correction, images of ground control points such as intersections of roads and roads that were clearly visible in both the Hyperion and ALI satellite imagery were selected. After these two stages, the image was prepared for performing research methods.

---

1. Visible-near infrared
2. Short wave infrared
3. Fast Line-of-sight Atmospheric Analysis of Spectral Hypercubes

3.3. Image Processing

After performing the preprocessing and geometric and atmospheric correction, the reflection image should be entered into the processing stage and extracted the required information, which is presented below:

3.4. Select a Band

Of the 242 Hyperion spectral band used in this study, 196 are calibrated and unique. If we eliminate water absorption bands and visualize and eliminate the bands that are rich in noise, then 5 15 bands will be processed into the processing stage.

Table2. Acceptable bands which enter processing

Acceptable bands	Spectrl range
8-57	VNIR range
79	SWIR range
83-119	
133-164	
183-184	
188-1220	

3.5. Minimum Noise fraction (MNF)

The use of metaphysical data needs to reduce noise and data dimensions. The MNF conversion is considered as a noise reduction transformer. This conversion is a linear transformation used to determine the dimension and size of the image, to separate the noise from other information, and reduce the processing speed at a later stage. In this conversion, the image is first converted into two parts of noise and non-noise, and then the non-noise part is recognized as the main component and noise is eliminated (Rangzan et al., 2011).

3.6. Pixel Purity Index(PPI)

The PPI algorithm is used to find pixels that have higher purity (end pixels) in over-spectral images. For this purpose, gave 10 of the first output bands of MNF transformation, which is non-noise, as input to the PPI algorithm, and the output of this algorithm is the image that identifies the pure pixels.

3.7. Extracting the Reference Spectrum (Endmember)

Many of the classification algorithms in ultra-spectral images require the introduction of spectral features of the members (to each class or the objects that are classified or detected in the metaphysical image) to begin processing.

3.8. Extraction of Endmembers by Identifying Pure Pixels

The Endmembers were extracted from the areas where the geological unit was identified. With 4 steps of field review and field mapping and geodetic coordinates registration using a high precision GPS device and using sampling points that were matched to the pure pixels extracted from the PPI algorithm, were able to extract the reference range of the units from the image itself and this reference spectrum was used as input for classification algorithms.

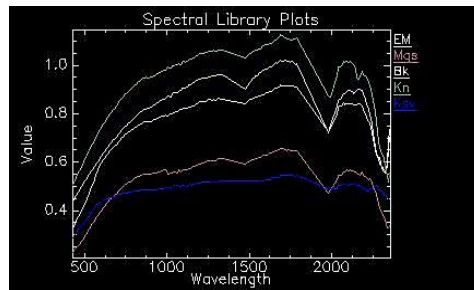**Figure 2.** The spectra extracted from the image of the geological units of the region

3.9. Ground Control Point
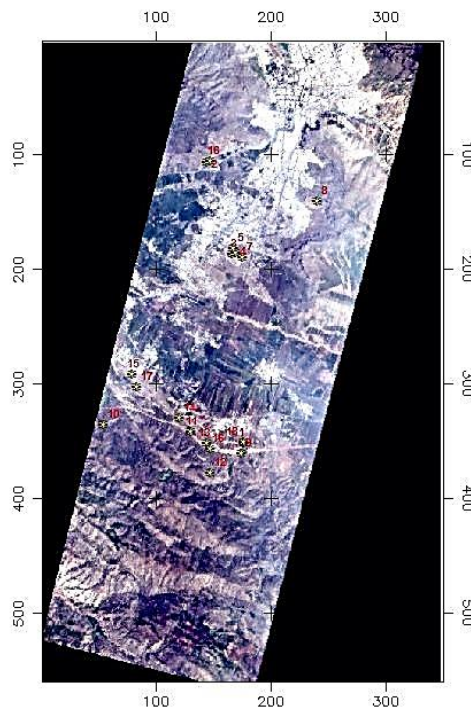
Figure 3. Location of samples taken from the study area

Table3. A number of sampling points

x	y	Zone	Formation	num
252771	252771	39	Sarvak	1
251385	3706698	39	Sarvak	2
251283	3706647	39	Sarvak	3

252558	3696929	39	Sarvak	4
252191	3703667	39	Sarvak	5
252174	3703477	39	Sarvak	6
252261	3703520	39	Sarvak	7
247732.95	3697558	39	Kashkan	8
250744.32	3697341.14	39	Kashkan	9
252493	3696589	39	Kashkan	10
251411	3696741	39	Asmari	11
248699	3699299	39	Asmari	12
250348	3697816	39	Asmari	13
251284	3696918	39	Asmari	14
251407	3695915	39	Asmari	15
248854	3698895	39	Gachsaran	16
252558	3696929	39	Bakhtiari	17
252549	3696968	39	Bakhtiari	18

4. Methods

4.1. Spectral Angle Mapper (SAM)

Spectral Angle Surveyor as a Guided Classification Method an Effective Method for Spectrum Comparison Images are relative to the standard range or reference spectrum. The algorithm of this method calculates the similarity between the two spectra by the spectral angle between the two. In fact, by transforming the spectra into a vector in space, the size of the number of bands, the angle between the two vectors is calculated. In this method, for calculating the angle, the direction of the vectors is important and not their length, and therefore the pixel brightness does not affect its classification. The angle between 0 and 1 if be low, the more accurate it will be. If the angle is one, the entire image is identified as the phenomenon. For example, to compare a pixel, the desired pixel spectrum with the same pixel spectrum is plotted between the reference spectra on two bands in a coordinate axis. The resulting points are then drawn to the origin and the angle between the two resulting lines is known as the pixel identification angle. To obtain the angle α between two vectors

$$\alpha = \cos^{-1}\left[\frac{\vec{r}.\vec{t}}{\|\vec{r}\|.\|\vec{t}\|}\right]$$

(2)

That way, it can also be written

$$\alpha = \cos^{-1}\left[\frac{\sum_{i=1}^{nb} t_i\, r_i}{\left[\sum_{i=1}^{nb} t_i^2\right]^{\frac{1}{2}}\left[\sum_{i=1}^{nb} r_i^2\right]^{\frac{1}{2}}}\right] \tag{3}$$

In this formula:

nb: number of bands t_i: spectrum tested r_i: reference spectrum

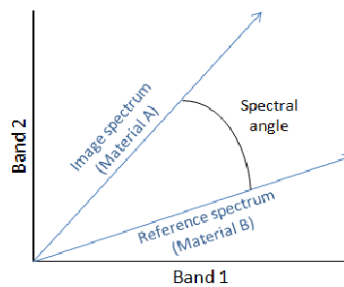**Figure 4.** The spectra of the tested spectrum and the standard range in the SAM process

The most important advantage of the SAM algorithm is its simplicity of structure and rapid use to display the spectral similarity between the image spectrum and the reference spectrum. The classification problem using this algorithm is not considering the problem of mixed pixels(Fahimnejad et al., 2007).
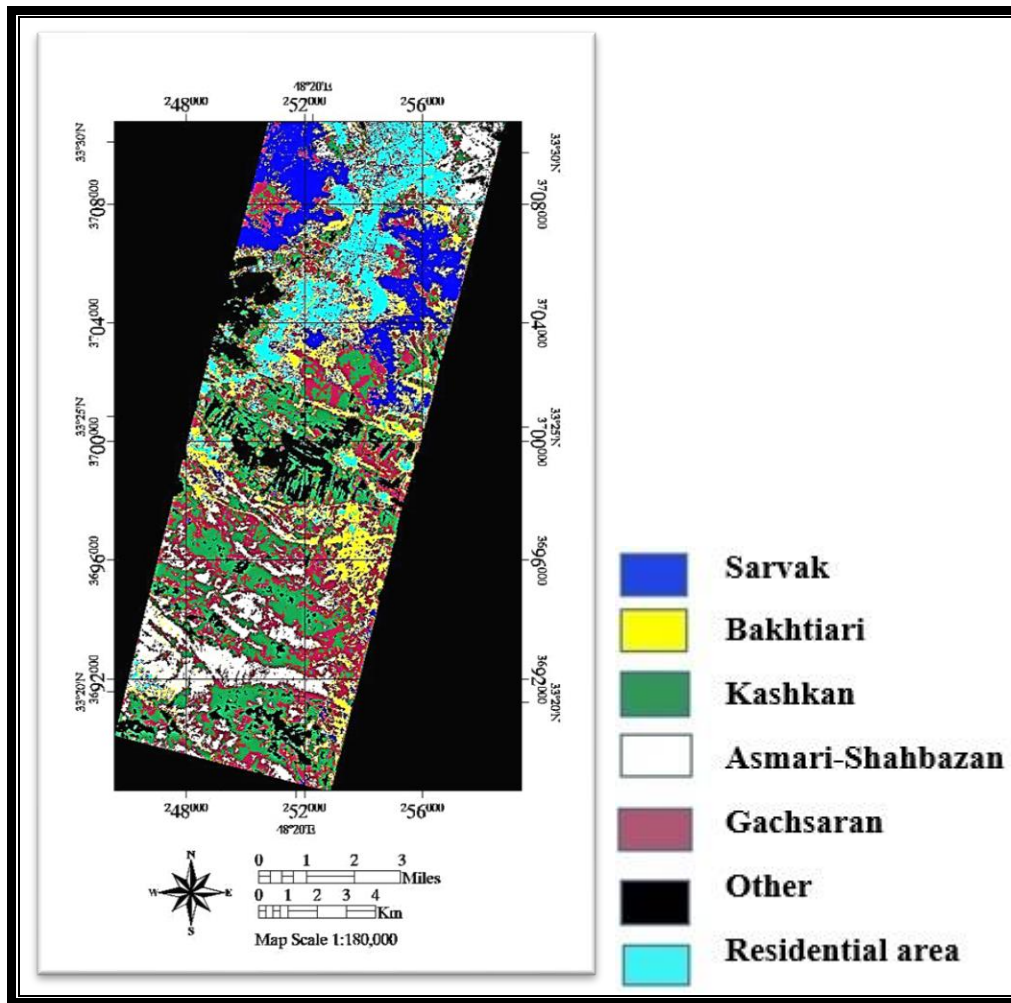
Figure 5. Classification result with SAM algorithm

4.2. Support Vector Machine (SVM)

Support vector machine is a useful technique for data classification(Abbasi et al., 2015). A classification task usually involves separating data into training and testing sets. Each instance in the training set contains one "target value" (i.e. the class labels) and several "attributes" (i.e. the features or observed variables). The goal of SVM is to produce a model (based on the training data) which predicts the target values of the test data given only the test data attributes(Wei Hsu et al., 2003).

Given a training set of instance label point $(x_i, y_i), i = 1, ..., l$ where $x_i \in R^n$ and $y \in \{1, -1\}^l$, the support vector machine(SVM) require the solution of the following optimization problem:

$$\min_{w, b, \hat{I}} \frac{1}{2} w^T w + C \sum_{i=1}^{l} \hat{I}_i \qquad \text{Subject to } y_i (w^T f(x_i) + b) \geq 1 - \hat{I}_i , \qquad (4)$$

$$\hat{I}_i \geq 0.$$

Here training vectors x_i is mapped into a higher (maybe infinite) dimensional space by the function ϕ. SVM finds a linear separating hyperplane with the maximal margin in this higher dimensional space. $C > 0$ is the penalty parameter of the error term. Furthermore, $K(x_i, x_j) = f(x_i)^T f(x_j)$ is called the kernel function. Though new kernels are being proposed by researchers, beginners may find in SVM books the following four basic kernels:

- Linear: $K(x_i, x_j) = x_i^T x_j$.

- Polynomial: $K(x_i, x_j) = (g\, x_i^T x_j + r)^d, g > 0.$

- Radial Basis Function(RBF): $K(x_i, x_j) = \exp(-g\, //x_i - x_j//^2), g > 0.$

- Sigmoid: $K(x_i, x_j) = \tanh(g\, x_i^T x_j + r).$

Here, γ, r are kernel parameters.

σ	C	Maximum precision(%)
≥0/001	100-200	62/57
0/005	100-200	81/70
0/01	100-200	59/96
0/05	100-200	63/01
0/1	100	55/78
	200	61/54
	200-2000	52/85
≥0/5	100-200	76/92
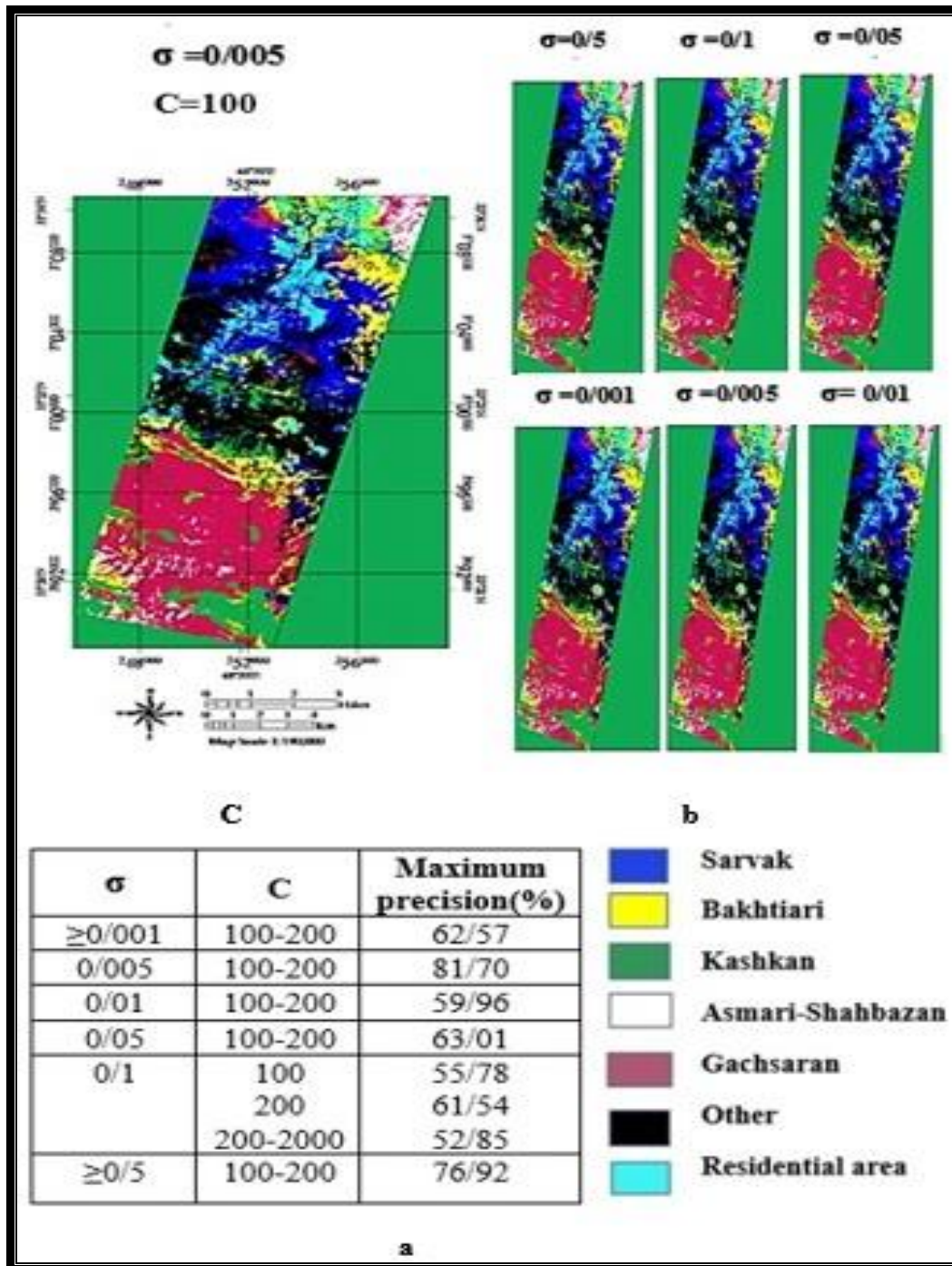
Figure 6. (a)Validation results for obtaining the best values of the SVM variables are σ and C .Maps of geological units of the region Studies for: (b) optimal amounts; and (c) varying amounts of variables

5. Results And Discussion

After compilation of classified pictures, to assess the accuracy of each method, the GPS points taken by ground observations were used as ground maps to determine the accuracy of the error matrix, the accuracy of classification in each method, and ultimately the best way to estimate the geological map of the units Introduced. The results of a health assessment are usually presented as an error matrix, whereby a variety

of parameters and values representing accuracy or some kind of error in the results are extracted from this matrix. This matrix is the result of a comparison of the pixels to the pixels, the pixels defined with the corresponding pixels in the classification results. In the error matrix, land data in the columns and data related to the classification results are given in the rows of this matrix. The numbers on the matrix's main diameter indicate the number of pixels whose labels match the two sets of data or, in the other hand, the number of pixels that are correctly categorized over this diameter. Non-diagonal elements are the set of errors. Based on the error matrix, several parameters are extracted for accuracy and error.

In this study, the results of the evaluation are presented as general and Kappa coefficients; the overall accuracy is the average of the accuracy of the classification, which represents the ratio of the correct pixels classified to the total of the pixels in question. The Kappa coefficient calculates the classification accuracy in a completely randomized manner, which means that the kappa gives the classification accuracy as compared to the state of a completely randomized image (Richard, J.A, 1995).

$$O.A = \frac{\sum_{n=1}^{c} E_{ii}}{N} \times 100 \tag{5}$$

C: number of classes

N: total number of pixels determined

Eii: Diameter members of the error matrix

The ratio of the calculation of this coefficient is as follows:

$$k = \frac{N \sum_{i=1}^{r} x_{ii} - \sum_{i=1}^{r} (x_{i+} * x_{+i})}{N^2 - \sum_{i=1}^{r} (x_{i+} * x_{+i})} \tag{6}$$

In this case, N is the total number of pixels of the ground plane, $+ xi$ the sum of the elements of the row i and $+ i$ is the sum of the elements of column i.

These algorithms were compared and verified in the classification of ultra-spectral images. The SVM algorithm has the highest accuracy (overall accuracy of 70/81 percent and kappa coefficient of 72/0) in classification and SAM algorithm with high accuracy (overall accuracy of 68/83 percent and Kappa coefficient was 0.49) but less than SVM algorithm. One of the influential issues in the SVM results is to allocate appropriate values to its variables, which was used for mutual validation.

The results showed that, by assigning optimal values to the variables c and σ, SVM has a high ability to classify the geological units of the region. However, the inappropriate values of these variables can greatly affect the classification accuracy.

After determining the optimal values for the variables c and σ, these values were used for SVM training. Finally, the SVM was trained to classify the study area. Because of the wide range of variable c as desirable values of 200-1000, and yet, the results are not very large, the only geological maps of the region for the values of c = 100 and 005 / σ = 0 are shown in Fig. 13-13 (b). Is.

Table 4. Error matrix, general accuracy, and kappa coefficients for the results of the SAM algorithm

Class	Ground data (experimental pixels)						
	Sarvak	Gachsaran	Asmari	Kashkan	Bakhtiari	Residential	**Full pixels**
Not classified	0.44	1.40	1.40	0.00	4.24	1.35	0.86
Sarvak	79.96	3.17	0.45	0	8.93	3.71	54.95
Gachsaran	2.88	31.81	9.75	17.47	12.75	1.05	9.18
Asmari	6.08	4.42	71.27	0	17.13	1.1	3.83
Kashkan	0.00	0.85	0	55.08	5.08	0	4.27
Bakhtiari	5.57	11.66	11.82	1.01	56.93	4.9	11.91
Residential	3.71	1.05	1,10	0	4.90	93.31	4.80
others	3.34	22.89	0	34.74	6.76	0	10.2
Full pixels	100.00	100.00	100.00	100.00	100.00	100.00	100.00
Kappa coefficient: 0.49				Total accuracy: 68.83			

Table 5. Error matrix, general accuracy and kappa coefficient for the results of the SVM algorithm

Class	Ground data (experimental pixels)						
	Sarvak	Gachsaran	Asmari	Kashkan	Bakhtiari	Residential	**Full pixels**
Not classified	0.00	0.00	0.00	0.00	0.00	0.00	0.00
Sarvak	69.17	0.01	0.00	0.39	0.00	0.00	24.75
Gachsaran	3.35	95.20	39.23	0.78	5.07	0.00	49.72
Asmari	0.03	4.74	59.83	3.29	11.66	0.00	8.86
Kashkan	0.02	0.00	0.20	89.53	1.01	0.00	2.03
Bakhtiari	7.70	0.05	0.75	4.07	81.08	0.00	4.93
Residential	3.21	0.00	0.00	0.19	0.84	100.00	2.15
others	۱۶٬۵۱	0	0	1.75	0.34	0	7.56
Full pixels	100.00	100.00	100.00	100.00	592	100.00	100.00
Kappa coefficient:0.72				Total accuracy:81.70			

The evaluation of the results of this study shows that the mapping of geological units mapped using SAM and SVM algorithms was carried out using maps previously provided by Geological Survey of Lorestan province and Geological Survey

The country that provided the fact that the SVM algorithm with a general accuracy of 81.70% and a kappa coefficient of 0.72% were more accurate than the SAM algorithm with a total accuracy of 68.63% and a coefficient of 0.44%, respectively(Table 3 and 4). Also, the results show that the SVM algorithm, taking into account the regional conditions, is an effective method for classifying the region based on existing geological units in geological mapping research. Due to the large capability of images in the resolution of phenomena, it is shown that the identification and separation of geological units using these images is easier and more accurate than other methods, such as the use of multidimensional images.

Table 6. Area of geological units using the algorithm used

Algorithm / Formation	SAM	SVM
Sarvak	2304,09	2523,69
Gachsaran	4387,32	4447,44
Asmari	1699,47	762,39
Kashkan	1984,59	16257,42
Bakhtiari	2371,05	1793,25

According to the results of calculating the area of different formations in the study area (see 5), the Kashkan Formation has the highest calculated area by the SVM class and Gachsaran Formation with the highest calculated area in the SAM classification method.

The accuracy of the detection of Sarvak, Gachsaran, Asmari, Kashkan and Bakhtiari formations by SAM and SVM algorithms is shown using the results of tables (4), (5) in the chart 6.
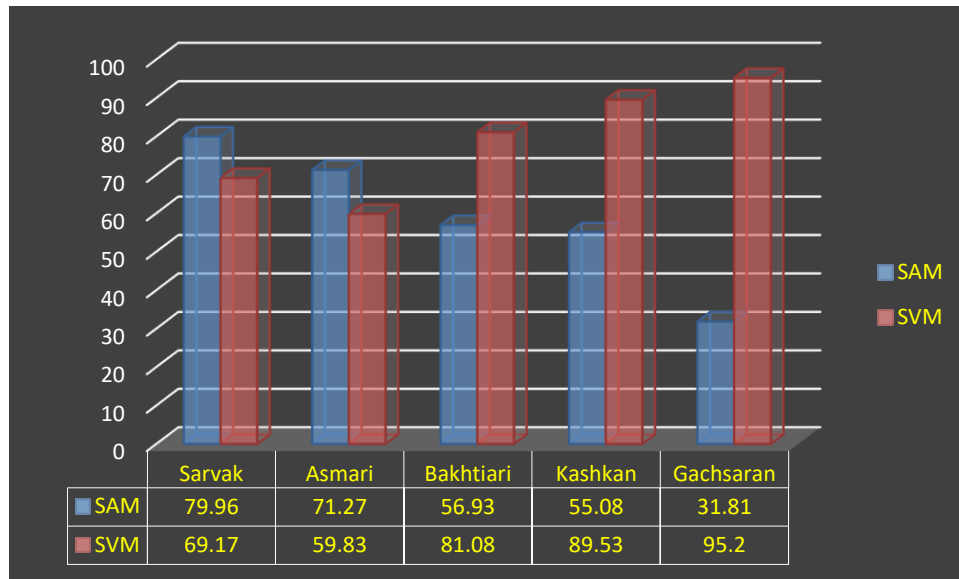

	Sarvak	Asmari	Bakhtiari	Kashkan	Gachsaran
SAM	79.96	71.27	56.93	55.08	31.81
SVM	69.17	59.83	81.08	89.53	95.2

Figure 7. Comparison of the accuracy of the different formations detection by classification algorithms

It is suggested that in future investigations, more powerful geodetic sensors than Hyperion (with a pixel size of 30 meters) are used to identify valuable geological units in order to produce higher precision maps.

6. Conclusion

The geological mapping over the years and extensive studies and studies has already reached the point that, instead of being in the field and doing fieldwork and spending a lot of time and money, using the

science of measuring and using metaphysical images in It can be done in a short time and with high precision.

In this research, SAM and SVM algorithms were used to identify geological units. One of the most important factors in the target's detection that affects the final evaluation of the algorithms is the choice of the threshold value that was determined by trial and error in this study. For better identification of geological units, we used MNF, PPI based on SVM and SAM composite. SVM classifier because of its kernels that used, has a better results. It may be its inner principal and its capabilities for identification of complex units. Because of SVM save boundaries of clases as well as, so it is usefull for classification and extraction of geological units. In this classification, in compariosion of SAM classifier that only uses of spectral similarity method for classes distinguishing, information of spectral and pixel location are key factors to pixels label.

References

Abbasi, B., Arefi, H., Bigdeli, B., & Roessner, S. (2015). Automatic generation of training data for hyperspectral image classification using Support Vector Machine, *36th International Symposium on Remote Sensing of Environment*, Berlin, Germany.

Blackburn, G, E. (2007). Hyperspectral remote sensing of plant pigments, *Journal of experimental botany*, Vol (58), pp. 855-867.

Bordoloi, L, J., Singh, A, K., Kumar, M., Patrisam., & Hazarika, S.(2013). Evaluation of nitrogen availability indices and their relationship with plant response on acidic soils of India, *Plant soil environ*, Vol(59), pp. 235-240.

Hsu, C, W., Chang, C. C., & Lin, C, J. (2003). A practical guide to support vector classification.

Torahi, A, A., & Rai, S, Ch. (2011). Land Cover Classification and Forest Change Analysis, Using Satellite Imagery - A Case Study in Dehdez Area of Zagros Mountain in Iran. *Journal of geographic information system*, Vol (3), pp. 1-11.

Fahimnejad, H. (2007). Resolution evaluation of Agriculture Products by Remote Sensing Data (Hyperion hyperspectral sensor). *M.A thesis*, *surveying college.Khaje Nasiraldin Tosi University*.

Kurtz,T,H., Buckley,S,J., & Becker,J,K.(2017). Hyperspectral imaging: a novel geological mapping technique for subsurface construction sites. *Proceeded of the world tunnel congress 2017*. Surface challenges, Bergen. Norway.

Rangzan, K., Saberi, A., Jokar, E., & Mohamadian, F (2011), Identification and Estimation of Area under Cultivation of Agriculture land by Hyperion sensor data, *Geometric Conference 90*.

Ramakrishnan, D., & Bharti. R. (2015). Hyperspectral remote sensing and geological applications. *Current science*.No.5, pp.879-891.

Seyyedin, A. Oil (hydrocarbon) span detection by detection methods in hyperspectral mages. *M.A thesis. Remote Sensing, GIS*, Tehran University.

Sharifi, A, R. (2008). Classification of Hyperspectral Images by Analyzing Spectral Signatures of Phenomena. *Master's Thesis, Field Student, and GIS*, Tehran University.

Alvipana,S.K (2013). "application of Remote Sensing in Geology" 4[th]version, Tehran. Tehran press. Hypersp». Scientific promotional *journal.Oil and Gas Detection & protection*.No.111, p.6-690.

Camps-Valls, G., Tuia, D., Bruzzone, L., & Benediktsson, J. A. (2014). Advances in hyperspectral image classification: Earth monitoring with statistical learning methods. *IEEE Signal Processing Magazine*, 31(1), 45-54.

Chang, C,I. (2003). Hyperspectral Imaging: Techniques for spectral Detection and Classification, Orlando. FL:Kluwer Academic.

Hasani Moghaddam,H., Torahi,A,A., & Zeaiean Firooz Abadi.P.(2019). Using discrete wavelet transform to increase the accuracy of hyperspectral and high resolution images fusion. *Jrors journal*, 1,pp. 22-30.

Chen, X., Warner, T. A., & Campagna, D. J. (2007). Integrating visible, near-infrared and short-wave infrared hyperspectral and multispectral thermal imagery for geological mapping at Cuprite, Nevada. *Remote Sensing of Environment*, 110(3), 344-356.

Oommen, T., Misra, D., Twarakavi, N. K., Prakash, A., Sahoo, B., & Bandopadhyay, S. (2008). An objective analysis of support vector machine based classification for remote sensing. *Mathematical geosciences*, 40(4), 409-424.

Rajendran, S., Srinivasamoorthy, K. and Aravindan, S. (2007). Mineal exploration: recent strategies. *New India Publishing*, 528.

Richards, J. A., & Jia, X. (1999). Remote Sensing Digital Image Analysis–Springer. Berlin, Germany.

Shrestha, D. P., Margate, D. E., Van der Meer, F., & Anh, H. V. (2005). Analysis and classification of hyperspectral data for mapping land degradation: An application in southern Spain. *International Journal of Applied Earth Observation and Geoinformation*, 7(2), 85-96.

Relationship between Land Cover Use and Urban Thermal Islands by Landsat 8: Case study of Sanandaj

Loghman Rahimi[a]*

[a] *Master of Remote Sensing and Geographic Information Systems, Yazd branch, Islamic Azad University, Yazd, Iran.*

Abstract

Increasing population (including natural increasing and migration) and rapid industrial growth are the main reasons of global climate change. Today, the most significant problem in urban areas is the increase in surface temperature due to changes in natural levels. In urban areas, depending on the type of land and vegetation used, areas with different temperatures develop from other areas. In this research, to answer the question that how different types of the urban usage affect the creation of high temperature areas with the aim of understanding the temperature difference between different regions of the city and the surrounding area in order to provide a thermal island map in Sanandaj, discharge and surface temperature in Sanandaj was estimated using Landsat 8 satellite data by Jenks method in summer and autumn. For this purpose, Envi and ArcGIS software were used, and finally, changes in surface temperature were evaluated in comparison with land uses, and the user role in the creation of surface temperature was determined. The results showed that wasteland, industrial and urban facilities have the highest temperature and commercial and green space has the lowest temperature. Thus, the influence of urban utilization in the emergence of current thermal conditions in Sanandaj indicates the relationship between the type of user and surface temperature.

---

* *Corresponding author Tel:* +98-9148433380.
E-mail address: loqman.rahimi@yahoo.com

1. Introduction

Nowadays, Urbanization has flourished, and this has led the Earth to be affected by various issues, loss in natural condition to a large extent, one of the consequences of which is the rise in temperature. With urban expansion after the 1930s, especially after World War II, local climate change appeared in urbanization (Bahreini, 1992). In the twentieth century, urbanization took place at a global scale. According to UN estimates, nearly half of the world's population lives in cities. In Western societies, it is higher than 75% (UN, 1999). The most important problem in urban areas is the increase in surface temperature due to changes occurring at natural levels, uncontrolled growth of cities, especially big cities, due to the natural urban population growth, the increase of rural migration, etc. They sought to increase the environmental degradation and the increasing number of contaminations (Wairmn yazdi, 2000). Urbanization has altered all kinds of land cover in urban areas, which has led to the formation of distinct urban weather (Rose.et al., 2009). Urban heating is one of the most well-known forms of local manipulation of the climate by mankind, so that changes in the use of land cover in urban areas can lead to an increase in urban temperatures relative to air temperatures in rural areas. Earth surface temperatures can provide useful information on the physical properties of land and climate that plays a significant role in environmental processes (Weng et al., 2004). The thermal island effect was first observed in London and other European cities in the 1930s, followed by cities such as New York and Chicago. The phenomenon is now an important environmental phenomenon, and wherever there are large cities, there is thermal island effect (Yamamoto, 2006). Urban areas are warmer than their surrounding countryside, for two reasons: First, the city's structure and morphology has the potential for absorbing and storing pure solar radiation, especially in the calm and smooth summer weather. This leads to overnight warming in the city center (business district) and the formation of a thermal island in the summer. The business center of big cities can be 6 to 8 degrees centigrade warmer than their suburbs. Second, large thermal islands are caused by the release of heat by human activities caused by processes such as fuel (especially in metropolises during winter). In addition, smoke and vapor coatings reduce the loss of heat by night-time wavelengths in urban areas, and consequently the greenhouse effect is exacerbated (Alavi panah, 2008). Due to the presence of suspended particles, the city receives less sun than the rural areas and is, however, warmer than neighboring rural areas. Because the city's environment, due to the heat generated by the use of fossil fuels, and because of the impermeable levels and high buildings, acts as a heat collector, resulting urban heat island is formed in the city. The specification of the city's thermal island increases the difference between the temperature of the city and its adjacent rural areas. The city is weathered by climate, local wind patterns, cloud and fog development, and rainfall rates, and in some cases leading to diseases such as asthma and respiratory diseases. Several important factors affect the thermal behavior of urban areas:

1. Physical properties of various components of urban areas
2. Geometric shape of the ground
3. Weather conditions

Research by the Lawrence Berkeley National Laboratory in Berkeley, California on the summer days in Los Angeles, the temperature rises to a degree Fahrenheit, increases the risk of mascara up to 3% (noak, 2000). The haze of smoke or surface ozone (in contrast to the ozone that protects the earth against ultraviolet radiation) is invisible pollutants which can permanently damage the lungs (Mhrgan, 2013).

Plant growth season in urban areas is fifteen days longer than rural areas and in addition to the effect of temperature, it produces secondary effects, such as local wind, cloud and fog, and accelerated precipitation. Likewise, building materials during the day store large quantities of thermal energy and it returns during the hours of the night. This process will delay the natural process and cool the city air; and the negative aspects that are very important are the studies that emphasized the impact of island heat on residents and urban life among the co-authors of Subrino, studying the thermal island of Madrid, assessed its role on thermal comfort throughout the day and night. Sue et al. determined the relationships between land cover and surface temperature on urban Thermal Island and its effects on population and showed that the city's thermal island was underestimated by the global model and the risk of disease has increased urban populations (Alavi panah, 2006).

The warming of the urban environment calls the steady rise of "thermal islands" steadily throughout the world and has created a difficult environmental situation for urban residents. Therefore, it is important to recognize these processes and make the appropriate decision for urban management (Nakamura, 2002). The thermal island in the cities can add a lot of heat to the city due to high thermal capacity of building materials,

industries, vehicles and thermal baths, air pollution, high-rise buildings and towers create heat exchange problems (Azizi, 2014). Urban thermal islands, in addition to the above, arise from the destruction of forests and the change in the surface cover of the surface to evaporated surfaces, such as asphalt and pavement (Alavi panah, 2006).

Thermal island studies are in the field of applied geography and climate (Alijani, 1992); which this research is seeking to know. Due to the irregular structure, it increases the energy consumption and doubles the temperature in the urban environment. Among the positive effects of heat island, the use of fossil fuels for heating homes during winter season and the growth of plants is due to increased food production in these areas (Soltaninjad, 2017). The study of the first urban thermal island was carried out using air temperature measurements of mobile and fixed urban stations based on ground data. However, the use of remote sensing data to estimate surface temperature is a relatively new method that greatly reduces the estimation cost of classical temperature (Miryaqobzadeh, 2009).

Remote sensing images due to extensive coverage, timelines and the ability to obtain information in the thermal range of the electromagnetic spectrum are a good source of information for the preparation of thermal maps and the estimation of surface radiation energy. Also, these images have different uses in the global analysis of land cover coverage of urban levels. Using these images, with proper resolution, urban thermal islands can be illustrated in different continental and regional scales, and quantitative data from the characteristics of the Earth's surface are generated by heterogeneous distribution, which results in a better understanding of urban and non-urban environments and urban temperature (Shakiba et al., 2009).

In order to generate a policy to reduce the thermal island, it is important to understand the relationship between the type of land cover and the formation of urban thermal. Remote sensing data from satellites and planes can provide infrared images through which surface temperatures can be extracted and linked to land cover and land use patterns (Mhrgan, 2013). Vegetation areas are colder than other urban areas during the day, while at night the vegetation is relatively warm. A low surface temperature during the day is due to the latent heat loss due to daily evapotranspiration (Alavi panah, 2008). The use of satellite data is a good way to prepare land cover map and it's monitoring - especially in large geographic areas (Yuan et al., 2005). Today, it is known that thermal data can complement other remote sensing data (reflection data) (Alavi panah, 2008). Thermal sensors are capable of recovering the islands of the terrestrial surface by recording the thermal radiation exerted from the surface of the areas in the sensory field of view (Balling and brazell, 1988). The study of this phenomenon and its mechanism or mechanism for urban planning are very important. Over the past two decades, there is a need for land surface temperature data for environmental studies and land resource management activities has identified the centers of thermal islands and the type of pollutants as one of the important scientific issues for their adjustment and control (Miller, 2011). By carrying out this research and its results, it can be used to understand the temperature data using geographic resources and instruments (GIS) and remote sensing methods. Their analysis is to identify places and determine higher temperatures points in the city and their contributing factors, as well as the optimal location of utilities, including polluting industries and urban transport systems, etc., by taking appropriate measures (Marofnjad, 2010).

During the process of industrialization of Iran, along with all parts of the world, the industrialization process has not been abandoned and the effects of population growth and industrialization in large cities of Iran have caused a lot of thermal islands, which requires a lot of research. Therefore, this research also investigated the relationship between the use of land cover and urban thermal islands using the Landsat 8 in Sanandaj city which gives a more precise results.

Hypotheses:
- There is a relationship between the types of uses in the city (case study) formation of thermal regions,
- There is a relationship between the green space and the average temperature,
- There is a relationship between industrial use and its average temperature.

Research purposes:
- To signify the temperature difference of regions and the surrounding area in Sanandaj and to determine the critical temperature areas,
- To determine the relationship between type and temperature at the city level,
- To determine of the effect of land cover and land use type on the surface temperature of the city.

2. Materials and Methods

In this research, different data sources, including Landsat 8 satellite imagery, urban land use map and temperature data from meteorological stations were used. Also, various software were used to correct and prepare the data and implement the techniques.

2.1. Data Used

2.1.1. Landsat Satellite Image 8

Table 1. Specifications of Landsat Satellite 8 images used in research

Satellite	Pass number	Row number	Year	Month	Day	Season
Landsat 8	167	35	2017	June (6)	28	Summer
Landsat 8	167	35	2017	December (12)	5	Fall

In this study, Landsat 8 satellite imagery, 167 and 35th row, were used on June 28 (7th of July) and December 5th (December 14th) in 2017. Some of the specifications with this satellite are summarized. The satellite, originally called LDCM, is a product of NASA and the United States Geological Survey (USGS).

With the retirement of Landsat 5 in early 2013, Landsat 7 was the only satellite on the orbit of the Landsat Satellite series Landsat 8 will receive continuous data and will ensure the availability of Landsat data using two sensors, one OLI imaging sensor and another infrared thermal sensor (TIRS). The two sensors collect image information for nine bands and two bands of thermal wavelength, respectively. Landsat 8 takes about 400 images a day, which has increased significantly in Landsat 7 compared to 250 images a day. Landsat 8 has a number of special features compared to the previous Landsat sensor:

OLI and TIRS sensors improve the signal-to-noise ratio (SNR) in radiometric performance, and as a result of this 12-bit data quantification, these more bits can better describe the ground cover.

1. In Landsat, the 8 Earth Field Imaging Device (OLI) uses the Push Broom system, which makes it more sensitive, less moving parts and better ground information.

2. The existence of two new spectral bands, the Blue Coastal band and the short infrared cirrus band, it allows specialists to measure the quality of water as well as high and thin clouds.

3. By registering TIRS data with OLI data, 12-bit Landsat 8 products will be produced Geometric, radiometric and terrestrial corrections have been applied to them. The table below shows the characteristics of the spectral bands of the OLI and TIRS sensors.

Table 2. Specifications of OLI Spectral Bands (NASA site)

Resolution	Wavelength	Spectral band
meters 30	Micrometer 0.433–0.453	Band -1- Band Coastal / Aerosol
meters 30	Micrometer 0.45- 0.515	Band 2 - Blue
meters 30	Micrometer 0.525 –0.60	Band 3- green
meters 30	Micrometer 0.63 – 0.68	Band 4 - Red
meters 30	Micrometer 0.845-0.885	Band 5 - Near Infrared
meters 30	Micrometer 1.56 –1.66	Band 6 - Infrared short wavelength
meters 30	Micrometer 2.100 – 2.300	Band 7 - Infrared short wavelength
meters 30	Micrometer 0.58-0.680	Band8-Panchromatic
meters 30	Micrometer 1.360 – 1.390	Band9-Cirrus

Table 3. Specifications of TIRS Spectral Bands (NASA site)

Resolution	Wavelength	Spectral band
meters 100	10.30 – 11.30	Band 10 - Infrared wavelength band
meters 100	11.50 –12.50	Band 11 - Infrared wavelength band

2.2. Application Used

In addition to general office software, the software uses various image processing and geographic information systems including Arc GIS, Envi 5 software.

2.3. Research method

The stages of this research work, the preparation of required data, heat image and thermal image of Sanandaj city. The role of topographic factors on thermal islands and ultimately determining the contribution of each urban application to the formation of thermal islands.

2.3.1. Preparing Data

2.3.1.1. Geometric Corrections

The Landsat 8 image, L1TP level, was presented in the GEOTIFF format, in which accurate geometric corrections were made and reference ground. There is no need to correct it.

2.3.2. Provide Thermal Map of TIRS Sensor Data

To prepare the thermal map, the 30-meter Band 10 at Nadir was used to study and determine temperature differences among complex urban phenomena and effective analysis of the urban climate. The image with a good atmospheric conditions, in the middle of the warm and cold season, allows us to compare the thermal islands. Since this study emphasizes on the differences in temperature among different phenomena and the extraction of information in the homogeneous spatial range taken at an atmospheric point of view, the sensor illumination temperature can be used to obtain surface temperature. The steps of preparing the surface temperature image are shown in Figures 1 and 2.
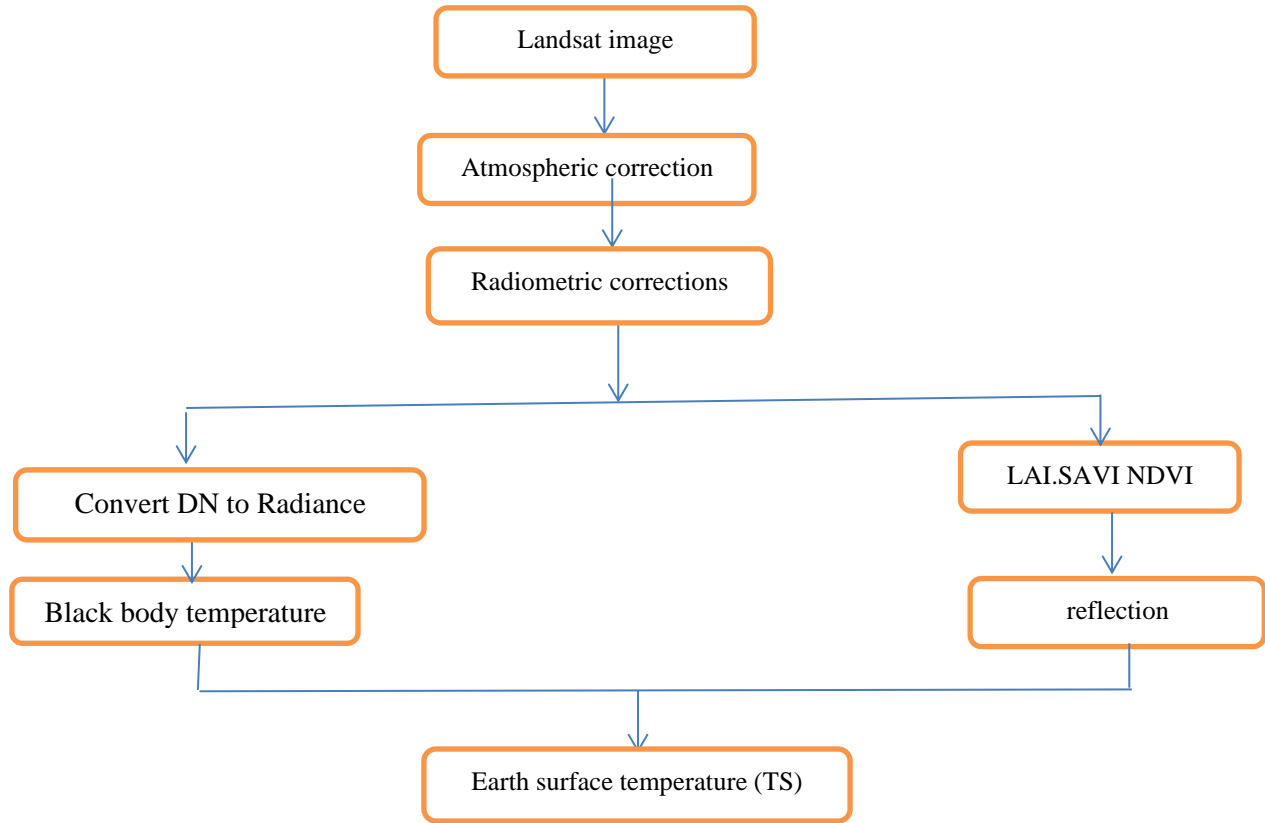
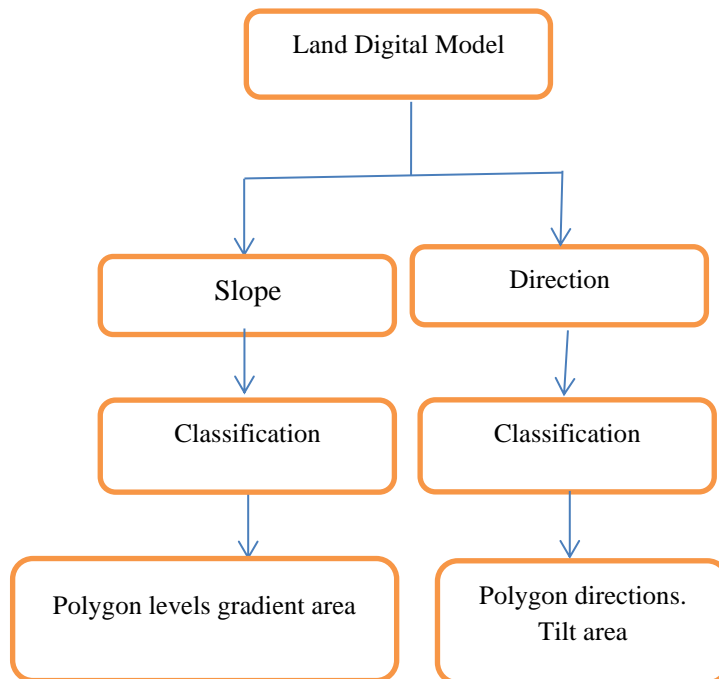Figure 1. Land surface temperature calculation process for Sanandaj

Figure 2. Steps for creating gradient and slope directions

2.3.2.1. Fluid Method for Calculating Surface Temperature

In this method, surface temperature is obtained by using corrected thermal radiations (Aleen et al., 2002). To calculate the corrected thermal radiance, there is a need to release the thermal bond. To calculate the emission in the thermal band, it is necessary to calculate the spectral radiance (λL), reflection in each band (λL) and Albudo is superficial.
Spectral Radiation (λL)
Spectral radius is the radiation emitted from the atmosphere by the detector. The radius of watts per square meter is in micrometers. Spectral radii for each band are obtained by relation (1) (Aleen et al., 2002):

$$L\lambda = \text{Gain*DN+Bias} \qquad (L_{max} - L_{min})/65535 = \text{Gain(1)}$$

DN = Grayscale pixels

$L_{min} = \text{Bias}$

Lmax and Lmin values (the maximum and minimum detectable spectral radii of any band by the sensor)
For OLI and TIRS sensors using the reference file, see Table 4.

Table 4. Highest and Lowest Detectable Radians in each band by Landsat 8

Band	Radiance - max	Radiance - min
1	755.65753	-62.40244
2	770.57178	-63.63407
3	705.58380	-58.26734
4	597.58630	-49.34887
5	362.62201	-29.94544
6	91.36265	-7.54476
7	29.72010	-2.45430
8	673.14319	-55.58838
9	149.01643	-12.30583
10	22.00180	0.10033
11	22.00180	0.10033

In this study, Landsat 8 satellite imagery, passage 167 and row 35, dated on June 28th and December 5th, 2017, were used. First, in all bands, the study area was sub-divided and stored (Figure 3 and 4).
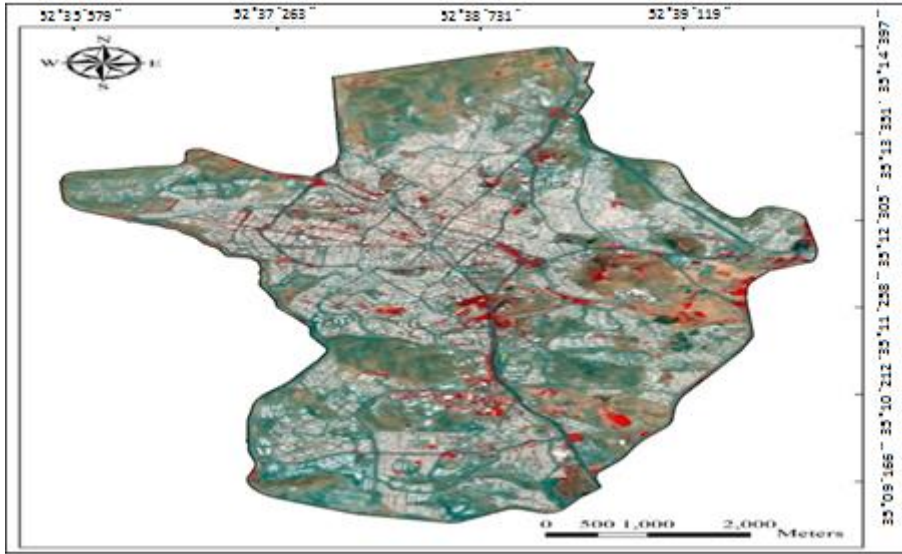
Figure 4. Landsat 8 satellite image from Sanandaj, date 5.12.2017, color combination of bands 5-4-3

2.3.2.2. Investigating the Relationship between Ground Temperature and Urban Usage

In order to investigate the role of each application in the creation of thermal islands and to increase the temperature of the earth surface, the static zoning command was used in the GIS environment. Figures 5 and 6 shows the average temperature of each runway in Sanandaj.
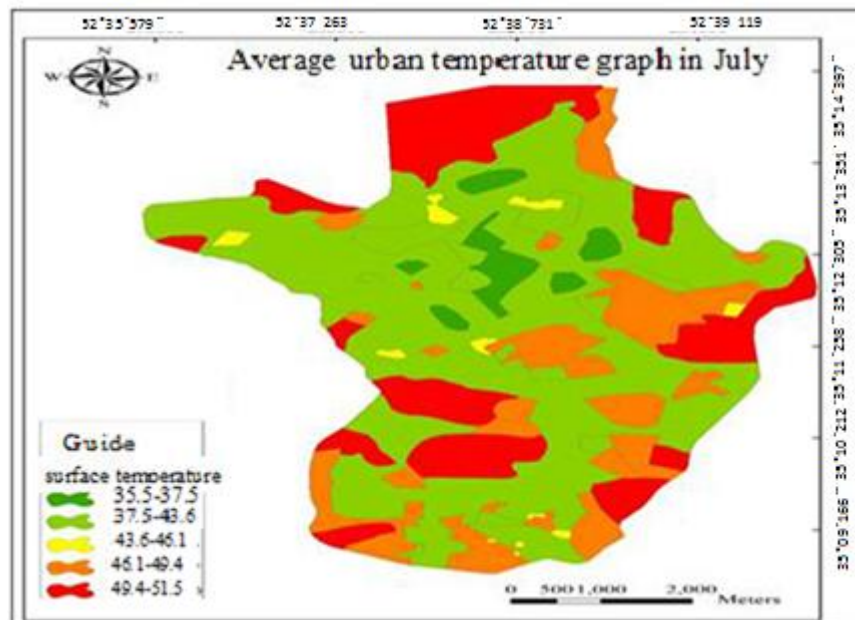

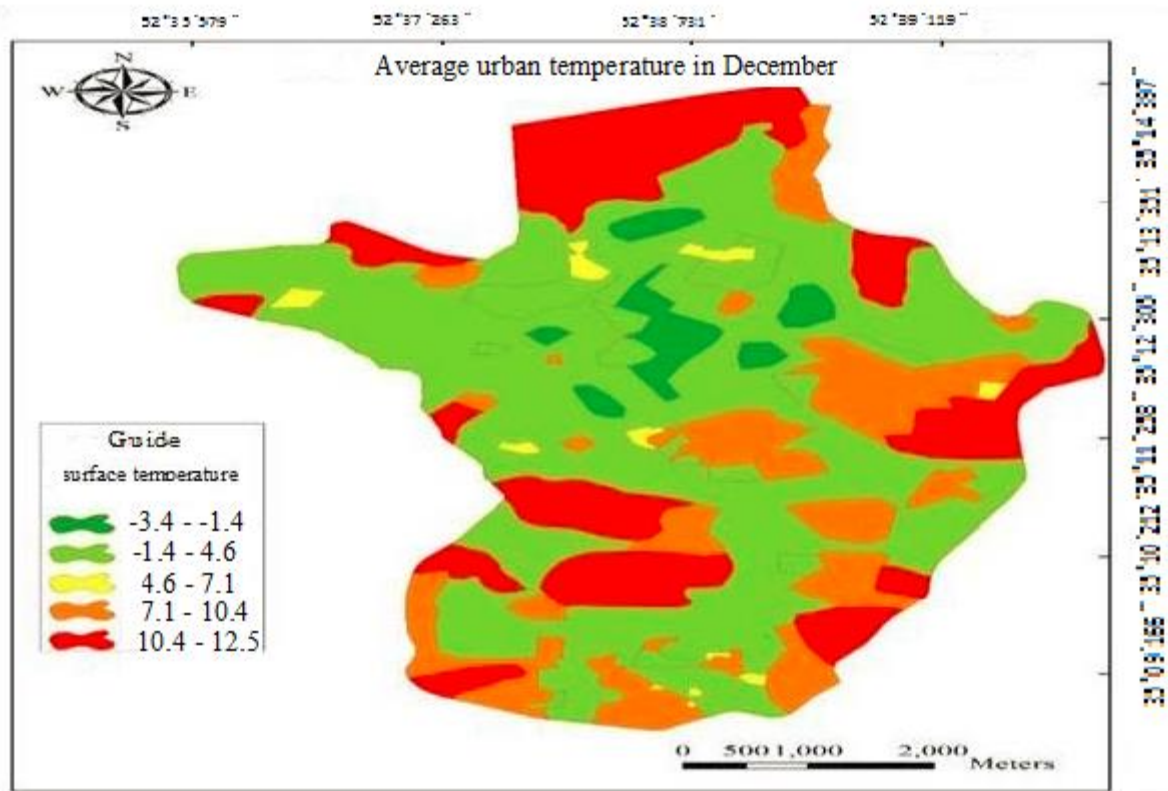**Figure 5**. Sanandaj average sanitation rate map on 28.6.2017

Figure 6. Sanandaj average sanitation rate map on 5.12.2017

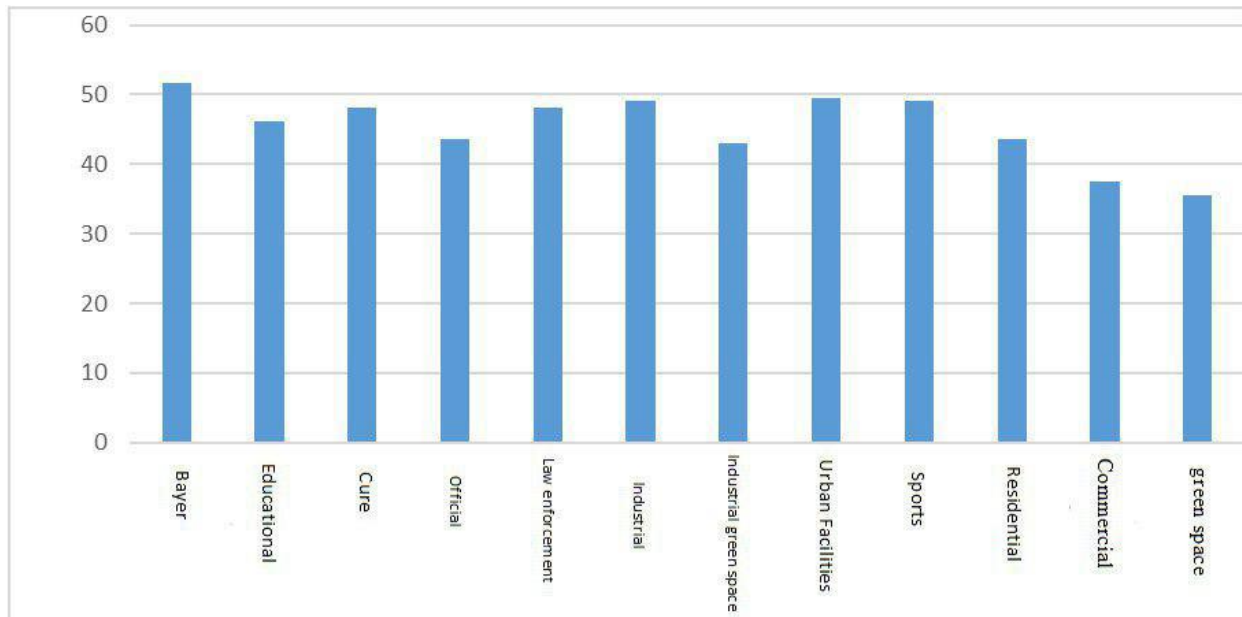Charts 1 and 2 Temperature-user relationship in July and December

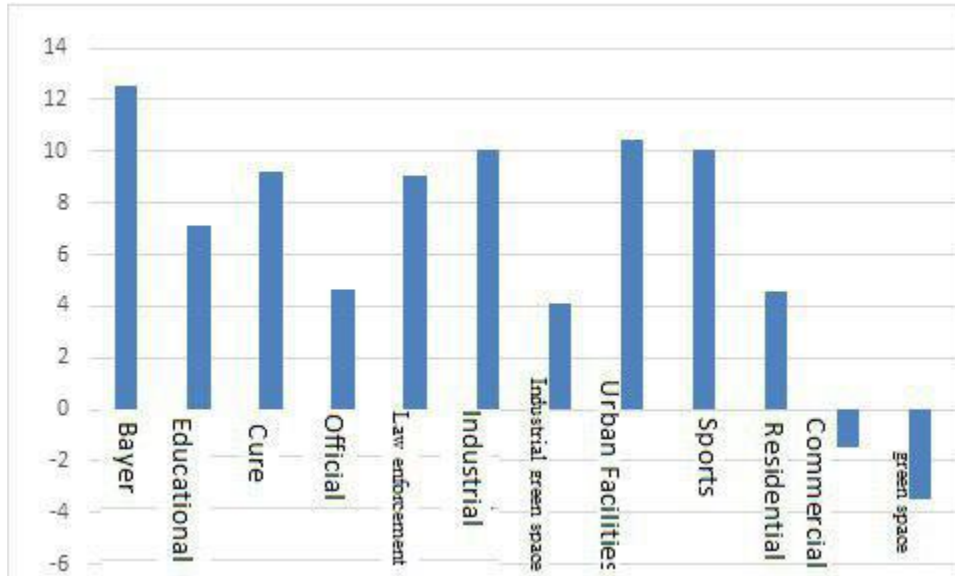**Chart 1.** Sanandaj urban-temperature on 28.6.2017

Chart 2. Sanandaj urban temperature on 5.12.2017

As it can be seen from the above charts in July, the best industrial and urban facilities had the lowest temperature, commercial use and green space. In December, Bayer (bare land), industrial and urban facilities had the highest temperatures and commercial use and green space.
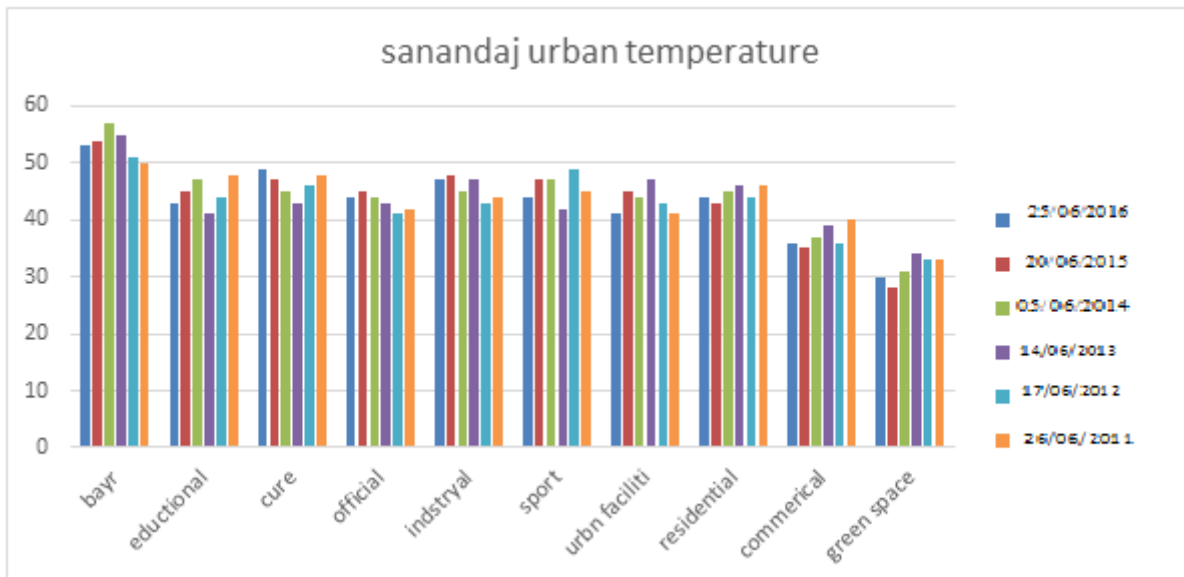

Chart 3. Sanandaj urban-temperature

Chart 3 shows that the temperature of Sanandaj city is different for different uses, and this over a period of 6 years, allows us to compare the user temperature, which indicates the temperature in the same time period (July).
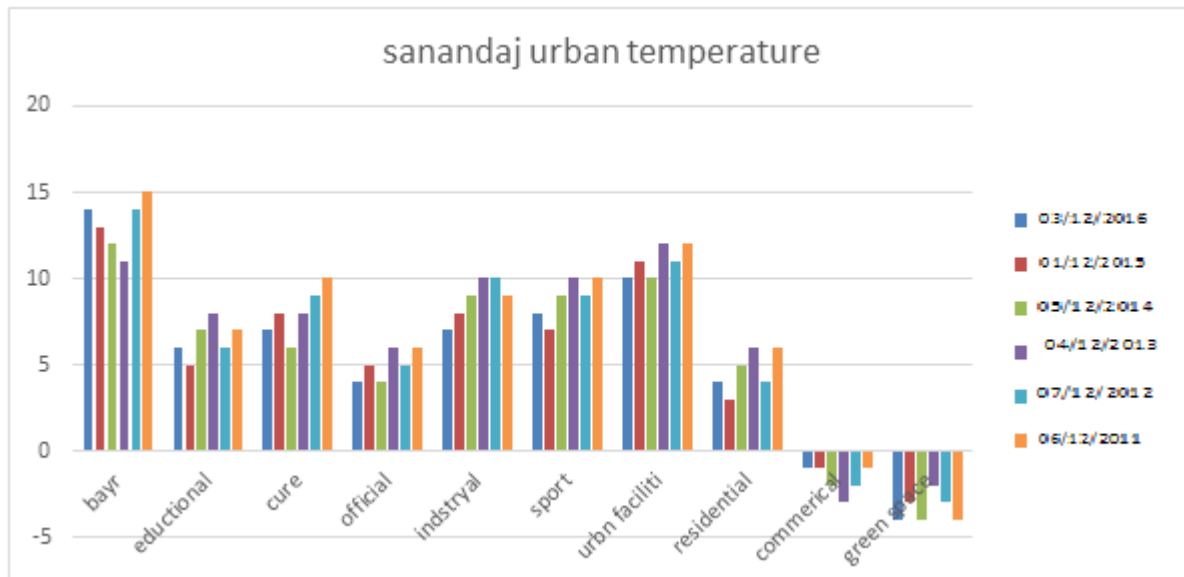
Chart 4. Sanandaj urban temperature

Chart 4 shows that the temperature of Sanandaj city is different for different uses, and this over a period of 6 years, allows us to compare the user temperature, which indicates the temperature in a similar time period (December). As you can see from the above, in July, the best industrial and urban facilities had the lowest temperature, commercial use and green space. In December, Bayer (bare land), industrial and urban facilities had the highest temperature, commercial use and green space.

3. Discussion and Conclusion

There is a relationship between the type of applications in the city (case study) and the formation of thermal regions. Feyzizadeh and Plazchak (2016), in their paper, calculated the surface temperature for the Maragheh city by the SEBAL method. The results show that there is a difference of 6% measured surface temperature (Faizizadeh et al., 2016).

Owen et al. (1998) at the University of Pennsylvania in a research entitled "Remote Sensing Surveillance Indicator Parameters in describing the quantitative climate impacts of urbanization" addressed the impacts of urban utilization on urban temperature determination and evaluated them (Owen, et al.,1998).

Carlson et al. (2000) investigated the effects of land use and vegetation changes in the Chester area of the United States. In his research, he used the TM and AVHRR imaging for NDVI and ISA extraction, and concluded that the magnitude of the ISA between two times (1996-1996) increased from 1.29 to 0.19 (Carlson et al., 2000). According to the urban utilization layer, Figures 1 and 2, it can be seen that there is a relation between urban type and formation of thermal regions which confirms the hypothesis. There is a relation between the hypothesis between the green space in a region and its average temperature.

Wang et al. (2003) proposed a successful way of determining the relationship between LST and land use patterns and land cover using remote sensing data and land echelon ecological methods. In this study, using the ETM + image of Indiana Police, images of green vegetation, soil, regions, or Albdeau highlands and landscapes with low albedo were obtained using spectral separation model.

Then impenetrable surfaces were extracted from high-resolution images and images with low albedra. Subsequently, a hybrid classification was used to develop the classification of fractional images into seven user levels and land cover. In fact, the Landscape pattern fragmentation images were obtained and the correlation of the subpixel image extracted with the Landscape fraction components was investigated. The results indicated that the extracted fragment images significantly reflect the morphology of the city, which showed a logical relationship with the city's bio-physical characteristics. The temperature was positively correlated with non-penetrating surfaces and negative relation with green vegetation (Wenget al., 2004).

Green space in the city depends on the location of the area so that there is enough green space in one of the factors not forming thermal islands in the densely populated urban areas. Conversely, there is a high temperature and the formation of thermal islands in the Bayer areas due to the lack of green space. So, one can conclude that there is a relation between the green space and the average temperature of that relationship is reversed, that is, lesser the green space lower is the temperature, so this hypothesis is also confirmed.

In the hypothesis, there is a relationship between the industrial user in one region and its average temperature.

Great islands are caused by the release of heat by human activities caused by processes such as fuel, especially in winter. In addition, the smoke and vapor coating caused by industrial activities reduce the loss of heat by night-time wavelengths in urban areas and, as a result, the greenhouse effect intensifies. The relationship between industrial user and temperature is clear and this relationship is as shown in Figures 1 and 2. It is straightforward that more the industrial centers, the higher the temperature in those areas which confirms the hypothesis.

-Earth surface temperature is one of the key factors, because it is equivalent to the air temperature of the lower layers of the urban atmosphere, which is the center of energy balance. It affects the lives and comfort of urban residents. Thermal islands are characterized by different atmospheric layers of the city, and are normally divided into two categories: the atmospheric thermal islands (Thermal Layer), and the thermal islands of the earth's surface layer.

-Thermal sensors are able to recover terrestrial thermal islands by recording the thermal radiation exerted from the surface areas in the sensor field. In general, LST is a large area of thermal islands. These islands are more visible in July.

At Sanandaj airport, especially the main passenger terminal of Saqez, low vegetation, existence of low asphalt surfaces with high thermal conductivity and the borderless areas of airports that do not perform moderating evaporation in the summer due to the lack of moisture, the formation of thermal islands in these areas. There is also a lot of cars and the presence of impermeable surfaces due to the increase in the temperature of passenger terminals in the city of Sanandaj.

-In streets and highways with high traffic on Sixth Bahman Avenue, Palestine Street, Iqbal Square, Sanandaj Highway - Hamadan and Sanandaj Highway - Kermanshah, the thermal islands of these areas, in addition to the mentioned factors, increase in the temperature of impermeable surfaces and increases the tangible heat. Heat and pollution are also due to fuel consumption. In the summer, one of the main causes of heat pollution is vehicle-related pollution. Cars produce nitrogen gas and carbon monoxide, which increases the temperature after absorbing long wavelengths and reflecting them into space.

-Residential areas of the city (such as Golshan, Farah, Farah, Sirous and Abbasabad) despite impermeable surfaces, the calculated temperature is related to the early hours of the morning, Residential buildings (roofs and bricks) are warmer than the industrial and industrial zones. That's why thermal islands are not formed in these areas.

-According to these results, thermal islands are not always located in city centers, but in the marginal areas of cities where the distribution of industries in these places is higher because of the presence of asphalt, concrete and pollution, as well as in the Bayer (bare land) areas in the city and the outskirts due to the lack of use evapotranspiration cooling mechanisms has high heat absorption capacities and low conductive capacity.

-According to the comparison of the results of terrain thermal images in July and land cover, it is evident that their spatial distribution has the same pattern, so that for the layers of application the highest is in the areas of waste, industrial and urban facilities, average temperatures to residential and administrative areas, the lowest temperatures to the regions is the commercial and green areas.

References

Alavi Panah, K. (2006). Thermal Detection and Application in Earth Sciences. *Tehran University Press*, p. 522

Alavi panah, K. (2008). Heat Detection and its Application in Earth Sciences. *Tehran University Press*.

Alijani, B., & Kaviani, M. R. (1992). *Basics of aerology*. side publications.

Allen, R., Tasumi, M., Trezza, R., & Wim, B. (2002). SEBAL; surface Energy glance Algorithms for Land, Version 1.0, Funded by a NASA EOSDIS/ Synergy Grant from the Raytheon Company through The Idaho Department of Water Resources.

Azizi, G. (2014). *Climate Change*. *Gomes Publishing*. p. 270.

Bahreini, A., & Zandniapour, H. (1992). Air Pollution Meteorology Studies and Application in Tehran. *Urban Design, Research Plan*, p. 83.

Balling, R., & Brazel, S. W. (1988). High-resolution surface temperature patterns in a complex urban terrain. *Photogrammetric Engineering and Remote Sensing*, *54*(9), 1289-1293.

Carlson, T. N., & Arthur, S. T. (2000). The Impact of Land Use – Land Cover Changes due to Urbanization on Surface Microclimate and Hydrology: a Satellite Perspective. *Global and Planetary Change*, (25), 49-65.

Faizizadeh, B., & Balaschak, T. (2013). Calculation of surface temperature for Maragheh city by SEBAL method. *Scientific and Research Journal of Geography and Planning (Tabriz University)*, No. 222 - 2217.

Marofnjad, A. (2010). The Role of Urban Use in the Geography of the Thermal Isles of the Cities (Case Study of Ahvaz City). *Environment, 3*(14), 90-66.

Mehregan, H., Rohami, M. B., & Khaknejad, A. S. (2013). Environmental management of urban thermal islands.

Miller, G. (2012). Living in the environment (Makhdoum, M. Trans.). Tehran: *Tehran University Press*.

Mir Yaghoubzadeh, M. H., & Ghanbarpour, M. R. (2009). The application of remote sensing data in land surface temperature estimation (A case study of the Westin watershed, East Azerbaijan). *Rangeland Scientific Journal*, 4, 723-734.

 Mohan, M., Kikegawa, Y., Gurjar, B. R, Kandya, Sh., Ogawa Koichi, A., (2012). Urban Heat Island Assessment for a Tropical Urban Air shed in India. *Atmospheric and Climate Sciences*, 2, 127-138.

Nakamura, M. (2002). Characterization of Urban Radiation Flux Using Remote Sensing Imagery. *Yasuoka Laboratory Institute of Industrial Science University of Tokyo*.

Noak, D. J. F. Dwyer, (2000). *Understanding the Benefits and Costs of Urban Forest Ecosyste*ms. In Handbook of Urban and Community Forestry in the Northeast. J. E Kuser, ed. New York: klawer Academic /Plenum Publishers.

Owen, R., & Andrew, N. (1998). Remote Sensing for the Earth Sciences, *New York: John Wiley and Sons.*

Rose, AL., & Devadas, M. D. (2009). Analysis of Land surface temperature and land use/ land cover types using remote sensing imagery a case in Chennai city, India. *The seventh Intonational conference on Urban Climate*, 29 June – 3 July 2009, Yokohama, Japan.

Roth, M., Oke, T. R., & Emery, W. J. (2009). Satellite derived urban heat islands from three coastal cities and the utilization of such data in urban climatology. *International Journal of Remote Sensing*, 10, 1699-1720.

Shakiba, A. R., Firoozabadi, P., Ashoorloo, D., & Namdari, S. (2009). The analysis of the relationship between land use and land cover and thermal islands in Tehran using ETM + data.

Shaqaygi, Sh., & Mofidi, M. (2008). The Relationship between Sustainable Development and Climatic Design in the Buildings of the Cool and Dry Areas of Tabriz. *Science and Technology for the Environment*, *10*(3), 120 - 105.

Sobrino, A., Juan, C., Jimenez, M., & Paolinib, L. (2004). Land Surface Temperature Retrieval from LANDSAT TM 5. *Remote Sensing of Environment*, 90, 434 -440.

Soltani Nejad, A. A. (2017). Environmental impacts of pollutant emissions from motor vehicles with emphasis on Tehran's great air. *Journal of Environmental Studies*.

Streutker, D. R., (2003). Satellite-measured growth of urban heat island of Houston, TX. *Remote Sensing of Environment*, 85, 282-289.

Wairmn Yazdi, M. (2000). The Role of Geographic Factors in the Physical Development of Ahvaz City. *Master's Degree in Geography and Urban Planning*, University of Isfahan. 153 pages.

Weng, Q., Lu, D., & Schubring, J. (2004). Estimation of land surface temperature- vegetation abundance relationship for urban heat island studies. *Remote sensing of Environment*, 89, 467-483.

Yamamoto, Y. (2006). Measure to mitigate urban heat islands. *Quarterly Review*, 18, 65-83.

Yuan, F., Bauer, M. E., Heinert, N. J., & Holden, G. R. (2005). Multi-level Land Cover Mapping of the Twin Cities (Minnesota) Metropolitan Area with Multi-seasonal Landsat TM/ETM+Data, *Geocarto International*, *2* (20), 5-14.